Development of Microfluidic Electrophoresis Separation Methods for Calmodulin Binding Proteins

By

2014

Thushara Nalin Samarasinghe

Submitted to the graduate degree program in Chemistry and the Graduate Faculty of the University of Kansas in partial fulfillment of the requirements for the degree of Doctor of Philosophy.

_____

Dr. Carey Johnson (Chairperson)

_____

Dr. Susan Lunte

_____

Dr. Michael Johnson

_____

Dr. David Weis

_____

Dr. Prajna Dhar

Date Defended: February 27th , 2015

The Dissertation Committee for Thushara Nalin Samarasinghe

certifies that this is the approved version of the following dissertation:

Development of Microfluidic Electrophoresis Separation Methods for Calmodulin Binding Proteins

_____

Dr. Carey Johnson (Chairperson)

Date approved: February 27th , 2015

Abstract

Calmodulin (CaM) is a Ca^{2+} signaling protein that regulates more than 100 different enzymes in many intracellular pathways. Investigation of this complex CaM-binding "interactome" requires a sensitive and rapid screening mechanism. The objective of this research work is to develop a highly sensitive fluorescence-based detection method coupled with microfluidic electrophoresis separation assay for CBPs. A functional microfluidic separation platform with red laser-induced fluorescent detection was developed. It is a semi-automated system with integrated functional modules, a separation module, an optical module, a detection module and a control module. AF647-labeled CaM, BSA and concanavalin A were separated to test the microchip platform. Different microfluidic devices, separation modes, and separation conditions were used to optimize the separation of a mixture of the standard proteins. Additionally, the three standards were separated in 100 s by capillary zone electrophoresis-based methods using glass chips. Si-nanoparticle colloidal array chips provided better resolution and separation efficiency in comparison with the glass chips. A photochemical bi-functional cross-linker was used to make a covalent link between AF647-labeled CaM and CBP to allow separation under denaturing conditions. Two CBPs, calcineurin (CN) and eNOS, were used as model proteins and photo cross-linked with CaM using different photochemical cross-linkers (BPM and NHS-diazirine). Mass spectrometric analysis of the in-gel digested sample revealed the presence of both CaM and CBPs in the sample, meaning that CaM and CBPs were successfully cross-linked. NHS-LC-SDA was used as the photo chemical cross-linker; and CaM-CN and CaM-eNOS photoproducts were separated on a PDMS/glass, PDMS/PMMA, glass and Si-nanoparticle colloidal array microfluidic device. CaMAF647 and the individual photoproducts were identified by different separation devices and modes. Overall, this work demonstrated the separation of CaM binding model proteins using different microfluidic devices operated under electrophoresis.

To my wife, Asha, and our children, Thehan, Yumethma and Ayansa.

Acknowledgements

First, I would like to sincerely thank my adviser, Dr. Carey Johnson, for his guidance and mentorship throughout this long journey. Working in his research laboratory helped me develop my own independent scientific ideas, as well as improve my technical research skills. I am very grateful for the scientific training that I received in his lab over the years.

Next, I would like to extend my gratitude to our collaborator, Dr. Susan Lunte, for her scientific insights and valuable suggestions on this project and for allowing me to use her laboratory. I would like to thank the members of my dissertation committee for their invaluable input at committee meetings and for serving on my committee: Dr. Susan Lunte, Dr. Michael Johnson, Dr. David Weis and Dr. Prajna Dhar. Additional thanks to Dr. Christopher Fischer for serving on my pre-defense committee meetings, and a special thanks to Dr. Susan Lunte and Dr. Michael Johnson for taking the extra time to read and edit my dissertation.

I would like to thank the Department of Chemistry for the great opportunity to study at the University of Kansas, especially Dr. Jon Tunge, Dr. Paul Hanson, and Dr. Jill Hedrick for helping me successfully complete the prerequisites to enter graduate school.

A special word of thanks goes to Ryan Grigsby (The Adams Microfabrication Facility, University of Kansas) for writing LabVIEW programs and sharing his expertise on microchip fabrication. Thanks to Dr. Craig Lunte for allowing me to use his laboratory and HPCE instrument, and to the past and present members of the C. Lunte group for teaching me how to use the instrument and for helping trouble-shoot when problems arose. I would like to thank Dr. Yong Zeng for providing Si-nanoparticle chips and discussing colloidal array separations with us. Also, I would like to thank the Zeng group members, Dr. Wenju Xu and Yiqiu Yin, for fabricating Si-nanoparticle chips for my project. Thanks to Dr. Christian Schöneich for allowing me to use his laboratory and instrumentation for photo-cross-linking experiments. Also, I would like to thank the Schöneich group members for helping me run SDS-PAGE and Western blot experiments; and I would like to especially thank Dr. Olivier Mozziconacci for instructing me on the use of their UV photoreactor and sharing his scientific knowledge on the photo-cross-linking

of proteins. Also, many thanks go to Jessica Bane for helping analyze MS data, with MassMatrix software and for reading some sections of my dissertation.

I would like to thank Dr. David Weis for allowing me to use his LC-MS instrument and for his input on intact protein analysis. I would like thank, Mohammed Al-Naqshabandi for both running my samples and for his assistance in analyzing the data. I thank Dr. Nadya Galeva (KU Mass Spectrometry/Analytical proteomics, University of Kansas) for her efforts in acquiring the ESI-LS/MS spectra and LTQ-FT spectra.

My special thanks go to the people who generously provided gifts of materials: Dr. Paul Stemmer (Wayne State University, Detroit, Michigan) provided calcineurin, Dr. David Arnett (Northwestern College, Orange City, Iowa) and Dr. Anthony Persechini (School of Biological Sciences, University of Missouri, Kansas City, Missouri) provided eNOS. I would also like to thank Dr. Kenneth Ratzlaff (Instrumentation Design Laboratory, Department of Chemistry) for designing and making high voltage relay for the experiments.

I would like to thank the many people in different departments that helped me complete this research work, especially the past and present members of S. Lunte group who graciously allowed me to use their laboratory and gave ideas and materials to solve my experimental problems. I would like to thank the past and present members of Johnson group, especially Dr. Shane Price and Dr. Mattew DeVore for instruction on calmodulin expression and labeling. Also, I would like to thank Dr. Christopher Culbertson (Kansas State University, Manhattan, Kansas) for his suggestions and discussions on microchip protein separations.

Finally, I would like to pay my gratitude to my parents for everything they have done for me, and to my mother-in-law for giving a helping hand to my family when we were really in need. Most importantly, I would like to thank my wife, Asha. This would have never be possible without her vision, love, encouragement, patience, and contribution. Most importantly, she gave me the most wonderful gifts of all, our children: Thehan, Yuma and Ayansa. They are the motivation in completion of this journey.

Table of Contents

Index of Figures

Scheme **Page**

Index of Tables **Page**

Abbreviations

CaM: Calmodulin

CBP: Calmodulin binding protein

MCE: Microchip capillary electrophoresis

LIF: Laser induced fluorescent

pI: Isoelectric point

EOF: Electro-osmotic flow

BGE: Background electrolyte

PDMS: Poly(dimethylsiloxane)

PETG: Polyethylene terephthalate glycol

SDS-PAGE: Sodium dodecyl sulfate polyacrylamide gel electrophoresis

PVC: Polyvinyl chloride

CZE: Capillary zone electrophoresis

CGE: Capillary gel electrophoresis

HPMC: Hydoxypropyl methylcellulose

HEC: Hydroxyethyl cellulose

HVPS: High voltage power supply

FL: Fluorescence

LED: Light emitting diode

MS: Mass spectroscopy

MEKC: Micellar electrokinetic chromatography

CIEF: Capillary isoelectric focusing

SDS: Sodium dodecyl sulfate

ICAT: Isotope-coded affinity tags

PMMA: Polymethyl methacrylate

2-D: Two dimensional

HV: High voltage

TCEP: Tris(2-carboxyethyl)phosphine

ESI: Electrospray ionization

APD: Avalanche photodiode

FT: Fourier transform

DAQ: Data acquisition

MWCO: Molecular weight cut-off

AF: Alexa Fluor

DMSO: Dimethyl sulfoxide

HEPES: 2-[4-(2-hydroxyethyl)piperazin-1-yl]ethanesulfonic acid

TBE: Tris-borate EDTA

BSA: Bovine serum albumin

ConA: Concanavalin A

HPCE: High performance capillary electrophoresis

DDM: n-Dodecyl-β-D-maltopyranoside

MeOH: Methanol

ACN: Acetonitrile

TTAB: Tetradecyltrimethylammonium bromide

LC: Liquid chromatography

NHS-SDA: Succinimidyl 4,4-azipentanoate

NHS-LC-SDA: Succinimidyl 6-(4,4′-azipentanamido) hexanoate

BPM: Benzophenone-4-maleimide

NHS: *N*-Hydroxysuccinimide

GRAVY: Grand average of hydrophathicity

Chapter One

Introduction

1.1. Objectives of dissertation

The objective of this research project is to develop sensitive and rapid methodology for the detection of calmodulin binding proteins (CBPs). The Ca^{2+}-signaling protein calmodulin (CaM) is involved in a network of cellular processes, and it is reported that CBP profiles represent the cell state, such as disease state at a given time (*1*). Consequently, a change in CBP profiles or expression in cells might indicate certain disease states, such as cancer (*2-6*). A change in expression levels of CBPs has been associated with many diseases, including cancer and neurodegenerative diseases (*7-9*). Hence, a subset of CBPs and their profiles could be used as a bio-marker for certain cell states, for example cancer cells versus healthy cells. Therefore, development of a rapid and sensitive assay to analyze CBPs is imperative.

Microfluidic electrophoresis separation methods are attractive tools for separating and analyzing biomolecules, including proteins (*10*). Microchip capillary electrophoresis (MCE) offers significant advantages over conventional analytical techniques, such as faster analysis, relatively small sample and solvent consumption, low cost including the possibility of miniaturization and interface with other modes of analysis, such as mass spectrometry (*10-12*). Hence, MCE is an ideal analytical technique to analyze CBPs. Our proposed method combines MCE with laser induced fluorescence (LIF) detection to achieve high sensitivity with the eventual possibility of single-cell analysis. The following studies were carried out with the goal of developing a methodology to separate CBPs on a microfluidic device, and the results obtained are discussed in detail in the following chapters:

Chapter 2 and 3: To develop a prototype microfluidic platform for a standard protein separation with LIF detection

Chapter 4: To photo cross-link fluorescently labeled CaM with two model CBPs, calcineurin and eNOS

Chapter 5: To separate and detect CaM-CBP complexes by microchip capillary electrophoresis with LIF

1.2. CaM and CBPs

CaM is a Ca^{2+} signaling protein that regulates numerous enzymes in many intracellular pathways (*13-15*). The intracellular Ca^{2+} concentration determines the cellular distribution, conformational state, and target protein interactions of CaM (*16-17*). CaM is an acidic (*pI* 4.5) protein consisting of ~148 amino acids (16.7 kDa), and it contains four EF-hands (helix-loop-helix Ca^{2+} binding motifs), which enable binding of up to four Ca^{2+} ions (*18-19*). Cooperative binding of Ca^{2+} ions induces a conformational change, exposing phenylalanine and methionine-rich hydrophobic surfaces that can, in turn, bind to a diverse group of target proteins (*15, 20-23*). CaM target proteins such as kinases, phosphatases, and ion channels can bind with CaM by Ca^{2+}-dependent (CaM-Ca^{2+}) or Ca^{2+}-independent (apo-CaM) manner (*20, 24-26*). Extensive studies have been carried out to recognize and characterize CBPs, and an online database exists for CBPs (*17, 27-28*). Current methods available for screening and characterizing CBPs in cell lysates involve conventional techniques, such as 1D and 2D gel electrophoresis, liquid chromatography and mass spectrometry, and immunoprecipitation (*29-31*). Almost all of these methods have limitations, such as long analysis times, labor-intensive processes, high limits of

detection (LOD), and large sample consumption (*32*). Consequently, there is a growing demand for rapid and sensitive techniques to characterize CBPs (*33*).

1.3. Microchip capillary electrophoresis

Electrophoresis separation is based on the migration of ions. Anions migrate towards the anode while cations migrate towards the cathode. Electroneutrality of the ionic solution is maintained by electrolysis at each electrode. As shown in the Figure 1.1A, electrolysis produces H^+ ions at the anode and OH^- ions at the cathode, and as a result, depletion of buffers occurs. Therefore, buffer pH and buffer capacity are very important parameters in capillary electrophoresis (*34*).

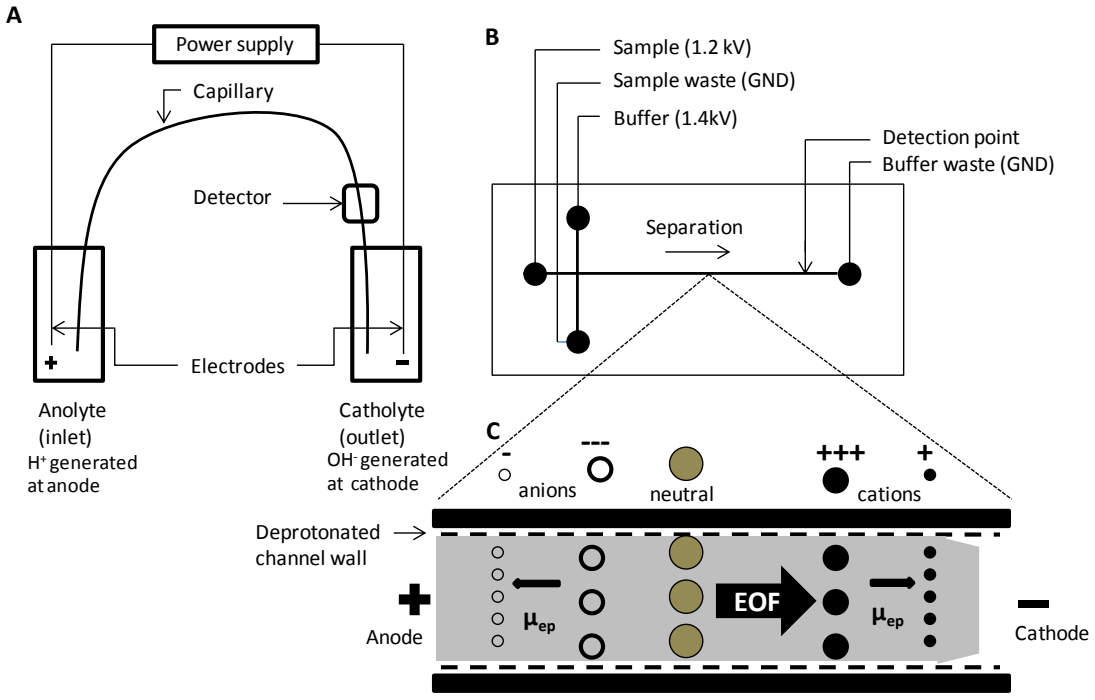

Figure 1.1. Capillary electrophoresis. (A) Basic schematic of a conventional capillary electrophoresis instrument. (B) Schematic of a microfluidic device. (C) Schematic representation of microchip capillary electrophoresis with normal polarity.

Application of a potential along a capillary or microchannel also generates electro-osmosis. Electroosmosis occurs due to the ζ-potential, which results from the surface charge on the inner wall of the capillary or microchannel (*34-35*). The ionization of silanol groups on the capillary wall (Figure 1.1C) generates the ζ-potential (*36*). The interaction of silanol groups with the background electrolyte (BGE) creates an electrical double layer at the surface. The potential of this double layer is called the ζ-potential. Anions in the run buffer are repelled by the negatively-charged capillary surface whereas cations are attracted. Ions that are close to the surface are immobile. Further from the surface are compact and mobile regions with relatively high level of cations. Upon application of a positive electric field, the mobile cations in compact and diffuse layers migrate towards the cathode (Figure 1.1). Since the ions and neutral molecules are solvated by water, water molecules in the run buffer are dragged along with migrating ions. This migration of ions and neutral molecules with water creates an electroosmotic flow (EOF) throughout the diameter of the capillary or micro channel (Figure 1.1). Even though anions are attracted to the anode relatively high EOF crates net flow towards the cathode (Figure 1.1C). Also, electroosmosis is one of the "pumping" mechanisms of capillary electrophoresis. An unmodified capillary, positive field and high pH buffers (as an example pH >3) will create cathodic EOF, and the electrophoresis can be described as a normal polarity-based separation. In this separation, the sample injection is performed at the anodic side (from the positive electrode) of the capillary or microchannel. Sometimes, reversing the EOF is beneficial for the separation. Reverse polarity creates anodic EOF and sample injection will be performed form the cathodic side (from the negative electrode). To generate anodic EOF, the channel surface charge must be modified from negative to positive. Also, negative voltages instead of positive voltages are applied to the buffer reservoir and sample reservoir (Figure 1.1B).

One of the most unique characteristics of microfluidics is that it utilizes small sample and reagent volumes (*12*). The separation mechanism in electrophoresis is based on the electrophoretic mobility (μ_e). Strong EOF makes it possible to detect anions, cations and neutral molecules simultaneously in a single separation. EOF can control different operations, such as injection and the direction of the fluid flow. The strength of EOF is determined by the applied field strength and the ζ-potential. The deprotonation of silanol groups (pK_a 2.9-4.9) is determined by the pH of the BGE and high EOF is generated at high pH (>8) conditions (*37-38*). Upon applying voltage the flow velocity generated by electroosmosis, v_{eo} in a microchannel can be determined by the Helmholtz-Smoluchowski equation (*39-40*):

$$v_{eo} = \varepsilon E \zeta / \eta \qquad (1)$$

where ε and η are dielectric constant and viscosity of BGE. The ζ-potential of the diffused layer is ζ and the applied electrical field is E. Adjustment of the EOF is required to optimize separation conditions. According to the Equation 1, the EOF depends on the properties of the BGE such as viscosity and dielectric constant (relative permittivity). Also, the strength of the EOF depends on the ζ-potential and applied field strength. The major parameter influencing the separation is electrophoretic mobility. However, high EOF can negatively affect the resolution and peak capacity. Separations that use normal polarity can utilize low EOF to improve the separation, and it can be achieved by either reducing the pH of the BGE or reducing the applied field strength. The electric field strength, BGE (pH, ionic strength), temperature, organic modifiers, solvents, and surfactants are some of the conditions used in optimizing separations. Further, a use of surface modification method is useful to obtain better separations.

In CE and MCE separations, transport is governed by the electrophoretic mobility, μ_{ep}, which is defined by Equation 2.

$$v = \mu_{ep} E \qquad (2)$$

where v is the velocity of analyte and E is the field strength. Under given separation conditions, EOF is constant and it will guide analytes towards the cathode (Figure 1.1). While moving towards the cathode, the analytes will be separated into zones based on their μ_{ep}. The two most important factors of electrophoretic zone separation are size (hydrodynamic radius) and net charge of the analyte. The relationship can be described by Equation 3.

$$\mu_{ep} = q/6\pi\eta r \qquad (3)$$

where μ_{ep} is the electrophoretic mobility of the analyte, q is net charge of the analyte, r is the hydrodynamic radius of the analyte and η is the viscosity of the BGE. The observed velocity of an analyte, v_{app}, is determined by μ_{ep} and μ_{eo} and shown in Equation 4.

$$v_{app} = (\mu_{ep} \pm \mu_{eo})E \qquad (4)$$

The apparent (observed) mobility of an analyte, μ_{app}, was calculated by Equations 5-7 where E is the field strength.

$$v_{app} = \frac{L_d}{t_m} \qquad (5)$$

$$\mu_{app} = \frac{v_{app}}{E} \qquad (6)$$

$$\mu_{app} = \frac{L_d/t_m}{V/L_t} \qquad (7)$$

Since the apparent mobility, μ_{app}, of the analyte is influenced by the EOF, determination of actual mobility requires measurement of μ_{eo}. The apparent electrophoretic velocity, υ_{app}, (cm/s) was calculated using detection length, L_d, (cm) and migration time, t_m (s). The apparent electrophoretic mobility, μ_{app}, [cm^2/ (Vs)] was calculated using υ_{app} and field strength, E, (V/cm) which was calculated using the applied voltage, V, (V) and the total length of the separation channel, L_t (cm).

Adjusting the pH of the BGE can change the net charge of analytes that are separated based on size-to-charge ratio. In capillary zone electrophoresis (CZE) and MCE, the net charge of an analyte plays an important role in separations (Equation 3). The separation of analytes that have very close size-to-charge ratio cannot be improved by adjusting the pH alone. Therefore, other CE modes have been introduced. In micellar electrokinetic chromatography (MEKC), micelles are formed by adding a surfactant above its critical micelle concentration (CMC) and have their own unique mobility in the BGE. In this mode, the mobility of an analyte is altered by the partitioning between micelles and BGE. The amount of time spent inside or interacting with the micelle is dependent on the ability of the analyte to partition between BGE and the micelles. As an example, the micelles formed by sodium dodecyl sulfate (SDS), interact with analytes and the complexes with micelles will have relatively different migration times. The separation mechanism of MEKC is based on mass transfer between micelles and BGE. A protein with a net negative charge can interact with SDS by available positively-charge residues and hydrophobic regions of the proteins.

Microchip capillary gel electrophoresis (MCGE) and microchip capillary isoelectric focusing (MCIEF) are adaptations of traditional slab gel electrophoresis. MCGE is more popular and commercial instruments are also available (*10*). In MCGE, the gel matrix provides the

mechanism of separation. These porous matrices are dissolved in the BGE and introduced into the microchip channel. The pore size of the three dimensional structure is determined by the concentration and type of polymeric material. Under the electric field, the size-based separation is determined by the pore size, and under conditions that suppress the EOF, the analyte mobility is inversely proportional to its size (*34*). This sieving based separation in a polymer network was described by several mechanisms such as Ogston and reptation models (*34*). Further, other sieving-based separation mechanisms such as colloidal arrays and nano or microstructures have been used to separate bio-polymers (*41-44*). The major separation modes and other criteria used in MCE with respect to protein separation were presented in Table 1.1

Electrophoresis-based separation techniques to separate biomolecules were first used in conventional capillary electrophoresis, and then transposed to MCE. MCE emerged in the early 1990s as a fast separation method for biomolecules, including proteins and DNA (*45*). MCE analysis comprises three steps: injection, separation and detection. There are two types of sample injection methods in MCE, pressure-driven and electokinetic injection. Electrokinetic injection is the most widely used method as it does not require pumps and valves to manipulate fluids during the injection process. It is discussed further in Chapter two.

Microchip construction and operation are the two main processes in the development of a microchip separation platform. Microchip construction includes microfabrication and substrate selection, which are determined by the objective of the analysis. Microchip operation, injection separation, and detection can be automatically controlled by software. The control of each of these processes is crucial to achieve sensitive and reproducible separations. Additionally, there are other factors, such as microfabrication, sample pre-treatment, detection, surface modification, and separation modes, that also contribute to a successful separation, and their involvement in

MCE separations will be addressed in detail in the following sections.

1.3.1. Microfabrication

Microfabrication is a technological process of constructing microstructures (*46*). Common microfabrication approaches use glass and silicon or polymer substrates. Glass and silicon chips offer higher-quality separation with respect to polymer substances (*47*). Glass chips have unique characteristics, such as high optical transparency (*48*). Glass offers surface characteristics similar to fused silica. However, glass is expensive and fragile, and therefore large-scale manufacturing is difficult. In addition, it requires clean room facilities.

Poly(dimethylsiloxane) (PDMS) is the most widely used polymer substance. Polymethyl methacrylate (PMMA), polyurethane, polyethylene terephthalate glycol (PETG), and polyvinyl chloride (PVC) are some of the polymer substrates also used in fabricating microchips (*49*). Besides their poorly understood surface chemistry, polymer material based devices are flexible, easy to fabricate and less expensive than glass, and as a result well-suited for research labs (*36*). Polymer-based microfluidic devices generate low EOF in comparison to glass based devices but have problems with adsorption.

1.3.2. Sample pretreatment

The protein analyte is frequently present in minute quantities and low concentrations in complex biological samples. Therefore, it is necessary to increase the target protein concentration by sample pre-concentration methods to enhance the sensitivity. Pre-concentration

improves the signal-to-noise ratio (S/N), and the detection of low abundant analytes. Some sample pretreatment techniques are solid-phase extraction, liquid-liquid extraction and filtration, and they often remove salts, solvents and biological matrix such as cell debris from the analyte protein (*50-52*). There are two types of on-line sample preconcentration techniques, dynamic and static. Stacking, sweeping, and preconcentration by focusing were used as dynamic and static sample preconcentration techniques (*53-56*). Solid-phase extraction is widely used in microchip capillary electrophoresis (*57*). Mello et al. and Lichtenberg et al. described microfluidic-based biological sample pretreatment methods in detail, and the implementation of dynamic pretreatment methods in the same microfluidic device, which is used to separate the sample (*51, 58*). In the work described in this dissertation, vacuum evaporation and size exclusion chromatography (off-chip methods) were used for sample pretreatment.

1.3.3. Surface modification

In electrophoresis-based separation modes, such as microchip zone electrophoresis (MCZE), the stability of EOF is important to obtain reproducible migration times (*35, 59-61*). The stability of EOF is affected by surface adsorption of analyte and buffer molecules as well as the interaction of analyte molecules with the channel wall (*62*). Similarly, the separation efficiency and reproducibility depend on the interactions of analyte molecules with the channel surface. Separation modes that use conditions that suppress EOF such as MCGE, offer higher separation efficiency than MCZE (*63*). Hence recent methodologies used in MCE have been focused on improving the surface chemistry of channels to minimize protein adsorption. There are two types of surface modifiers, dynamic coatings and permanent coatings (*64*). In dynamic

coating, surfactants and polymers, such as hydoxypropyl methyl cellulose (HPMC) and hydroxyethyl cellulose (HEC) are added to run buffers, and those surface-active molecules adsorb at the surface. In contrast, in permanent coating, chemical compounds are covalently attached to the channel surface. However, surface modifiers often adversely affect the separation. As an example, polymer additives like HPMC affect peak shapes due to local variation of the EOF that occurs as a result of uneven coating of channel walls (*35*).

1.3.4. Detection of proteins in microfluidic devices

Optical detection, mass spectrometry, and electrochemical detection are the three main detection methods widely used in microfluidic separation methods. Sample miniaturization is one of the most important features in microfluidics; however, it has inherent limitations, such as low sensitivities in small sample volumes. Many approaches have been proposed to overcome this problem, as an example, increasing the sensitivity by coupling with LIF detection (*65*). Microchip capillary electrophoresis coupled with LIF has been extensively used for analyzing biological samples (*66*). Derivatives of fluorescent dyes can react with amino, carboxylate and thiol groups of proteins, and bind covalently or interact by affinity (*67*). Incomplete labeling and multi-site labeling are the other drawbacks associated with complex protein mixtures (*68*). Similarly, native fluorescence, which results from aromatic amino acid residues, such as tryptophan, tyrosine and phenyl-alanine, can also be used for detection (*69*). Using native fluorescence eliminates the labeling, but it requires using deep-UV light for excitation, and UV-transparent chip substrates, and creates high background signal due to Rayleigh scattering of excitation light and background fluorescence (*70-71*).

Fluorescence (FL) based detection is widely used in MCE platforms due to its positive attributes, such as high sensitivity and selectivity (*65, 67, 72*). However, it is preferable to use an excitation source with wavelengths above 300 nm to minimize auto fluorescence, and as a result, most of the analytes must be derivatized prior to the detection (*72-74*). Derivatization performed within the microfluidic device is called on-chip derivatization, and it can be done before (pre-channel derivatization) or after (post-channel derivatization) the separation (*74*). Proteins can be derivatized during the sample preparation steps or fluorogenic domains can be introduced through genetic modification, as an example CaM-green fluorescence fusion protein (GFP-CaM) (*18, 73, 75-76*). Zhang and co-workers used CE-LIF to separate CaM and CaM-CBP complexes (*76*). They used GFP-CaM and OsCBK, a CBP kinase. GFP eliminates multiple labeling, which is a disadvantage associated with conventional FL probes. Gottschilich and co-workers reported a MCE method for post-separation labeling of proteins and peptides prior to FL detection (*77*). They integrated different functions into the microfluidic device, such as enzymatic reduction, electrophoretic separation and post-separation labeling. In their work, naphthalene-2,3-dicarboxaldehyde was used to label the A and B chains of insulin after on-chip reduction of disulfide bridges of bovine insulin. Also, Kennedy et.al have reported the pre-separation labeling of insulin in a competitive immunoassay with MCE (*78*). A 4-cm long reaction channel was used to mix insulin, FITC-insulin and anti-insulin antibody, and using a 1.5-cm long separation channel, FITC-insulin and FITC-insulin-antibody complex were separated with the detection limit of 3 nM. Based on the excitation source, FL detection can be divided into three categories; laser induced FL, lamp based-FL, and LED based-FL detection (*72, 79-81*).

LIF detection is the most easily adopted FL detection method in MCE for protein separation (*72-73*). The dimensions of the laser beam and the dimensions of the micro channels

are compatible, and the coherence and low divergence of laser beams makes it easy to focus on very small detection volumes with very high irradiation (*72*). LIF has offered one of the lowest detection limits of any detection method used in MCE protein separations (*82*). Mainly, epifluorescence microscopy has been used for MCE-LIF proteomic analysis (*79*). Several research groups (Zare et al., Harrison et al. and Landers et al.) have developed confocal microscopy based methods to detect single molecules in microfluidic devices (*65, 82-83*). Huang et al. reported single cell manipulation and detection of low copy-number proteins by MCE with confocal microscopy (*82*). This single-molecule counting method used an especially designed microfluidic device and high efficiency confocal LIF detection. To improve the counting efficiency in single-molecule detection with conventional confocal spectroscopy, they widened the laser focus using cylindrical optics with a tight focus. As a result, the number of single-molecules detected in a unit time was increased by 60%. Also, they proposed a method to manipulate, lyse, derivatize, separate and quantify low-abundant proteins. Jiang et al. used a red diode laser-based detection to achieve a very low limit of detection, 9 pM (900 molecules of Cy-5) using MCE (*83*). They also separated Cy-5 labeled ovalbumin in an MCE based-immunoassay in less than 30 s. Further, they demonstrated the use of confocal epifluorescence microscopy in MCE. Johnson and Landers reported the instrumental requirements of the detection module to achieve sub-zeptomole and sub-picomole detection limits in micro-analytical systems (*65*).

Coupling of MCE with MS is another promising technique used in protein analysis (*84*). It offers sensitive and fast detection along with relatively small sample consumption. However, interfacing of MCE with MS is challenging, and only electrospray ionization (ESI) has been interfaced successfully (*85-86*). Direct electrochemical detection of unlabeled molecules is another method integrated with MCE, and it functions with small volumes and low potential

(*87*). Easy miniaturization and selectivity are two advantages of combining MCE with electrochemical detection (*88*). However, only conductivity-based electrochemical detection was used in protein detection (*89*).

1.3.5. Separation modes

There are various separation modes in protein electrophoresis on microchips, such as MCZE, MEKC, MCGE, and MCIEF. MCZE is one of major modes of separation used in microchip protein analysis. Analytes are separated according to their electrophoretic mobilities and size-to-charge ratio. Even though the separation is based on the electrophoretic mobilities of the ions, at pH > 3 EOF governs the fluid flow, and both charged and uncharged analytes can be detected with the same detector placed before the cathode (Figure 1.1). Surface adsorption is a major drawback in this mode and dynamic coating methods have been predominantly used to minimize adsorption problems (*10, 72*). Usually SDS (lower than critical micellar concentration, CMC) is added to both the sample and BGE solution to modify not only channel walls (PDMS) and EOF but also the sample (*90*).

In MEKC, a surfactant-modified BGE and sample buffer are used. Separation is based on analyte partitioning between surfactant micelles and buffers. The mobility of analytes is determined by the type and the amount of surfactant (above the CMC) used. Additionally, surfactants enhance protein solubility, and hence reduce the adsorption at the surface (*91*).

MCGE is a widely used method in protein analysis. In MCZE the separation is based on the size-to-charge ratio of analytes while MCGE uses a sieving matrix and the separation will be based on the size of analytes (*92*). Normally, SDS and heat denatured proteins (all negatively

charged) migrate to the anode and the detector is placed before the anode. In MCGE, linear or entangled polymers have been used as sieving media and EOF suppressors, and subsequently, high efficiency separations were obtained (*42*). The net flow of analytes is determined by the electrophoretic mobility of BGE, and the sieving depends on the pore size of polymer media. The separation of SDS-protein complexes in MCGE is based on the molecular weights. An overview of mainly used separation modes in MCE-based protein separations is shown in Table 1.1.

Table 1.1 A brief overview of different separation modes used in MCE for proteins

Criterion	*MCZE* (*89-90, 93-95*)	*MCGE* (*96-102*)	*MEKC* (*103-105*)	*MCIEF* (*106-107*)	*Sieving with colloidal arrays and nano/micro structures* (*41, 43-44, 108-109*)
EOF	Prominent at high pH	Suppress	Prominent	Suppress	Suppress
Electrophoretic mobility (μ_{ep})	Important	Important	Important	Important	Important
BGE	High or low pH, surfactants below CMC	pH>7, surfactant high concentration	High pH, surfactants above CMC	pH gradient using a ampholyte mixture	High pH
Injection mode	Gated or Cross	Cross	Gated or cross	Cross and pressure	Cross or pressure
Separation mechanism	Size-to-charge	Size (Mass)	Affinity to micelles (mass transfer)	p*I*	Size (Mass)
LOD & Reproducibility	Good	Very good	Moderate	Moderate	Good
Challenges	High surface adsorption, low resolution, low peak capacity,	EOF, difficulty of handling viscous polymeric media	Moderate resolution, low peak capacity, variable affinities of proteins with surfactants	Low resolution, low peak capacity, EOF, pH drift and compression	EOF, unstable structures, drying and reproducibility

Merits	Easy and fast	Low surface adsorption, high resolution, high peak capacity	Increase of protein solubility, reduced adsorption	Not depend on separation distance, pressure mobilization, whole column scanning	Good resolution, high peak capacity
Integration with other modes	Poor	Very good	Good	Good	Has a good potential

1.4. Protein separations by microchip capillary electrophoresis

Proteomics demands fast and sensitive methods for separation and analysis. The basic tasks in proteomics involve separation, identification and characterization of constituent proteins from a complex biological sample. Over the years many techniques have been introduced; however, the lack of superior techniques to address extremely complex biological samples demands novel, rapid and sensitive methods. Two-dimensional gel electrophoresis combined with mass spectrometry is one of the major techniques used for proteomic studies over the years. Although 2D gel analysis provides adequate information about a protein sample, it is labor intensive, time consuming and difficult to automate (*110*). There are other common techniques, such as isotope-coded affinity tags (ICAT), isotope-coded protein labeling, and multi-dimensional protein identification technology (MudPit) (*111-113*). Although these methods address the complexity of a protein mixture and provide a great amount of information, they are inadequate in providing other information, such as post-translational modifications (*114*). MCE is a powerful method that is able to process complex samples, such as proteins, and generate very fast and highly efficient separations (*115-116*). Therefore, MCE has become a useful alternative to the traditional techniques (*36, 117*). Some applications of MCE-based protein separation with different separation modes are discussed in following paragraphs.

An automated CGE method was used to identify heat-shock proteins in Jurkat cells and it required sample denaturing buffers and heat denaturation (*118*). Soluble proteins from Jurkat cells (a human lymphoblastic T-cell line) were separated using the Agilent 2100 Bioanalyzer which contained an MCE-LIF platform (FL dye that was included in the Agilent Protein 200 Plus LabChip Kit had excitation/emission 650/680 nm), without denaturation. More than 20 proteins were separated within 45 s and sub-picogram sensitivity of a single protein was obtained. The same sample was analyzed after heat denaturation and only one new heat-shock protein was identified. This automated method is suitable to detect changes in protein expression levels (*118*). Similarly, an Agilent 2100 Bioanalyzer was used in proteomic analysis of bacteria like *Pseudomonas* strains and fungal cells of *Candia albicans* (*119-120*). Agilent Protein 200 Plus LabChip Kit was used for chip conditioning, protein denaturation and in-channel labeling. MCGE-LIF was performed for molecular weight-based separations and detection. Molecular weight standards (6-207 kD) that were included in the kit were used to estimate the separated proteins from cell lysates.

There are many single-cell based proteomic applications that are based on microfluidic separations (*121-123*). There are a number of microchip applications employed for immunological and cancer related investigations (*122*). These microfluidic methods were used to identify multiple proteins from single cells and study protein-protein interactions (*122, 124*). Wei et al. discussed advances of single-cell proteomic platforms with respect to microfluidic methods, and the applications of single-cell microfluidic platforms in fundamental proteomic research and clinical applications, especially immunology and cancer research (*123*). Chips can manipulate small numbers of cells and require very small volumes of reagents (*125*). Most importantly, chips can be customized to carry out multiple functions such as cell incubation, cell

labeling, cell sorting and cell lysis (*123*). Single-cell based microfluidic platforms can be divided into two main categories based on the method of detection. Some methods use whole cell staining to identify target proteins, while other methods detect target proteins by surface immunoassays, including protein chips and protein micro arrays (*125-128*).

Highly complex matrices affect the separation of proteins in biological fluids (*129*). MCE-based protein separations have been used as diagnostic tools in hospitals recently, but only a limited number of analyses have been reported with respect to biological samples such as blood, urine, and other body fluids (*130-131*). Albumins were labeled with 2-toluidinonapthaline-6-sulfonate (TNS) to detect different human serum proteins in a "synthetic" serum solution (*131*). The authors were able to separate all target albumins under 60 s with this post-column labeling method, but the separation of a real sample of human serum was unsuccessful. However, albumins were detected as a single peak in 50 times diluted human serum sample using MCE.

Chan and co-workers successfully used MCE separation and quantification for urinary albumins as a bio-marker of microalbuminuria. Urinary albumins were correlated with diabetes and cardiovascular disease (*132*). Unlike a conventional immunoassay, this method detected both immunoactive and non-immunoactive isoforms of albumins in urine. In another application, low-temperature bonded quartz chips were used to separate serum lipoproteins by MCZE-LIF detection (*133*). A lipophilic fluorescent dye (NBD-ceramide) was used to selectively label lipoproteins in a serum sample.

After a traumatic head injury, neurological dysfunctions are common, and the presence of inflammatory cytokines can be used as a prognosis-screening assay to determine the level of

head trauma (*134*). Six cytokines were successfully separated using a microchip based immunoaffinity separation. First, cytokines were isolated and captured by six separate antibodies, and they were labeled with AF633 on the chip, followed by MCZE in less than 2 min. The accuracy and precision associated with this MCE based assay were similar to a conventional ELISA assay (*134*).

A commercially available Agilent 2100 Bioanalyzer was used to analyze therapeutic proteins and secreted antibodies from cell cultures (*72*). Further, the instrument was used for quality control of recombinant proteins, and the concentration and purification process of antibodies (*10, 135*). As an example, Ohashi et al. reported the separation of immunoglobulins (IgGs) according to the size using hybridoma cell cultures, followed by quantification (*135*).

An MCE-based competitive immunoassay was developed to detect changes of insulin in mice. Insulin was mixed with FITC-insulin in a 4-cm reaction channel before mixing with anti-insulin antibody (*78*). Then the mixture of FITC-insulin and FITC-insulin-antibody complexes was separated using a 1.5 cm separation channel with 5 s separation time. Also, they demonstrated the ability to resolve secretary profiles of insulin by total protein analysis with 15 s intervals and the LOD of insulin was 3 nM.

The composition of glutenin, a wheat protein, is related to the dough quality of bread (*136*). Using the Agilent 2100 Bioanalyzer, Uthayakumaran et al. analyzed a set of 40 Australian wheat varieties to determine the subunits of glutenin composition. The same group developed a lab-on-a-chip procedure to quantify high molecular-weight subunits of glutenin. Rhazi et al. reported the separation and quantification of glutenin using another commercially available MCE platform, LabChip90 (Caliper LifeSciences), and it was used to evaluate 130 French wheat

varieties (*137*). The analysis time (45 s) was 100 times faster than that of reverse phase-HPLC (80 min) for the same sample.

The quality of chemical composition of food is very important aspects of human health. Biochemical differences in protein expression in different aquaculture methods were investigated by Monti et al. using the Agilent Bioanalyzer MCE platform (*138*). In a fish (*D. labrax*) muscle sample, 13 proteins were separated and quantified, and the expression levels of 9 out of 13 of those proteins revealed significant changes between wild-caught and farmed raised fish.

MCE separation of proteins is an attractive tool in lab-on-a-chip applications (*10*). Integration of miniaturized analytical-processes in the same device with high separation performance is well utilized in recent developments (*10, 95, 117*).

The integration of MCE with ESI-MS detection widens the capabilities of analyzing proteins in complex biological samples (*10, 84*). This has been integrated with multiple processing steps in proteomics, such as cell lysis, enzymatic digestion, pre-concentration and peptide separation.

CE-based traditional methods, such as CZE, MEKC, CGE, and CIEF have been transposed to MCE with faster analysis times. CGE is the most commonly used and most successful separation mode for protein separation by MCE (*10*). Additionally, this method has been widely used as a result of commercially available automated-CGE platforms (*139*). To improve separation performance, two modes have been orthogonally combined in multidimensional separation schemes such as 2-D-MCE (*79*). In these 2-D assays researchers faced challenges to combine 1-D separation modes in tandem without compromising the performance, and also to control the physiochemical properties between the dimensions (*117*).

Other non-traditional methods, such as counter flow gradient focusing, colloidal array and nano-structure based sieving methods, have been demonstrated in successful protein separation by MCE (*41, 140-142*).

1.5. Conclusion

MCE is a fast growing technique used in analyzing biomolecules, including proteins. In terms of protein separation, MCE solves many problems associated with conventional analytical methods, such as long analysis time and large sample consumption. Different fabrication methods offer customized solutions for different modes of microchip protein separations. It is important to improve the surface chemistry of microfluidic devices and interfacing approaches for 2-D separations. Based on the rate of novel developments of MCE separation methods, applications of the lab-on-a-chip concept (developing a miniaturized total analysis system that functions in a single device) could be applied in clinical settings in the near future. Proteomic analysis often handles complex biological samples, which are limited in quantity and concentration, and therefore, MCE would be an ideal technique in proteomic applications.

1.6. References

1. O'Day, D. H. (2003) CaMBOT: profiling and characterizing calmodulin-binding proteins, *Cell. Signal. 15*, 347-354.
2. Karp, C. M., Shukla, M. N., Buckley, D. J., and Buckley, A. R. (2007) HRPAP20: a novel calmodulin-binding protein that increases breast cancer cell invasion, *Oncogene 26*, 1780-1788.

3. Mine, N., Yamamoto, S., Saito, N., Yamazaki, S., Suda, C., Ishigaki, M., Kufe, D. W., Von Hoff, D. D., and Kawabe, T. (2011) CBP501-calmodulin binding contributes to sensitizing tumor cells to cisplatin and bleomycin, *Mol Cancer Ther 10*, 1929-1938.
4. Flory, M. R., Moser, M. J., Monnat, R. J., Jr., and Davis, T. N. (2000) Identification of a human centrosomal calmodulin-binding protein that shares homology with pericentrin, *Proc Natl Acad Sci U S A 97*, 5919-5923.
5. Hamada, T., Souda, M., Yoshimura, T., Sasaguri, S., Hatanaka, K., Tasaki, T., Yoshioka, T., Ohi, Y., Yamada, S., Tsutsui, M., Umekita, Y., and Tanimoto, A. (2014) Anti-apoptotic effects of PCP4/PEP19 in human breast cancer cell lines: A Novel Oncotarget, *Oncotarget 5*, 6076-6086.
6. Chang, S.-W., Tsao, Y.-P., Lin, C.-Y., and Chen, S.-L. (2011) NRIP, A novel calmodulin binding Protein, activates calcineurin to dephosphorylate Human Papillomavirus E2 Protein, *J Virol. 85*, 6750-6763.
7. Berggard, T., Arrigoni, G., Olsson, O., Fex, M., Linse, S., and James, P. (2006) 140 mouse brain proteins identified by Ca2+-calmodulin affinity chromatography and tandem mass spectrometry, *J Proteome Res 5*, 669-687.
8. Al-Lamki, Z., Wali, Y. A., Wasifuddin, S. M., Zachariah, M., Al-Mjeni, R., Li, C., Muralitharan, S., Al-Kharusi, K., Gunaratne, P., Peterson, L., Gibbs, R., Gingras, M. C., and Margolin, J. F. (2005) Identification of prognosis markers in pediatric high-risk acute lymphoblastic leukemia, *Pediatr Hematol Oncol 22*, 629-643.
9. Bergamaschi, A., Kim, Y. H., Kwei, K. A., La Choi, Y., Bocanegra, M., Langerod, A., Han, W., Noh, D. Y., Huntsman, D. G., Jeffrey, S. S., Borresen-Dale, A. L., and Pollack, J. R. (2008) CAMK1D amplification implicated in epithelial-mesenchymal transition in basal-like breast cancer, *Mol Oncol 2*, 327-339.
10. Tran, N. T., Ayed, I., Pallandre, A., and Taverna, M. (2010) Recent innovations in protein separation on microchips by electrophoretic methods: an update, *Electrophoresis 31*, 147-173.
11. Mellors, J. S., Black, W. A., Chambers, A. G., Starkey, J. A., Lacher, N. A., and Ramsey, J. M. (2013) Hybrid capillary/microfluidic system for comprehensive online liquid chromatography-capillary electrophoresis-electrospray ionization-mass spectrometry, *Anal Chem 85*, 4100-4106.
12. Whitesides, G. M. (2006) The origins and the future of microfluidics, *Nature 442*, 368-373.
13. Kaleka, K. S., Petersen, A. N., Florence, M. A., and Gerges, N. Z. (2012) Pull-down of calmodulin-binding proteins, *J Vis Exp*.
14. Moorthy, A. K., and Murthy, M. R. (2001) Conformation and structural transitions in the EF-hands of calmodulin, *J Biomol Struct Dyn 19*, 47-57.
15. Clapham, D. E. (2007) Calcium signaling, *Cell 131*, 1047-1058.

16. Chin, D., and Means, A. R. (2000) Calmodulin: a prototypical calcium sensor, *Trends Cell Biol 10*, 322-328.
17. Shen, X., Valencia, C. A., Szostak, J. W., Dong, B., and Liu, R. (2005) Scanning the human proteome for calmodulin-binding proteins, *Proc Natl Acad Sci U S A 102*, 5969-5974.
18. Allen, M. W., Urbauer, R. J., Zaidi, A., Williams, T. D., Urbauer, J. L., and Johnson, C. K. (2004) Fluorescence labeling, purification, and immobilization of a double cysteine mutant calmodulin fusion protein for single-molecule experiments, *Anal Biochem 325*, 273-284.
19. Lakowski, T. M., Lee, G. M., Okon, M., Reid, R. E., and McIntosh, L. P. (2007) Calcium-induced folding of a fragment of calmodulin composed of EF-hands 2 and 3, *Protein Sci 16*, 1119-1132.
20. Jones, E. M., Squier, T. C., and Sacksteder, C. A. (2008) An altered mode of calcium coordination in methionine-oxidized calmodulin, *Biophys J 95*, 5268-5280.
21. Hoeflich, K. P., and Ikura, M. (2002) Calmodulin in action: diversity in target recognition and activation mechanisms, *Cell 108*, 739-742.
22. Yuan, T., Ouyang, H., and Vogel, H. J. (1999) Surface exposure of the methionine side chains of calmodulin in solution. A nitroxide spin label and two-dimensional NMR study, *J Biol Chem 274*, 8411-8420.
23. Okano, H., Cyert, M. S., and Ohya, Y. (1998) Importance of phenylalanine residues of yeast calmodulin for target binding and activation, *J Biol Chem 273*, 26375-26382.
24. Ikura, M., Osawa, M., and Ames, J. B. (2002) The role of calcium-binding proteins in the control of transcription: structure to function, *Bioessays 24*, 625-636.
25. Carruthers, N. J., and Stemmer, P. M. (2008) Methionine oxidation in the calmodulin-binding domain of calcineurin disrupts calmodulin binding and calcineurin activation, *Biochemistry 47*, 3085-3095.
26. Mondragon, A., Griffith, E. C., Sun, L., Xiong, F., Armstrong, C., and Liu, J. O. (1997) Overexpression and purification of human calcineurin alpha from Escherichia coli and assessment of catalytic functions of residues surrounding the binuclear metal center, *Biochemistry 36*, 4934-4942.
27. Jang, D. J., Guo, M., and Wang, D. (2007) Proteomic and biochemical studies of calcium- and phosphorylation-dependent calmodulin complexes in Mammalian cells, *J Proteome Res 6*, 3718-3728.
28. http://calcium.uhnres.utoronto.ca/.
29. Klimmeck, D., Mayer, U., Ungerer, N., Warnken, U., Schnolzer, M., Frings, S., and Mohrlen, F. (2008) Calcium-signaling networks in olfactory receptor neurons, *Neuroscience 151*, 901-912.

30. Tuerxun, H., Zhang, Y., Ji, F., Aili, A., Yang, X., and Ding, Y. (2014) Application of two-dimensional electrophoresis and mass spectrometry to screen endometriosis-related proteins, *Mol Med Rep 10*, 95-100.
31. Zybailov, B. L., Glazko, G. V., Jaiswal, M., and Raney, K. D. (2013) Large scale chemical cross-linking mass spectrometry perspectives, *J Proteomics Bioinform 6*, 001.
32. Issaq, H., and Veenstra, T. (2008) Two-dimensional polyacrylamide gel electrophoresis (2D-PAGE): advances and perspectives, *Biotechniques 44*, 697-698, 700.
33. O'Connell, D. J., Bauer, M. C., O'Brien, J., Johnson, W. M., Divizio, C. A., O'Kane, S. L., Berggard, T., Merino, A., Akerfeldt, K. S., Linse, S., and Cahill, D. J. (2010) Integrated protein array screening and high throughput validation of 70 novel neural calmodulin-binding proteins, *Mol Cell Proteomics 9*, 1118-1132.
34. Weinberger, R. (2000) Practical capillary electrophoresis, 2 ed., Academic Press, New York.
35. Doherty, E. A., Meagher, R. J., Albarghouthi, M. N., and Barron, A. E. (2003) Microchannel wall coatings for protein separations by capillary and chip electrophoresis, *Electrophoresis 24*, 34-54.
36. Henry, C. S. (2006) Microchip capillary electrophoresis: an introduction, *Methods Mol Biol 339*, 1-10.
37. Horvath, J., and Dolnik, V. (2001) Polymer wall coatings for capillary electrophoresis, *Electrophoresis 22*, 644-655.
38. Fan, H. F., Li, F., Zare, R. N., and Lin, K. C. (2007) Characterization of two types of silanol groups on fused-silica surfaces using evanescent-wave cavity ring-down spectroscopy, *Anal Chem 79*, 3654-3661.
39. Nguyen, N.-T., and Wereley,S.T., (Ed.) (2004) Fundermentals and application of microfluidics, Vol. Chapter 2, 2 ed., Artech House Boston.
40. Delgado, A. V., (Ed.) (2002) Interfacial electrokinetics and electrophoresis, Vol. pp 1-54, Marcel Decker, New York.
41. Han, J., Fu, J., and Schoch, R. B. (2008) Molecular sieving using nanofilters: past, present and future, *Lab Chip 8*, 23-33.
42. Han, J., and Singh, A. K. (2004) Rapid protein separations in ultra-short microchannels: microchip sodium dodecyl sulfate-polyacrylamide gel electrophoresis and isoelectric focusing, *J Chromatogr A 1049*, 205-209.
43. Zeng, Y., and Harrison, D. J. (2007) Self-assembled colloidal arrays as three-dimensional nanofluidic sieves for separation of biomolecules on microchips, *Anal Chem 79*, 2289-2295.
44. Yasui, T., Kaji, N., Mohamadi, M. R., Okamoto, Y., Tokeshi, M., Horiike, Y., and Baba, Y. (2011) Electroosmotic flow in microchannels with nanostructures, *ACS Nano 5*, 7775-7780.

45. Woolley, A. T., and Mathies, R. A. (1994) Ultra-high-speed DNA fragment separations using microfabricated capillary array electrophoresis chips, *Proc Natl Acad Sci U S A 91*, 11348-11352.
46. Jacobson, S. C., Ramsey, J. M. (1997) Electrokinetic focusing in microfabricated channel structures, *Anal. Chem. 69*, 3212-3217.
47. Paegel, B. M., Hutt, L. D., Simpson, P. C., and Mathies, R. A. (2000) Turn geometry for minimizing band broadening in microfabricated capillary electrophoresis channels, *Anal Chem 72*, 3030-3037.
48. Voldman, J., Gray, M. L., and Schmidt, M. A. (1999) Microfabrication in biology and medicine, *Annu Rev Biomed Eng 1*, 401-425.
49. Barker, S. L., Tarlov, M. J., Canavan, H., Hickman, J. J., and Locascio, L. E. (2000) Plastic microfluidic devices modified with polyelectrolyte multilayers, *Anal Chem 72*, 4899-4903.
50. Xiang, F., Lin, Y., Wen, J., Matson, D. W., and Smith, R. D. (1999) An integrated microfabricated device for dual microdialysis and on-line ESI-ion trap mass spectrometry for analysis of complex biological samples, *Anal Chem 71*, 1485-1490.
51. de Mello, A. J., and Beard, N. (2003) Dealing with real samples: sample pre-treatment in microfluidic systems, *Lab Chip 3*, 11N-19N.
52. Yakhnin, A. V., Vinokurov, L. M., Surin, A. K., and Alakhov, Y. B. (1998) Green fluorescent protein purification by organic extraction, *Protein Expr Purif 14*, 382-386.
53. Monton, M. R., and Terabe, S. (2006) Sample enrichment techniques in capillary electrophoresis: focus on peptides and proteins, *J Chromatogr B Analyt Technol Biomed Life Sci 841*, 88-95.
54. Breadmore, M. C., Thabano, J. R., Dawod, M., Kazarian, A. A., Quirino, J. P., and Guijt, R. M. (2009) Recent advances in enhancing the sensitivity of electrophoresis and electrochromatography in capillaries and microchips (2006-2008), *Electrophoresis 30*, 230-248.
55. Pan, Q., Zhao, M., and Liu, S. (2009) Combination of on-chip field amplification and bovine serum albumin sweeping for ultrasensitive detection of green fluorescent protein, *Anal Chem 81*, 5333-5341.
56. Foote, R. S., Khandurina, J., Jacobson, S. C., and Ramsey, J. M. (2005) Preconcentration of proteins on microfluidic devices using porous silica membranes, *Anal Chem 77*, 57-63.
57. Sueyoshi, K., Kitagawa, F., and Otsuka, K. (2008) Recent progress of online sample preconcentration techniques in microchip electrophoresis, *J Sep Sci 31*, 2650-2666.
58. Lichtenberg, J., de Rooij, N. F., and Verpoorte, E. (2002) Sample pretreatment on microfabricated devices, *Talanta 56*, 233-266.

59. Gilges M, K. M., and Schomburg G. (1994) Capillary zone electrophoresis separation of baisc and acidic protiens using poly(vinyl alcohol) coating in fused silica capillaries, *Anal Chem 66*, 2038-2046.
60. Locascio, L. E., Perso, C. E., and Lee, C. S. (1999) Measurement of electroosmotic flow in plastic imprinted microfluid devices and the effect of protein adsorption on flow rate, *J Chromatogr A 857*, 275-284.
61. Hjertén, S., and Kubo, K. (1993) A new type of pH- and detergent-stable coating for elimination of electroendosmosis and adsorption in (capillary) electrophoresis, *Electrophoresis 14*, 390-395.
62. Belder, D., and Ludwig, M. (2003) Surface modification in microchip electrophoresis, *Electrophoresis 24*, 3595-3606.
63. Nikcevic, I., Lee, S. H., Piruska, A., Ahn, C. H., Ridgway, T. H., Limbach, P. A., Wehmeyer, K. R., Heineman, W. R., and Seliskar, C. J. (2007) Characterization and performance of injection molded poly(methylmethacrylate) microchips for capillary electrophoresis, *J Chromatogr A 1154*, 444-453.
64. Naruishi, N., Tanaka, Y., Higashi, T., and Wakida, S. (2006) Highly efficient dynamic modification of plastic microfluidic devices using proteins in microchip capillary electrophoresis, *J Chromatogr A 1130*, 169-174.
65. Johnson, M. E., and Landers, J. P. (2004) Fundamentals and practice for ultrasensitive laser-induced fluorescence detection in microanalytical systems, *Electrophoresis 25*, 3513-3527.
66. Ban, E., and Song, E. J. (2013) Recent developments and applications of capillary electrophoresis with laser-induced fluorescence detection in biological samples, *J Chromatogr B Analyt Technol Biomed Life Sci 929*, 180-186.
67. Garcia-Campana, A. M., Taverna, M., and Fabre, H. (2007) LIF detection of peptides and proteins in CE, *Electrophoresis 28*, 208-232.
68. Craig, D. B., and Dovichi, N. J. (1998) Multiple labeling of proteins, *Anal Chem 70*, 2493-2494.
69. Lee, T. T., and Yeung, E. S. (1992) High-sensitivity laser-induced fluorescence detection of native proteins in capillary electrophoresis, *J Chromatogr 595*, 319-325.
70. Schulze, P., and Belder, D. (2009) Label-free fluorescence detection in capillary and microchip electrophoresis, *Anal Bioanal Chem 393*, 515-525.
71. Schulze, P., Ludwig, M., and Belder, D. (2008) Impact of laser excitation intensity on deep UV fluorescence detection in microchip electrophoresis, *Electrophoresis 29*, 4894-4899.
72. Peng, Y., Pallandre, A., Tran, N. T., and Taverna, M. (2008) Recent innovations in protein separation on microchips by electrophoretic methods, *Electrophoresis 29*, 157-178.

73. Johnson, C. K. (2007) Fluorescence techniques for proteins, In *Wiley Encyclopedia of Chemical Biology*, John Wiley & Sons, Inc.

74. Giordano, B. C., Jin, L., Couch, A. J., Ferrance, J. P., and Landers, J. P. (2004) Microchip laser-induced fluorescence detection of proteins at submicrogram per milliliter levels mediated by dynamic labeling under pseudonative conditions, *Anal Chem 76*, 4705-4714.

75. Nagai, T., Sawano, A., Park, E. S., and Miyawaki, A. (2001) Circularly permuted green fluorescent proteins engineered to sense Ca2+, *Proc Natl Acad Sci U S A 98*, 3197-3202.

76. Zhang, J. F., Ma, L., Liu, X., and Lu, Y. T. (2004) Using capillary electrophoresis with laser-induced fluorescence to study the interaction of green fluorescent protein-labeled calmodulin with Ca2+- and calmodulin-binding protein, *J Chromatogr B Analyt Technol Biomed Life Sci 804*, 413-420.

77. Gottschlich, N., Culbertson, C. T., McKnight, T. E., Jacobson, S. C., and Ramsey, J. M. (2000) Integrated microchip-device for the digestion, separation and postcolumn labeling of proteins and peptides, *J Chromatogr B Biomed Sci Appl 745*, 243-249.

78. Roper, M. G., Shackman, J. G., Dahlgren, G. M., and Kennedy, R. T. (2003) Microfluidic chip for continuous monitoring of hormone secretion from live cells using an electrophoresis-based immunoassay, *Anal Chem 75*, 4711-4717.

79. Shadpour, H., and Soper, S. A. (2006) Two-dimensional electrophoretic separation of proteins using poly(methyl methacrylate) microchips, *Anal Chem 78*, 3519-3527.

80. Chirica, G., Lachmann, J., and Chan, J. (2006) Size exclusion chromatography of microliter volumes for on-line use in low-pressure microfluidic systems, *Anal Chem 78*, 5362-5368.

81. Yao, B., Luo, G., Wang, L., Gao, Y., Lei, G., Ren, K., Chen, L., Wang, Y., Hu, Y., and Qiu, Y. (2005) A microfluidic device using a green organic light emitting diode as an integrated excitation source, *Lab Chip 5*, 1041-1047.

82. Huang, B., Wu, H., Bhaya, D., Grossman, A., Granier, S., Kobilka, B. K., and Zare, R. N. (2007) Counting low-copy number proteins in a single cell, *Science 315*, 81-84.

83. Jiang, G., Attiya, S., Ocvirk, G., Lee, W. E., and Harrison, D. J. (2000) Red diode laser induced fluorescence detection with a confocal microscope on a microchip for capillary electrophoresis, *Biosens Bioelectron 14*, 861-869.

84. Koster, S., and Verpoorte, E. (2007) A decade of microfluidic analysis coupled with electrospray mass spectrometry: an overview, *Lab Chip 7*, 1394-1412.

85. Wen, J., Lin, Y., Xiang, F., Matson, D. W., Udseth, H. R., and Smith, R. D. (2000) Microfabricated isoelectric focusing device for direct electrospray ionization-mass spectrometry, *Electrophoresis 21*, 191-197.

86. Wang, Y. X., Zhou, Y., Balgley, B. M., Cooper, J. W., Lee, C. S., and DeVoe, D. L. (2005) Electrospray interfacing of polymer microfluidics to MALDI-MS, *Electrophoresis 26*, 3631-3640.

87. Xu, X., Li, L., and Weber, S. G. (2007) Electrochemical and optical detectors for capillary and chip separations, *Trends Analyt Chem : TRAC 26*, 68-79.

88. Lacher, N. A., Garrison, K. E., Martin, R. S., and Lunte, S. M. (2001) Microchip capillary electrophoresis/electrochemistry, *Electrophoresis 22*, 2526-2536.

89. Abad-Villar, E. M., Tanyanyiwa, J., Fernandez-Abedul, M. T., Costa-Garcia, A., and Hauser, P. C. (2004) Detection of human immunoglobulin in microchip and conventional capillary electrophoresis with contactless conductivity measurements, *Anal Chem 76*, 1282-1288.

90. Wang, H., Wang, H. M., Jin, Q. H., Cong, H., Zhuang, G. S., Zhao, J. L., Sun, C. L., Song, H. W., and Wang, W. (2008) Microchip-based small, dense low-density lipoproteins assay for coronary heart disease risk assessment, *Electrophoresis 29*, 1932-1941.

91. Badal, M. Y., Wong, M., Chiem, N., Salimi-Moosavi, H., and Harrison, D. J. (2002) Protein separation and surfactant control of electroosmotic flow in poly(dimethylsiloxane)-coated capillaries and microchips, *J Chromatogr A 947*, 277-286.

92. Zhu, Z., Lu, J. J., and Liu, S. (2012) Protein separation by capillary gel electrophoresis: a review, *Anal Chim Acta 709*, 21-31.

93. Dang, F., Kakehi, K., Nakajima, K., Shinohara, Y., Ishikawa, M., Kaji, N., Tokeshi, M., and Baba, Y. (2006) Rapid analysis of oligosaccharides derived from glycoproteins by microchip electrophoresis, *J Chromatogr A 1109*, 138-143.

94. Abad-Villar, E. M., Kuban, P., and Hauser, P. C. (2005) Determination of biochemical species on electrophoresis chips with an external contactless conductivity detector, *Electrophoresis 26*, 3609-3614.

95. Shadpour, H., Hupert, M. L., Patterson, D., Liu, C., Galloway, M., Stryjewski, W., Goettert, J., and Soper, S. A. (2007) Multichannel microchip electrophoresis device fabricated in polycarbonate with an integrated contact conductivity sensor array, *Anal Chem 79*, 870-878.

96. Werling, J., Kocsis, B., Dean, D., and Kustos, I. (2008) Characterisation of protein composition and detection of IgA in cervicovaginal fluid by microchip technology, *J Chromatogr B Analyt Technol Biomed Life Sci 869*, 54-58.

97. Chen, X., Tang, K., Lee, M., and Flynn, G. C. (2008) Microchip assays for screening monoclonal antibody product quality, *Electrophoresis 29*, 4993-5002.

98. Okada, H., Kaji, N., Tokeshi, M., and Baba, Y. (2008) Poly(methylmethacrylate) microchip electrophoresis of proteins using linear-poly(acrylamide) solutions as separation matrix, *Anal Sci 24*, 321-325.

99. Mohamadi, M. R., Kaji, N., Tokeshi, M., and Baba, Y. (2008) Dynamic cross-linking effect of Mg2+ to enhance sieving properties of low-viscosity poly(vinylpyrrolidone) solutions for microchip electrophoresis of proteins, *Anal Chem 80*, 312-316.

100. Park, C. C., Kazakova, I., Kawabata, T., Spaid, M., Chien, R. L., Wada, H. G., and Satomura, S. (2008) Controlling data quality and reproducibility of a high-sensitivity immunoassay using isotachophoresis in a microchip, *Anal Chem 80*, 808-814.

101. Chen, H., Hansen, M. J., Jones, J. E., Vlahos, R., Anderson, G. P., and Morris, M. J. (2008) Long-term cigarette smoke exposure increases uncoupling protein expression but reduces energy intake, *Brain Res 1228*, 81-88.

102. Makamba, H., Huang, J. W., Chen, H. H., and Chen, S. H. (2008) Photopatterning of tough single-walled carbon nanotube composites in microfluidic channels and their application in gel-free separations, *Electrophoresis 29*, 2458-2465.

103. Xu, Y., Li, J., and Wang, E. (2008) Microchip micellar electrokinetic chromatography based on one functionalized ionic liquid and its excellent performance on proteins separation, *J Chromatogr A 1207*, 175-180.

104. Huang, B., Kim, S., Wu, H., and Zare, R. N. (2007) Use of a mixture of n-dodecyl-beta-D-maltoside and sodium dodecyl sulfate in poly(dimethylsiloxane) microchips to suppress adhesion and promote separation of proteins, *Anal Chem 79*, 9145-9149.

105. Kitagawa, F., and Otsuka, K. (2008) Micellar electrokinetic chromatography on microchips, *J Sep Sci 31*, 794-802.

106. Shimura, K. (2009) Recent advances in IEF in capillary tubes and microchips, *Electrophoresis 30*, 11-28.

107. Silvertand, L. H., Torano, J. S., van Bennekom, W. P., and de Jong, G. J. (2008) Recent developments in capillary isoelectric focusing, *J Chromatogr A 1204*, 157-170.

108. Wirth, M. J. (2007) Separation media for microchips, *Anal Chem 79*, 800-808.

109. King, S. B., and Dorfman, K. D. (2013) Role of order during Ogston sieving of DNA in colloidal crystals, *Anal Chem 85*, 7769-7776.

110. Rogowska-Wrzesinska, A., Le Bihan, M. C., Thaysen-Andersen, M., and Roepstorff, P. (2013) 2D gels still have a niche in proteomics, *J Proteomics 88*, 4-13.

111. Florens, L., Washburn, M. P., Raine, J. D., Anthony, R. M., Grainger, M., Haynes, J. D., Moch, J. K., Muster, N., Sacci, J. B., Tabb, D. L., Witney, A. A., Wolters, D., Wu, Y., Gardner, M. J.,

Holder, A. A., Sinden, R. E., Yates, J. R., and Carucci, D. J. (2002) A proteomic view of the Plasmodium falciparum life cycle, *Nature 419*, 520-526.

112. Gygi, S. P., Rist, B., Gerber, S. A., Turecek, F., Gelb, M. H., and Aebersold, R. (1999) Quantitative analysis of complex protein mixtures using isotope-coded affinity tags, *Nat Biotechnol 17*, 994-999.
113. Coombs, K. M. (2011) Quantitative proteomics of complex mixtures, *Expert Rev Proteomics 8*, 659-677.
114. Lion, N., Rohner, T. C., Dayon, L., Arnaud, I. L., Damoc, E., Youhnovski, N., Wu, Z. Y., Roussel, C., Josserand, J., Jensen, H., Rossier, J. S., Przybylski, M., and Girault, H. H. (2003) Microfluidic systems in proteomics, *Electrophoresis 24*, 3533-3562.
115. Manabe, T. (1999) Capillary electrophoresis of proteins for proteomic studies, *Electrophoresis 20*, 3116-3121.
116. Righetti, P. G. (2001) Capillary electrophoretic analysis of proteins and peptides of biomedical and pharmacological interest, *Biopharm Drug Dispos 22*, 337-351.
117. Tia, S., and Herr, A. E. (2009) On-chip technologies for multidimensional separations, *Lab Chip 9*, 2524-2536.
118. Tabuchi, M., Kuramitsu, Y., Nakamura, K., and Baba, Y. (2003) Rapid subpicogram protein detection on a microchip without denaturing, *J Proteome Res 2*, 431-435.
119. Kustos, I., Nyul, A., Lorand, T., Kocsis, B., and Kilar, F. (2006) Effect of antifungal agents on protein composition of Candida albicans studied by capillary electrophoresis and chip technology, *J Biochem Biophys Methods 69*, 57-65.
120. Kustos, I., Andrasfalvy, M., Kustos, T., Kocsis, B., and Kilar, F. (2005) Effect of iron restriction on outer membrane protein composition of Pseudomonas strains studied by conventional and microchip electrophoresis, *Electrophoresis 26*, 3789-3795.
121. Ma, C., Fan, R., Ahmad, H., Shi, Q., Comin-Anduix, B., Chodon, T., Koya, R. C., Liu, C. C., Kwong, G. A., Radu, C. G., Ribas, A., and Heath, J. R. (2011) A clinical microchip for evaluation of single immune cells reveals high functional heterogeneity in phenotypically similar T cells, *Nat Med 17*, 738-743.
122. Ma, C., Cheung, A. F., Chodon, T., Koya, R. C., Wu, Z., Ng, C., Avramis, E., Cochran, A. J., Witte, O. N., Baltimore, D., Chmielowski, B., Economou, J. S., Comin-Anduix, B., Ribas, A., and Heath, J. R. (2013) Multifunctional T-cell analyses to study response and progression in adoptive cell transfer immunotherapy, *Cancer Discov 3*, 418-429.

123. Wei, W., Young Shik, S., Chao, M., Jun, W., Elitas, M., Rong, F., and Heath, J. R. (2013) Microchip platforms for multiplex single-cell functional proteomics with applications to immunology and cancer research, *Genome Medicine 5*, 1-12.

124. Shi, Q., Qin, L., Wei, W., Geng, F., Fan, R., Shin, Y. S., Guo, D., Hood, L., Mischel, P. S., and Heath, J. R. (2012) Single-cell proteomic chip for profiling intracellular signaling pathways in single tumor cells, *Proc Natl Acad Sci U S A 109*, 419-424.

125. Varadarajan, N., Kwon, D. S., Law, K. M., Ogunniyi, A. O., Anahtar, M. N., Richter, J. M., Walker, B. D., and Love, J. C. (2012) Rapid, efficient functional characterization and recovery of HIV-specific human CD8+ T cells using microengraving, *Proc Natl Acad Sci U S A 109*, 3885-3890.

126. Brouzes, E., Medkova, M., Savenelli, N., Marran, D., Twardowski, M., Hutchison, J. B., Rothberg, J. M., Link, D. R., Perrimon, N., and Samuels, M. L. (2009) Droplet microfluidic technology for single-cell high-throughput screening, *Proc Natl Acad Sci U S A 106*, 14195-14200.

127. Huebner, A., Srisa-Art, M., Holt, D., Abell, C., Hollfelder, F., deMello, A. J., and Edel, J. B. (2007) Quantitative detection of protein expression in single cells using droplet microfluidics, *Chem Commun (Camb)*, 1218-1220.

128. Love, J. C., Ronan, J. L., Grotenbreg, G. M., van der Veen, A. G., and Ploegh, H. L. (2006) A microengraving method for rapid selection of single cells producing antigen-specific antibodies, *Nat Biotechnol 24*, 703-707.

129. Selvaraju, S., and Rassi, Z. E. (2012) Liquid-phase-based separation systems for depletion, prefractionation and enrichment of proteins in biological fluids and matrices for in-depth proteomics analysis--an update covering the period 2008-2011, *Electrophoresis 33*, 74-88.

130. Song, H., Wang, H., Ju, S., Jin, Q., Jia, C., and Cong, H. (2014) Simplified microchip electrophoresis for rapid separation of urine proteins, *J Clin Lab Anal 28*, 104-109.

131. Colyer, C. L., Mangru, S. D., and Harrison, D. J. (1997) Microchip-based capillary electrophoresis of human serum proteins, *J Chromatogr A 781*, 271-276.

132. Chan, O. T., and Herold, D. A. (2006) Chip electrophoresis as a method for quantifying total microalbuminuria, *Clin Chem 52*, 2141-2146.

133. Zhuang, G., Jin, Q., Liu, J., Cong, H., Liu, K., Zhao, J., Yang, M., and Wang, H. (2006) A low temperature bonding of quartz microfluidic chip for serum lipoproteins analysis, *Biomed Microdevices 8*, 255-261.

134. Phillips, T. M. (2004) Rapid analysis of inflammatory cytokines in cerebrospinal fluid using chip-based immunoaffinity electrophoresis, *Electrophoresis 25*, 1652-1659.

135. Ohashi, R., Otero, J. M., Chwistek, A., and Hamel, J. F. (2002) Determination of monoclonal antibody production in cell culture using novel microfluidic and traditional assays, *Electrophoresis 23*, 3623-3629.

136. Uthayakumaran, S., Listiohadi, Y., Baratta, M., Batey, I. L., and Wrigley, C. W. (2006) Rapid identification and quantitation of high-molecular-weight glutenin subunits, *Journal of Cereal Science 44*, 34-39.

137. Rhazi, L., Bodard, A. L., Fathollahi, B., and Aussenac, T. (2009) High throughput microchip-based separation and quantitation of high-molecular-weight glutenin subunits, *Journal of Cereal Science 49*, 272-277.

138. Monti, G., De Napoli, L., Mainolfi, P., Barone, R., Guida, M., Marino, G., and Amoresano, A. (2005) Monitoring food quality by microfluidic electrophoresis, gas chromatography, and mass spectrometry techniques: effects of aquaculture on the sea bass (Dicentrarchus labrax), *Anal Chem 77*, 2587-2594.

139. Li, S. F., and Kricka, L. J. (2006) Clinical analysis by microchip capillary electrophoresis, *Clin Chem 52*, 37-45.

140. Meighan, M. M., Staton, S. J., and Hayes, M. A. (2009) Bioanalytical separations using electric field gradient techniques, *Electrophoresis 30*, 852-865.

141. Han, J., and Craighead, H. G. (2000) Separation of long DNA molecules in a microfabricated entropic trap array, *Science 288*, 1026-1029.

142. Fu, J., Schoch, R. B., Stevens, A. L., Tannenbaum, S. R., and Han, J. (2007) A patterned anisotropic nanofluidic sieving structure for continuous-flow separation of DNA and proteins, *Nat Nano 2*, 121-128.

Chapter Two

Development of a Microchip Capillary Electrophoresis Platform with Laser Induced Fluorescence Detection

2.1. Introduction

Microfluidic-based analytical platforms are used to separate different biomolecules including proteins and DNA (*1*). MCE-based protein separation methods are generally adopted from the conditions that were optimized using conventional CE. Different separation and detection methods have been utilized to improve the performance of MCE-based protein separations (*2-8*). Despite the novel techniques described in the literature, the development of prototype protein separation microfluidic devices is still challenging due to the unique characteristics of proteins (*4, 6*). As a result, the development of a microfluidic platform varies depending on the individual research objective and mode of analysis.

The goal of this chapter is to explain the development of a microfluidic electrophoresis platform for protein separation. The developed separation platform is capable of being integrated with sample pre-concentration techniques, and can potentially be adopted for single cell analysis (*9-10*). The platform consists of four main modules, a separation module, an optical module, a detection module, and a control module. The separation module consists of a microfluidic device, fluorescently-labeled analytes, electrodes, HV power supply and a BGE. The microscope, an objective lens, other optics, and a fluorophore that is compatible with the laser, are components of the optical module. The detection module contains a laser source, an avalanche photodiode (APD) and optics. The control module comprises a USB-interfaced data acquisition (DAQ) card, a PC, and LabVIEW-based software, and it regulates the other three modules including data acquisition and recording. The assembly and formulation of different

modules in this functional microfluidic separation platform with laser induced fluorescent detection and derivatization of Cys-mutated CaM will be discussed in detail in the following sections.

2.2. Materials and methods

All reagents and samples were prepared with doubly-deionized water from an ultrapure water system (Barnstead, Dubuque, IA). *E. coli* cultures of single mutated CaM (Thr-34 was replaced with a Cys in T34C-CaM and Thr-44 was replaced with a Cys, T44C-CaM) were available in the laboratory of Dr. Carey Johnson (University of Kansas, Lawrence, KS). The protein was expressed in *E. coli,* and purified using a phenyl sepharose column according to a previously published method (*11-13*). The T34C-CaM was conjugated with Alexa Fluor 647 or 488 (AF647 C_2-maleimide or AF488 C_5-maleimide) maleimide (Molecular Probes, Eugene, OR). SU8 10 negative photo resist and silicon wafers were purchased from Micro-chem (Newton, MA) and Silicon (Boise, ID), respectively. PDMS (polydimethylsiloxane) and a curing agent were purchased from Ellsworth Adhesive (Minneapolis, MN), and Si-nano beads were purchased from Bangs Laboratories (Fishers, IN). All the other reagents were purchased from Sigma-Aldrich (St. Louis, MO).

2.2.1. Expression and purification of T34C-CaM

A sample of *E. coli* expressing mutant calmodulin (T34C-CaM) was available in the laboratory Dr. Carey Johnson (University of Kansas, KS). T34C-CaM was expressed in *E. coli*. and purified according to a previously published method (*13*). Briefly, 50 mL of the initial culture was used to inoculate 1 L of Luria-Bertani (LB) medium, which was incubated at 37°C

with shaking until the optical density reached 0.6 at 600 nm. Next, 120 mg of isopropyl β-D-1-thiogalactopyranoside (IPTG) was added to induce the bacteria cell growth. The bacterial culture was grown at 37°C for 3-4 hrs, and harvested by centrifugation at 6000 g for 10 min. The pellet was resuspended in Tris buffer and the cells were lysed by adding lysozyme and incubated at 37°C, followed by sonication. The cell sap was separated from the cell debris by centrifugation at 4000 rpm at 4°C. Calcium chloride was added to the supernatant to a final concentration of 5 mM, and then, the supernatant was purified on an Akta FPLC with a 25 mL bed of phenyl sepharose 6 Fast Flow (high-sub) in an XK 16/20 column (GE Health Care). Fractions were collected from the FPLC and concentrated using 10,000 molecular weight cut-off (MWCO) filters to approximately 1.5 mL for FPLC gel filtration using a Superdex size exclusion column (GE Healthcare). Collected fractions were dialyzed with high Ca^{2+} HEPES buffer, and the protein samples were aliquoted to 2.1 mg/mL stocks and stored at -80ºC. A detailed description of purification of CaM mutants with FPLC can be found in DeVore et al. (*13*) .

Gene encoding of wild-type chicken CaM was described previously (*11*). The mutants were separately purified by affinity chromatography on a phenyl sepharose column (*11*). The phenyl resin binds CaM with high affinity under a high Ca^{2+} environment. To remove non-specific binding of other proteins, the resin was washed with high ionic strength buffer (50 mM Tris.HCl, 0.5 M NaCl, pH 7.4). The CaM mutant was eluted from the sepharose column by a buffer (10 mM HEPES, pH 7.4) containing EDTA. High Ca^{2+} affinity EDTA sequestered Ca^{2+} from the buffer and triggered the Ca^{2+} release from the CaM mutant, and at the same time this action disrupted the binding of the CaM-mutant with the resin. This purification procedure of the CaM mutant indicates that the Cys mutation still retains CaM affinity to the target (resin) and

Ca^{2+}. The Cys mutation did not alter the CaM-stimulated activity of plasma membrane Ca^{2+}-APTase (*11*).

2.2.2. Labeling of T34C-CaM and purification of fluorescently labeled T34C-CaM

The Cys residue in T34C-CaM was labeled with AF647 through maleimide reaction chemistry as previously described in a single labeling protocol (*12*). The protein (2.1 mg/mL or 125 nmoles in 1 mL) was added to 500 nmoles (100 µL of 5 mM solution) of tris(2-carboxyethyl)phosphine (TCEP), followed by addition of 2 mmoles (1 mL of 2 M NaCl) of NaCl in the 10 mM HEPES buffer containing 2 mM Ca^{2+}. A solution of AF647 was prepared by dissolving 1 mg in 1 mL of DMSO. It was added to the protein mixture while stirring, followed by one hour incubation in the dark. Unreacted AF647 in the solution was removed from the AF647-labeled protein by size exclusion chromatography (G-25 Sephadex column, GE Healthcare Life Sciences, Pittsburgh, PA). The collected protein fractions were dialyzed to ensure complete AF647 removal, and the labeled T34C-CaM was concentrated using 10 kDa MWCO centrifugal filters (Millipore, Ireland). Purified T34C-CaM, which was labeled with AF647, was analyzed by ESI-LC-MS.

The maleimide group reacts selectively with the sulfhydryl group by nucleophilic addition at the physiological pH (*11, 14-15*). A probe with a maleimide functional group, attached with a linker, was reacted with thiol moiety of the Cys residue in the mutant protein under physiological pH under reduced conditions. The single thiol group in mutated CaM gives one reaction site for the specific maleimide reaction and also avoids the multiple labeling of the protein with dye.

The mutants T34C-CaM and T44C-CaM were labeled with AF647 C_2-maleimide separately. Disulfide bonds of protein dimers were reduced by TCEP and an excess of AF647 was used to maximize the labeling efficiency. NaCl was used to increase the ionic strength and change the conformation of the protein to facilitate the dye-protein conjugation reaction. Also, the high ionic strength would minimize the non-specific adsorption of dye on to the proteins. To enhance the reaction efficiency, AF647 was dissolved in DMSO prior to mixing with the proteins.

2.2.3. Automation and remote controlling of instruments and data collection

The schematic of the electrophoresis platform used in this study is depicted in Figure 2.1. The platform was first tested using AF647 (λ_{ex}= 651 nm, λ_{em} = 670 nm). A 633 nm He-Ne laser was used as an excitation source. A high voltage was applied between the reservoirs of the microfluidic device using four independently controlled high voltage power supply (HVPS) channels (UltraVolt, Ronkonkoma, NY). The reservoirs were connected to the HVPS channels using Pt leads. The LabVIEW program (written by Ryan Grigsby, Adams Micro-Fabrication facility, University of Kansas) was used for controlling the HVPS and data collection. The LabVIEW program was interfaced with a digital and analog data acquisition (DAQ) card, NI-USB 6229 (National Instrument, Austin, TX), and it facilitated the control of the high voltage (HV) relay box (designed and built by the Instrumentation Design Laboratory, Department of Chemistry, University of Kansas, KS), APD and HVPS.

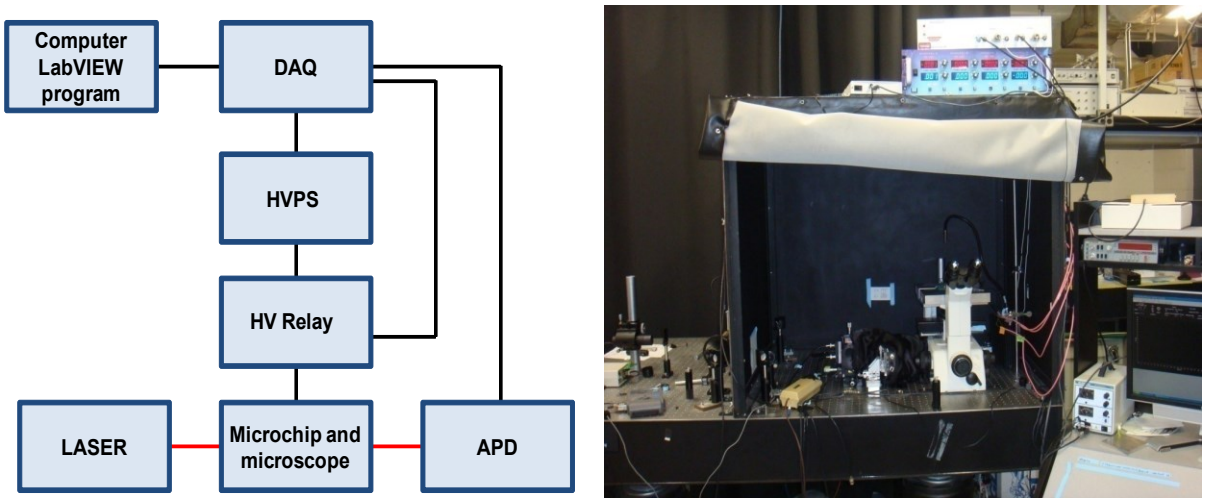

Figure 2.1. Semi-automated microfluidic electrophoresis separation platform with laser induced fluorescent detection.

The LabVIEW program was designed to import user-defined parameters for separation and detection, such as applied voltages and their durations, injection time, separation time, and priming microfluidic channels including collecting and monitoring photon counts during the course of separations. In this microfluidic platform, sample injection and separation were controlled by an automated electrokinetic injection mechanism. Gated injection and pinch injection with "pull back" were used to manipulate the sample plug introduction into the separation channel. The HV-relay box was used to perform switching and floating of HV leads during the pinch injection.

As depicted in Figure 2.1, the microfluidic separation platform is semi-automated. The laser and optic adjustments, fluid handling, and translational stage were manually controlled while all other operations were computer controlled. During the microchip electrophoresis separation, the HVPS, HV relay and photon counting module were controlled by the LabVIEW program, and it was interfaced with the devices by the DAQ card connected to the computer. The

HV relay was used during the pinch injection only, and to avoid arcing during voltage switching while providing smooth transitions of voltages into the HV leads (Figure 2.5).

2.2.4. Laser induced fluorescence detection

Figure 2.2 shows the optical setup with a microfluidic device integrated with a conventional LIF detection. The chip was mounted on X-Y translational stage (Newport, Irvine, CA). A Nikon TE 300 microscope was used in this LIF detection. A 633 nm He-Ne laser was used as an excitation source, and the laser beam was focused inside the microscope by an open-beam optical setup.

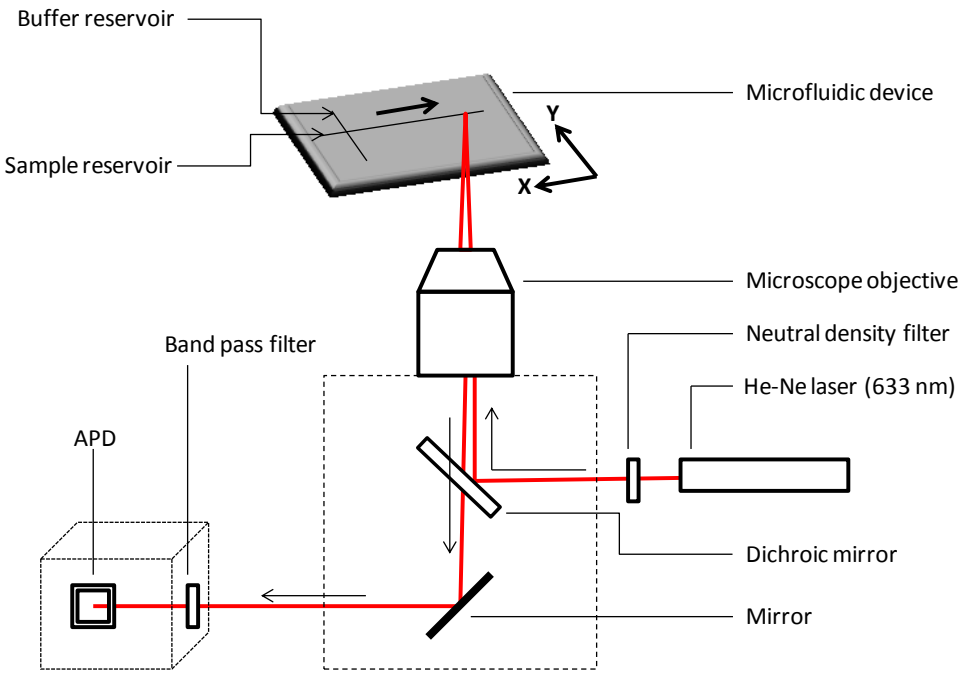

Figure 2.2. Epifluorescence setup for AF647 detection on a microfluidic device

Initially, the laser beam was passed through the neutral density filter (Newport, Irvine, CA), and the power of the beam that goes into the microscope was controlled by adjusting the

filter. The power of the laser beam coming through the neutral density filter was measured by an optical power meter (Pro-lite Technology, Bedfordshire, UK). Then the laser beam was reflected by the dichroic mirror (Chroma, Bellows Falls, VT), which was in line with the microscope objective; 40X, 0.4 NA, 2.5 mm working distance (Olympus), and focused inside the microchannel. During the microfluidic separation, the fluorescence emission that passed through the dichroic mirror was collected from the same objective. Then the emission was reflected out from the microscope by a mirror and captured by the APD that was a part of the photon counting module (PerkinElmer, Fremont, CA). The counting module was placed in line with the C-port of the microscope and a band-pass filter (Chroma, Bellows Falls, VT) was mounted on the module before the APD as shown in the Figure 2.2.

2.2.5. Fabrication of microfluidic devices

2.2.5.1. Fabrication of PDMS/glass microfluidic chips

PDMS-based microchips were fabricated using standard soft lithography at the Adams Micro-Fabrication facility (University of Kansas, KS) as described previously (*16*). To develop a raised structure (mold) for electrophoresis channels, an SU-8 negative photoresist was spin-coated on a 4-inch silicon wafer up to the thickness of ~16 μm using a spin coater (Brewer Science, Rolla, MO). The wafer was soft baked using a programmable hot plate (Thermo Scientific, Ashville, NC) at 65°C for 2 minutes, followed by 95°C for 5 minutes. AutoCad LT 2004 (Autodesk, San Rafael, CA) was used to create microfluidic channel designs, and those designs were printed onto a transparency film at a resolution of 50,000 dpi (Infinite Graphics, Minneapolis, MN). The transparency film was aligned on top of the photoresist coated wafer and

exposed to UV light using a UV source (ABM, San Jose, CA). After the exposure, the wafer was baked at 65°C for 2 minutes, followed by 95°C for 10 minutes. SU-8 developer was used to develop the channel structures, and the wafer was washed with isopropyl alcohol and dried with nitrogen gas. Finally, the developed wafer was "hard baked" at 175°C for 2 hours. The depth of the PDMS microfluidic channels, which represent the thickness of the raised photoresist structure, was measured with a surface profiler (Alfa Step-200, Tencor Instruments, Mountain View, CA). PDMS microfluidic channels were casted using a 10:1 mixture of the elastomer and the curing agent, respectively. The approximate width and the depth of the channels are ~40 and ~16 μm. In this study, two different types (simple "T" and 10-cm serpentine) of PDMS/glass chips were used. PDMS/PMMA hybrid chips were also fabricated. As describe above PDMS replica was fabricated and to form bottom layer of the device instead of piece of glass a piece of PMMA was used.

2.2.5.2. Fabrication of glass microchips

Glass microchips with different channel structures were fabricated by The Adams Micro-Fabrication facility (University of Kansas, KS), using the glass chip fabrication procedure described in Scott et al. and Allen et al. (*17-18*).

2.2.5.3. Si-nanoparticle microfluidic device fabrication and assemble

Si-nanoparticle chips were kindly provided by Dr. Yong Zeng (University of Kansas, KS). Briefly, a chip with simple "T" wafer (10 mm separation channel and 4 mm long side arms)

was made. An approximately 5-mm thick PDMS layer was cured at 60°C overnight and reservoirs were made using a 2-mm biopsy puncher. The separation devices were assembled by sealing the replicas to clean glass slides with oxygen plasma oxidation (*19*). The process of the colloidal self-assembly was carried out as previously described (*19*). Monodisperse plain silica beads were 160, 170, and 400 nm in diameters (10% w/v, <10% deviation) were obtained.

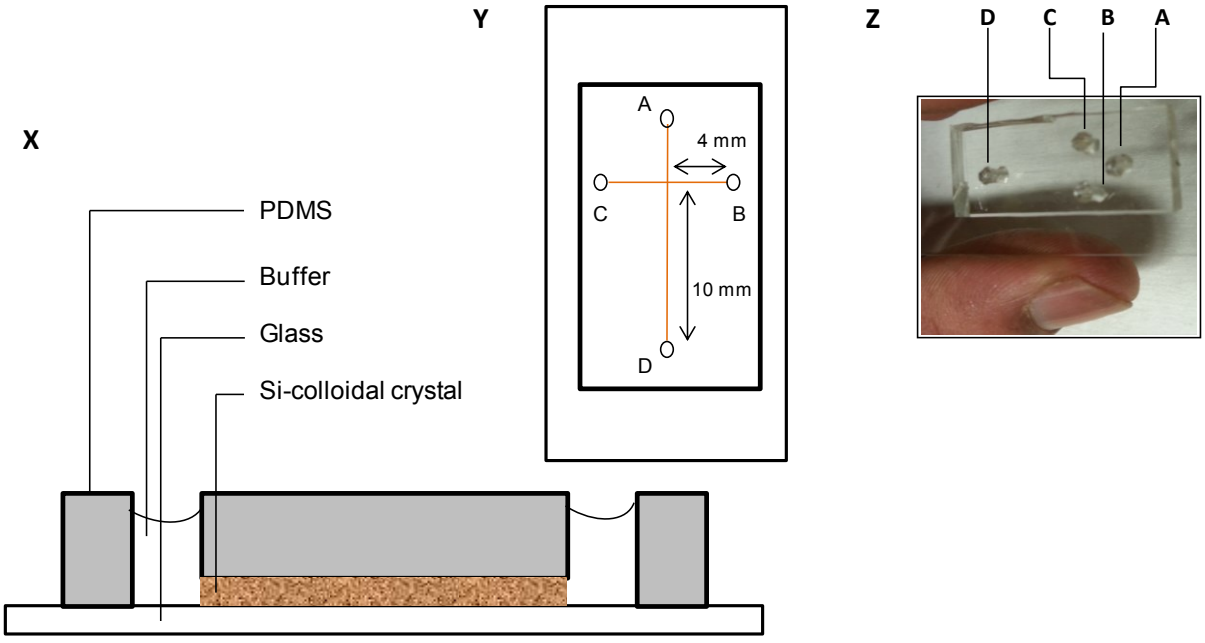

Figure 2.3. Layout of self assembled Si-nanoparticle microfluidic device. (X) Schematic of self assembled colloidal array inside of a PDMS/glass microfluidic device. (Y) Schematic of 10 mm PDMS/glass microfluidic device that was used to assemble colloidal array. The layout of reservoirs of the chip: A-buffer, B-sample, C-sample waste, D-buffer waste. (Z) An actual PDMS/glass colloidal array microfluidic device.

As graphically depicted in Figure 2.3, a sonicated ~20 μL of Si-nanoparticle colloidal suspension was added into reservoirs of A, B, and C in PDMS/glass simple "T" chip. The aqueous suspension filled the channels by capillary action and formed a water meniscus at outlets in the reservoirs. When all the channels were filled with water, reservoir D was left open

whereas reservoirs A, B, and C were covered with pieces of PDMS to block evaporation and to induce colloidal growth inside the channels. Once the growth of the colloidal array was completed, unwanted growth was stopped by replacing the colloidal suspension in the reservoirs with water. The water in the reservoirs was replaced with the run buffer before the electrophoresis and the microfluidic device was equilibrated for ~30 min.

Si-nanoparticle chips were operated under conditions that suppress EOF and the separation is based on sieving. Simple "T" PDMS/glass microchips were used to form the device, and relatively small channel structures (10 mm) were used. The net flow (EOF) was suppressed by a high ionic strength 4X TBE (356 mM Tris-borate, 8 mM EDTA, pH 8.3) buffer and physically hindered by the colloidal array (*19-20*). Furthermore, the relatively small channel structure reduces the length of colloidal array, which eases assembly and minimizes drying. Comparatively wide channels (~100 um and 20 um in depth) were cast using a mold with a thick PDMS layer (~5 mm), resulting in relatively deep reservoirs. This accommodates adequate volumes (~20 μL) in reservoirs, and hence decreases the drying effect of the colloidal array. The buffer and sample injection channels were ~5-mm long, and the separation channel was 10-mm long. Additionally, the diameters of reservoirs were kept 4 mm for conventional PDMS/glass chips, and 1.5 mm for Si-nanoparticle chips, respectively. Si-nanoparticle chip-based electrophoresis used relatively low electric fields (40 V/cm) to decrease the Joules heating.

Assembly and growth of the colloidal array were induced by controlled evaporation of water from the buffer waste reservoir (Figure 2.3Y) (*19*). The growth of the array can be stopped by replacing the colloidal suspension in the reservoirs with water. The colloidal arrays were assembled inside the microchannels arranged as a three dimensional structure with different order (*21-22*), but the order of structure does not affect the sieving-based separation of

biomolecules (*22*). This self-assembly method reduces the assembly time in comparison with conventional methods, which use gravity and vertical depositions (*23-24*), and avoids the formation of cracks caused by drying. It is also reported that different sizes of nanoparticles create different pore sizes that can be used to separate a wide array of biomolecules with size base separation. In this project, two different colloidal arrays (particle size 170 and 400 nm) were used to separate SDS-protein complexes.

2.2.6. Electrokinetic injection methods

Based on separation modes and types of chip, two electrokinetic injection methods were employed. They were gated injection and pinched injection with "pull back" voltages (Figures 2.4 and 2.5). In both injection methods, a sample plug was introduced to the separation channel of the device by manipulating the applied voltages in the reservoirs of the device. Example voltage programs are depicted in Figure 2.4 and 2.5. Visual detection of the initial injection process was performed using fluorescein injections and a UV lamp. Optimum applied voltages for leak-free injections were also obtained with the fluorescein injections. Further, multiple injections of CaMAF647 were used to test a consistent injection volume with different injection times after selecting the optimum voltages using fluorescein. During the test, the laser was focused 3-4 mm away from the cross-junction of separation and sample channels.

2.2.6.1. Gated injection

In the separation state, high voltages were applied to the reservoir B and A, and the sample and the run buffer fluid flow established a gated cross section at the intersection, where the vertical and horizontal channels meet (Figure 2.4). With a desired injection time (for example 0.3 s), the potential of the A reservoir was switched to zero, and with the cathodic-EOF the sample flowed through the cross junction. Once the potential of the lead A was reestablished, a plug of sample was introduced into the separation channel, and the fluid gate was re-established. Manipulation of voltages in the reservoirs was performed by a LabVIEW program. With EOF, the sample plug migrated towards reservoir D. This injection method was employed in both PDMS/glass and glass microfluidic separations with EOF and with the conditions that reduce EOF.

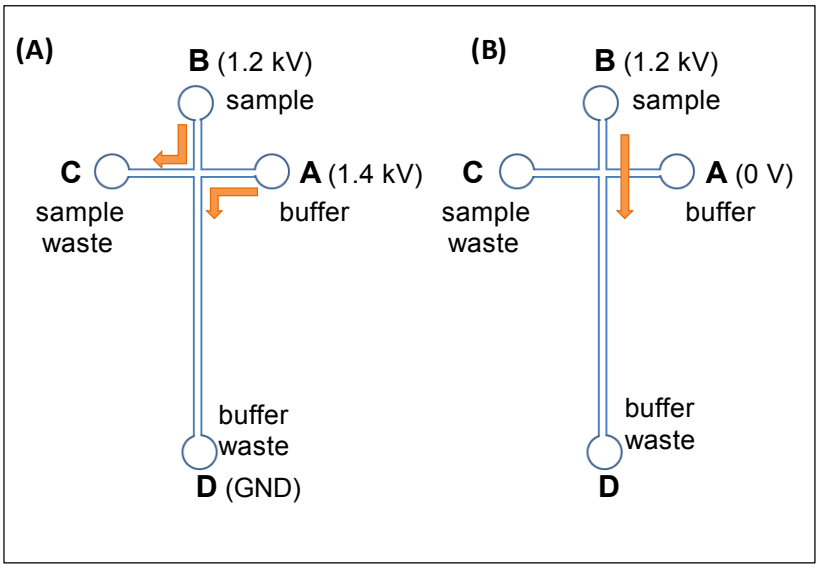

Figure 2.4. Schematic of sample flow and run buffer flow in elctrokinetic gated injection (*25*). A-D labels represent microfluidic reservoirs and arrows indicate the flow direction during the separation state and injection state of the device. (A) shows the separation or idle state of the microchip operation. (B) illustrates the sample injection mode during the device operation.

2.2.6.2. Pinched injection with pull back mechanism

A sample containing mostly negatively charged species (properties of the proteins are discussed in Chapter three) was injected under conditions that suppress EOF, and the sample moved from B to A reservoir (Figure 2.5) while the voltages in reservoirs C and D were floated. In the second step, voltages of reservoirs A and B were reduced to a certain level, and a relatively high positive voltage was applied to reservoir D, and reservoir C was simultaneously grounded (example voltages were shown in Figure 2.5). The sample migration and injection were based on the electrophoretic mobility of the ions, and the direction of separation was as same as the direction of the bulk flow.

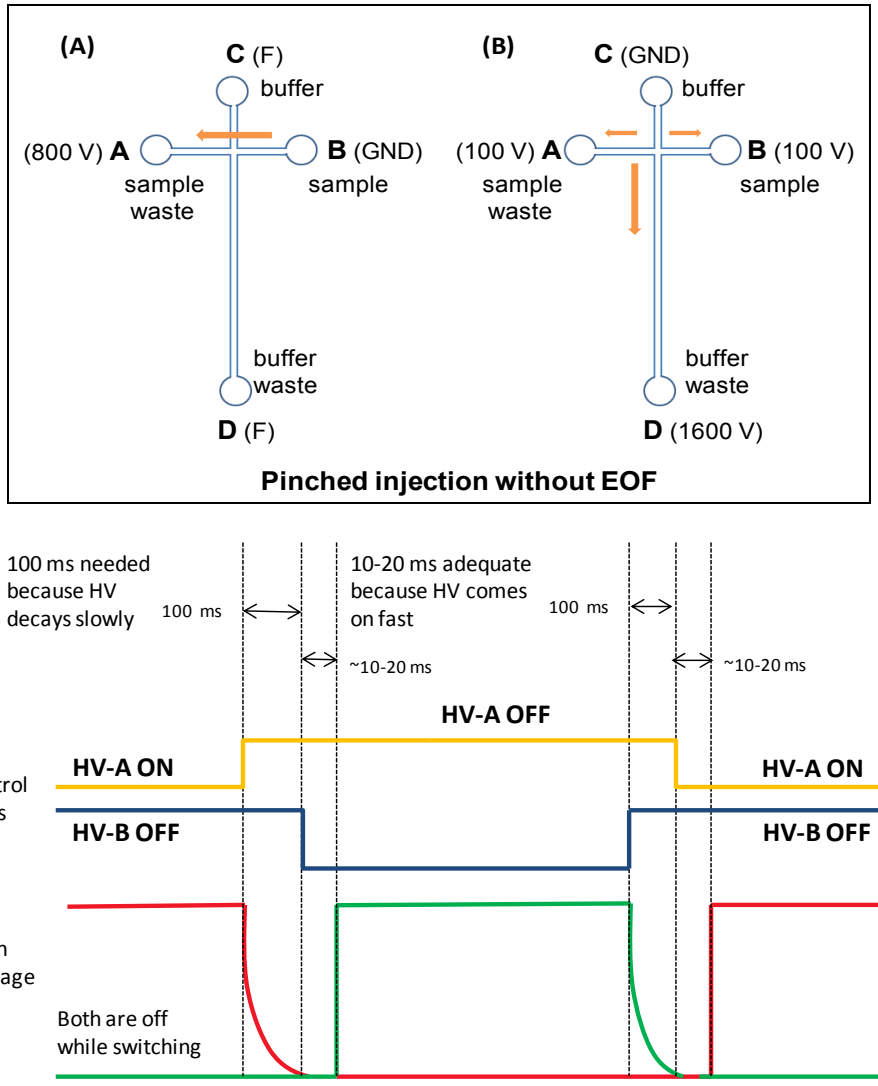

Figure 2.5. Schematic of sample flow and run buffer flow (top) and a timing chart of a HV voltage switching (bottom) in electrokinetic pinched injection (*26-27*). Top: A-D labels represent microfluidic reservoirs and arrows indicate the flow direction during the separation state injection state of the device. (A) depicts the idle state of the electrokinetic fluid manipulation and (B) shows both injection and separation states of the manipulation. Bottom: A timing chart of a HV switching in pinch injection. Blue and yellow lines show HV relay outputs. Red and green lines show HVPS outputs. During switching, HV decay of 100 ms was allowed, and 10 -20 ms was allowed for the new voltage, and the total time delay was ~120 ms. (The timing chart diagram was kindly provided by Dr. Kenneth Ratzlaff, Instrumentation Design Laboratory, University of Kansas, KS).

2.2.7. Separation modes

Different separation modes were tested under conditions with or without EOF (Chapter three, Scheme 1). With EOF, mainly MCZE and MEKC were tested using different microfluidic devices with different substrates. Conditions that suppress the EOF were used for the method development as well as protein separation. To suppress the EOF, buffer constituents and high ionic strengths were used (Chapter three, Table 3.2, and section 3.3.2.3) (*2, 19, 27*).

2.2.8. Signal intensity and laser power study

A simple 'T' PDMS/glass microchip (3.5-cm long separation channel) was used to separate AF488-labeled T34C-CaM under MCZE separation conditions (Figure 2.7). The separation was carried out with gated injections (0.3 s), and multiple injections were performed with different laser powers (5-100 μW) for the LIF detection, and the laser power was adjusted using neutral density filter and was measured using a laser power meter. The relationship between the laser power and the signal (peak heights of the CaMAF488 peaks) was investigated.

2.3. Results and discussion

2.3.1. Derivatization of CaM mutant

From a group of CaM mutants (which were constructed previously in the laboratory of Dr. Carey Johnson), T34C-CaM and T44C-CaM were selected to facilitate the labeling and minimize the changes in CBP affinity due to changes in the CaM sequence. SDS-PAGE analysis

indicated that the mutant was relatively pure. AF647 was selected for the labeling due to relatively low autofluorescence and scattering associated with red laser excitation.

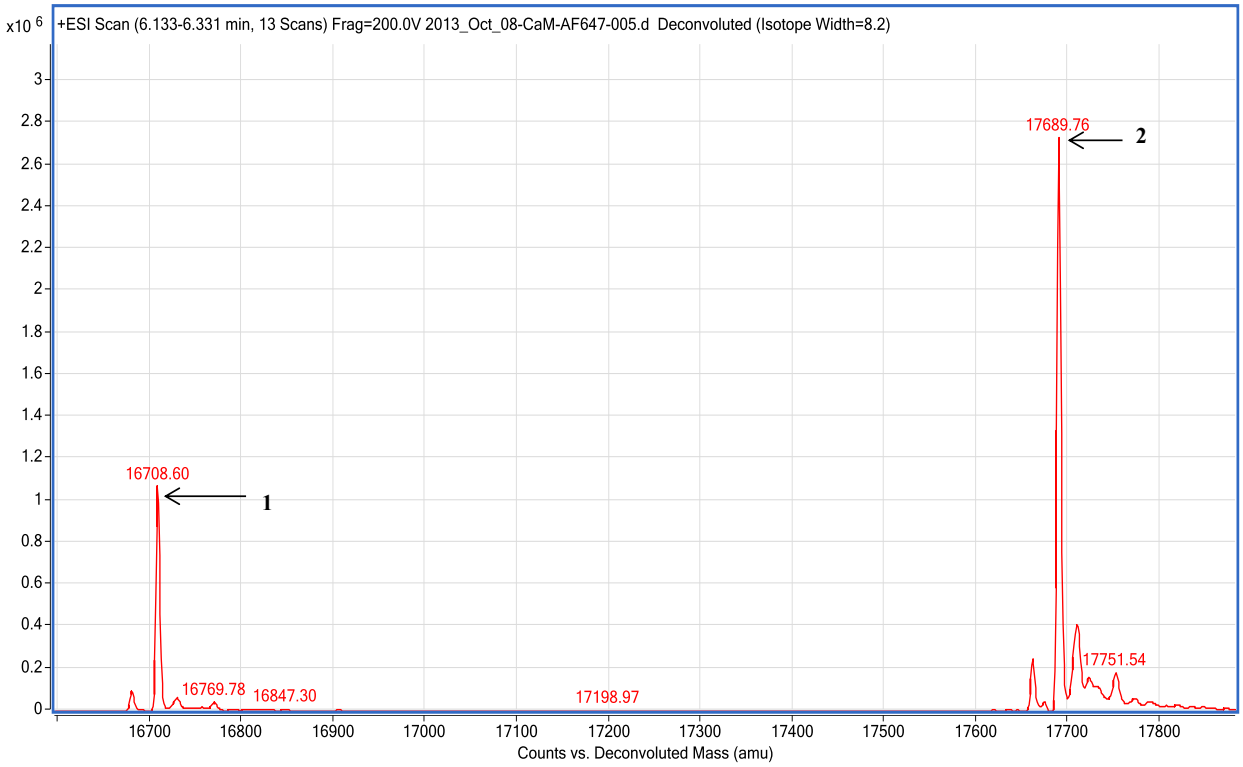

Figure 2.6. Charge deconvoluted ESI-LC mass spectrum of T34C-CaM and T34C-CaM labeled with AF647. In the spectrum, peak 1 is T34C-CaM (16708.60 Da) and the peak 2 is AF647 labeled T34C-CaM. The mass corresponding to peak 2 is 17689.76 Da and the molar mass of the AF647 is ~981 Da.

2.3.2. Fluorescent labeling of T34C-CaM

The purity of mutants was verified by ESI-LC-MS analysis. Figure 2.6 shows the mass spectrum of a sample of T34C-CaM after labeling with AF647. The expected molecular weight of the T34C-CaM mutant was 16708.40 Da. Therefore, peak 1 (16708.60 Da) was assigned as the CaM mutant (Figure 2.6). Within a given error margin (1 Da), the MS result conforms the

purity of the mutant. According to the manufacturer's catalog, the molecular weight of AF647 C_2-maleimide is ~1250 Da; however, the exact chemical structure or chemical formula of AF647 C_2-maleimide was not published. Hence the expected mass of the labeled mutant could not be verified. The major mass peak at (17689.76 Da) was assigned to the labeled mutant (CaMAF467).

2.3.3. Laser induced fluorescence detection

During the separation, analytes in the separation channel move towards the buffer waste reservoir. A red (633 nm) laser beam was focused inside the separation channel as depicted in Figure 2.2. The AF647 labeled proteins were excited and the emission was collected as shown in Figure 2.2. Photons collected by the photon-counting module transformed the signal into counts as a function of time, and using the LabVIEW program an electropherogram was developed during the separation. Against background counts, signal counts coming from the excited fluorophore created a peak and separate peaks indicated different analyte bands. The collected electropherogram data was automatically stored as an Excel file in the pre-selected location of computer, and at the same time the electropherogram was displayed on the lab view software window.

Both CaMAF488 and CaMAF647 samples were tested with the developed platform and a 488 nm blue laser or 633 nm red laser, respectively. Based on the fluorophore and the laser, the dichroic mirror and filters were changed in the system. To investigate signal sensitivity and saturation limit of the LIF detection method, an experiment was carried out with a PDMS/glass chip to test the signal against laser power levels (Figure 2.7). The blue laser (488 nm) excitation

creates relatively high autofluorescence and scattering. CaMAF488 (~160 nM) was used in this experiment. In PDMS/glass devices with gated electrokinetic injection, the sample plug of the analytes was injected into the separation channel and electropherogram data was collected as previously explained. With the same injection volumes (~30 pL), six (n=6) injections were performed per selected laser power as shown the Figure 2.8. The peak height of CaMAF488 was proportional to the fluorescence signal (photon counts) of AF488. Over the selected laser power range, a fit to the signal shows a linear relationship. The results indicate that for the selected laser power range the signal was not saturated. Within the selected laser power range, the experiments were conducted without saturating the APD.

The developed platform was sensitive and utilizes a cost effective detection method with the possibility of upgrading to confocal detection (*28*). With confocal detection, the LOD will be decreased to single molecular level (*29*). This detection system can be upgraded by placing a special pinhole at the confocal plane of the tube-lense to eliminate out-of-focus fluorescence signals (*28*). Single molecule level detection was obtained by Zare et al. using a red laser and AF647-labeled proteins (*30*). They used a nontraditional optical method using a cylindrical objective with confocal detection (curtain detection). The laser beam was expanded throughout the cross section of the separation channel by the cylindrical objective, and it collected fluorescence signal from the whole area. In this experiment point detection (where the laser was focused inside the separation channel) was used instead of curtain detection to test the saturation of the signal during MCE. Also, the optical setup required for the curtain detection was relatively complex and expensive. A relatively small focal area inside the separation channel produced an adequate signal in the LIF detection. Hence, the idea of confocal and/or curtain detection was eliminated.

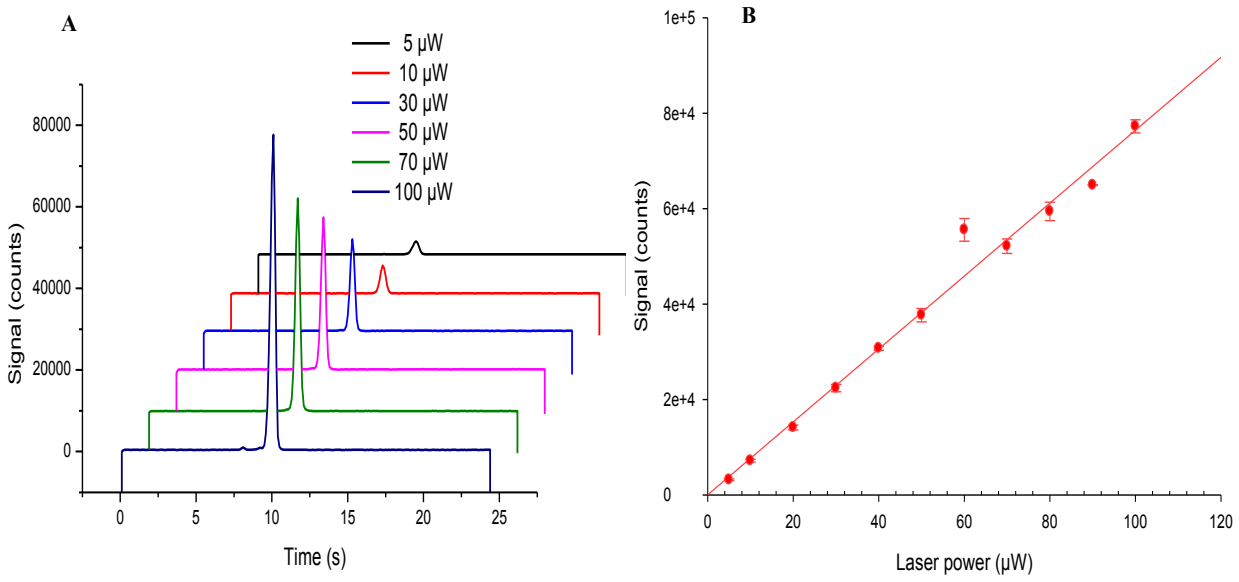

Figure 2. 7. Analysis of laser power and fluorescence signal intensity. (A) Separation of 160 nM T34C-CaM labeled with AF488 and different laser powers. The range of laser power was 5-100 µW and for each designated laser power six separations were performed (n=6). In the separation gated injection with 3.5 cm PDMS/glass microchip used. BGE was 25 mM boric acid, pH 9.2, 3.5 mM SDS and detection length, ~1.5 cm. For each separation a constant injection time of 0.3 s was used with an injection voltage of 1.2 kV. A constant separation voltage was used, 1.4 kV (~400 V/cm). (B) Relationship between laser power and signal intensity.

Since 488-nm-laser excitation did not saturate the signal, it was approximately assumed that 633 nm laser excitation (with relatively less autofluorescence and scattering) may not saturate the signal for similar excitation powers. With 633 nm laser excitation 5 nM CaMAF647 was detected with signal-to-noise ~6. As shown in Figure 2.8, the LIF module has the ability to detect less than 5 nM very easily (n=5). Gated injection with a 3.5-cm PDMS/glass chip was used. The BGE was 100 mM boric acid, pH 9.2, and 3.5 mM SDS. The separation field strength was 400 V/cm and the injection time was 0.3 s. The laser excitation power was 20 µW. The LOD obtained for the developed method was adequate for the detection of the CBPs in relatively large concentrations.

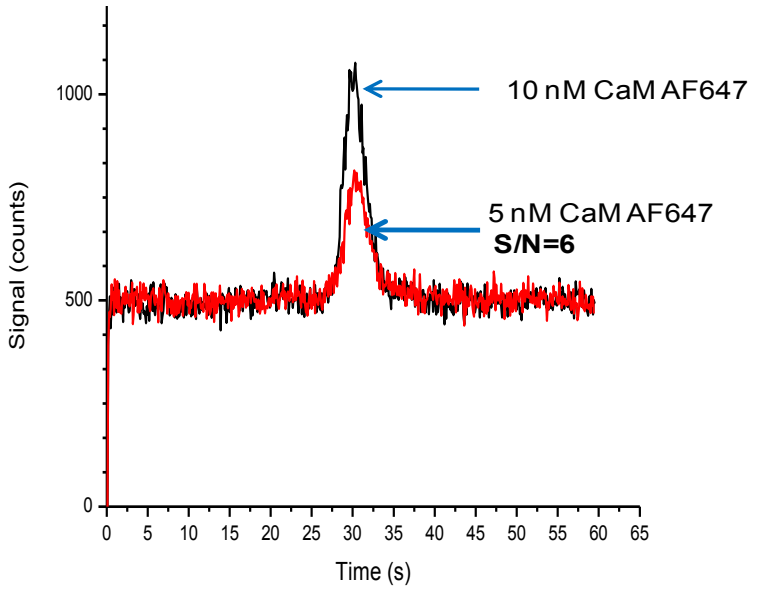

Figure 2. 8. Investigation of limit of detection of CaMAF647 in MCE separation. In the separation gated injection with a 3.5-cm PDMS/glass chip was used. LOD was 5 nM with signal-to-noise ratio (S/N), 6. The separation conditions are, BGE was 100 mM boric acid, 3.5 mM SDS, pH 9.2, and detection length ~3 cm. The injection time was 0.3 s, and injection voltage and separation voltage were 1.2 kV and 1.4 kV (~ 400 V/cm), respectively. The laser excitation power was 20 μW.

2.3.4. Fabrication and assembly of PDMS/glass microfluidic devices

Polymeric microfluidic devices are less expensive than quartz, silicon and glass-based devices, and they involve a simple and relatively inexpensive fabrication procedure (*16, 31*). Different polymer-based chips have been reported including polyurethane, polycarbonate, polymethyl methacrylate (PMMA), polystyrene, polyethylenetetraphthalate glycol (PETG), polyvinylchloride, polyethylene, and poly(dimethylsiloxane) (PDMS) (*32*). In comparison to other materials, PDMS microfluidic devices are easy to fabricate and inexpensive. They are fabricated by casting the polymer against a pre-casted mold before crosslinking with a curing agent (*16*).

Both simple “T” PDMS/glass chips and serpentine chips were used in the initial method development and to separate proteins. During the electrophoresis to avoid Joule heating, buffer depletion due to electrolysis, and to minimize the evaporation of buffer and samples reservoirs, after few runs the sample and the buffer in the other reservoirs were replaced with new reagents (*16*). The assembled chips were used as soon as possible because old chips show uneven injections and run-to-run migration time differences. This may be due to uneven channel surfaces caused by drying and changes in surface chemistry (*33-35*). A polymer to curing agent ratio of 10:1 was used in casting PDMS chips, and the proper degassing of the mixture was essential to avoid air bubbles trapping inside the cured polymer. Air bubbles in the PDMS create problems, such as leaking, unstable current and uneven channel surfaces.

It is has been reported that the wet etching and glass bonding procedures were challenging (*18*). In this study, some of the glass chips had defects in channel surfaces. The wet etching procedure had to be optimized to get relatively uniform channel structures in the glass substrate (*16*). Degradation of the acid formulation and poor quality of the glass substrate created uneven etching and serrated channel edges. These defective channel structures gave irreproducible migration times and injection volumes. Further, they were more susceptible to clogging.

Glass chips are more expensive and difficult to fabricate in bulk quantities in comparison to hybrid PDMS/glass chips (*16*). Also, the maintenance of the chip can be time consuming for repetitive use. Once clogged, they are difficult to unclog. In addition, proteins tend to stick to the glass surface during a separation, and thus the viability of chips was reduced over the time. Relatively large diameter reservoirs (4-5 mm) in a chip are needed to minimize the effects of evaporation and Joule heating. Drilling of larger diameter reservoirs is highly susceptible for

glass breakages. To minimize breakages during drilling, the reservoir size was kept small (2-3 mm); however, small volume reservoirs were subject to high Joule heating and clogging with air bubbles, and buffer depletion. To solve these problems, pipette-tip necks were glued onto the top of the chips covering the reservoirs to increase the volume of the reservoirs.

Permanent coating of the channel wall with modifiers generates neutrally charged walls (*2, 27*), and physically obstructing polymers (*27, 36*) or other sieving materials, such as a colloidal array (*19*), can be used to suppress the EOF. The developed microfluidic electrophoresis platform is compatible with different separation modes with the laser induced fluorescent detection. The separation of proteins using different separation modes and devices will be discussed in detail in the following chapters. Also, a summary of different chips and separation methods used in this study is included in Chapter three Scheme 3.1 and Table 3.2.

2.3.5. Electrokinetic injection modes

Standard analysis by microfluidic electrophoresis involves injection, separation and detection steps. The sample flow and the injection of the sample plug into the separation channel can be regulated by employing a pressure driven method or by an electrokinetic method (*16*). Electrokinetic injection is by far the most convenient and commonly used injection method since it does not require an additional pumping mechanism to move the sample fluid (*16*). Improved electrokinetic injection methods such as pinched injection with “pull back” voltages generated a defined sample plug and leakage-free injections. Well defined sample plugs and leakage-free injections are imperative to obtain a high separation efficiency and reproducibility (*27*).

Different electrokinetic strategies have been reported, and a selection of injection mode depends on the mode of separation and the analyte (*37*). Two common modes of electrokinetic injections have been utilized in microchip electrophoresis, gated injection and pinched injection. Gated injection can be performed only with EOF-driven flow, and pinched injection can be performed with or without EOF driven sample flows (*19, 27, 37*). In gated injection, the fluid gate is established between the sample and buffer solutions. The establishment of a leakage-free fluid boundary is contingent on the ionic strength, pH, and the field strength applied during the injection. For selected buffers, applied voltages should be adjusted with injection time to obtain the optimum leakage-free gating. Fluorescein was used to visualize the fluid flow at the cross junction of the sample channel and the separation channel. No mixing of buffer and the sample solution at the fluidic gate was observed because the interaction time is small, and therefore, diffusion is minimized (*37-38*). To inject a good sample plug into the separation channel, the ionic strength and the pH of the sample solution should be similar to the BGE (*39*). The size of the sample plug is determined by the time between "on" and "off" voltages in the buffer reservoir lead. This injection mode is simple; however, it has sample bias such as cation migration over anion migration due to higher apparent mobility of cations under cathodic-EOF (*40-44*).

Gated injection based on anodic EOF was tested with a 5-cm PDMS/glass chip. Tetradecyltrimethylammonium bromide (TTAB), 2 mM, was used to dynamically coat the channel surfaces with positive charge. Negative potentials were applied to establish reverse EOF (anodic-EOF). It was difficult to establish reproducible gating with reverse EOF and therefore reverse polarity-based separations were discontinued.

Electrophoresis-based separation of proteins with MCZE (with normal polarity) shows relatively low resolution in protein separation (Chapter three, table 1.2). Reproducible gated injections were difficult to obtain under conditions that reduce or suppress EOF. As a result, pinched injection with "pull back" was introduced to obtain injections under conditions that suppress EOF.

The most widely used electrokinetic injection mode is the pinched injection mode (*37*). The pinched injection with "pull back" mechanism is more complicated than gated injection and can be used for different types of analytes, such as small to large bio-molecule separation (*19, 44*). This mode is mainly used under conditions that suppress EOF, such as microchip gel electrophoresis and other sieving-based methods. As depicted in the Figure 2.5, voltage switching introduced a sample plug into the separation channel. The volume of the injected sample is defined by the volume of the channel intersection. Relatively small "pull back" voltages were applied to the sample and sample waste reservoirs to prevent leakage into the separation channel (*19, 27, 44*). The amount of injection depends on the potential applied to each of the HV leads during the injection phase and the separation phase. It has been reported that a significantly lower amount of sample is introduced by pinch injection in comparison to an uncontrolled pinched injection (without "pull back" voltages) (*44*), and thus the pinched injection (with "pull back" voltages) creates lower detection limits as a result of smaller injection volumes and leak free injections (*44*). Similarly, the injection of a narrow sample plug provides higher separation efficiency.

Si-nanoparticle-based separation will be discussed in detail in Chapters three and five. For these separations, pinched injection under relatively low voltages (60-80 V) was used.

Migration times of Si-nanoparticle-based separations were significantly longer than those of other chip-based separations.

2.4. Conclusion

A functional prototype microfluidic separation platform with red laser induced fluorescent detection was developed. It is a semi-automated system with integrated functional modules, including a separation module, an optical module, a detection module and a control module. In the separation module, different microfluidic devices were fabricated and tested, and they were compatible with the optical and control modules. The detection module comprised a red He-Ne laser and AF647-labeled analytes, which were suitable for very sensitive detection with relatively low scattering and auto-fluorescence in the epifluorescence microscope. Expression and purification of CaM mutants and labeling with AF647 were achieved successfully. A detection module, which contained an APD, was utilized to detect a concentration of 5 nM CaMAF647 with high signal-to-noise ratio (S/N=6). This system can be easily converted to detect different analytes by changing the laser and dichroic mirror, and by selecting a compatible fluorophore.

2.5. References

1. Sanders, G. H., and Manz, A. (2000) Chip-based microsystems for genomic and proteomic analysis, *TrAC: Trends Analyt Chem 19*, 364-378.
2. Tran, N. T., Ayed, I., Pallandre, A., and Taverna, M. (2010) Recent innovations in protein separation on microchips by electrophoretic methods: an update, *Electrophoresis*

31, 147-173.

3. Escarpa, A., Gonzalez, M. C., Lopez Gil, M. A., Crevillen, A. G., Hervas, M., and Garcia, M. (2008) Microchips for CE: breakthroughs in real-world food analysis, *Electrophoresis 29*, 4852-4861.
4. Dishinger, J. F., and Kennedy, R. T. (2008) Multiplexed detection and applications for separations on parallel microchips, *Electrophoresis 29*, 3296-3305.
5. Sinville, R., and Soper, S. A. (2007) High resolution DNA separations using microchip electrophoresis, *J Sep Sci 30*, 1714-1728.
6. Wirth, M. J. (2007) Separation media for microchips, *Anal Chem 79*, 800-808.
7. Fu, L. M., Hong, T. F., Wen, C. Y., Tsai, C. H., and Lin, C. H. (2008) Electrokinetic instability effects in microchannels with and without nanofilm coatings, *Electrophoresis 29*, 4871-4879.
8. Song, Y.-A., Chan, M., Celio, C., Tannenbaum, S. R., Wishnok, J. S., and Han, J. (2010) Free-flow zone electrophoresis of peptides and proteins in PDMS microchip for narrow pI range sample prefractionation coupled with mass spectrometry, *Anal Chem 82*, 2317-2325.
9. Price, A. K., and Culbertson, C. T. (2007) Chemical analysis of single mammalian cells with microfluidics. Strategies for culturing, sorting, trapping, and lysing cells and separating their contents on chips, *Anal Chem 79*, 2614-2621.
10. Zare, R. N., and Kim, S. (2010) Microfluidic platforms for single-cell analysis, *Annu Rev Biomed Eng 12*, 187-201.
11. Allen, M. W., Urbauer, R. J., Zaidi, A., Williams, T. D., Urbauer, J. L., and Johnson, C. K. (2004) Fluorescence labeling, purification, and immobilization of a double cysteine mutant calmodulin fusion protein for single-molecule experiments, *Anal Biochem 325*, 273-284.
12. Price, E. S., DeVore, M. S., and Johnson, C. K. (2010) Detecting intramolecular dynamics and multiple Forster resonance energy transfer states by fluorescence correlation spectroscopy, *J Phys Chem B 114*, 5895-5902.
13. Devore, M. S., Gull, S. F., and Johnson, C. K. (2013) Reconstruction of calmodulin single-molecule FRET states, dye-interactions, and CaMKII peptide binding by MultiNest and classic maximum entropy, *Chem Phys 422*.

14. Kuiper, J. M., Pluta, R., Huibers, W. H., Fusetti, F., Geertsma, E. R., and Poolman, B. (2009) A method for site-specific labeling of multiple protein thiols, *Protein Sci 18*, 1033-1041.
15. Spratt, D. E., Taiakina, V., Palmer, M., and Guillemette, J. G. (2007) Differential binding of calmodulin domains to constitutive and inducible nitric oxide synthase enzymes, *Biochemistry 46*, 8288-8300.
16. Henry, C. S. (2006) Microchip capillary electrophoresis: an introduction, *Methods Mol Biol 339*, 1-10.
17. Scott, D. E., Grigsby, R. J., and Lunte, S. M. (2013) Microdialysis sampling coupled to microchip electrophoresis with integrated amperometric detection on an all-glass substrate, *Chemphyschem 14*, 2288-2294.
18. Allen, P. B., and Chiu, D. T. (2008) Calcium-assisted glass-to-glass bonding for fabrication of glass microfluidic devices, *Anal Chem 80*, 7153-7157.
19. Zeng, Y., and Harrison, D. J. (2007) Self-assembled colloidal arrays as three-dimensional nanofluidic sieves for separation of biomolecules on microchips, *Anal Chem 79*, 2289-2295.
20. Yasui, T., Kaji, N., Mohamadi, M. R., Okamoto, Y., Tokeshi, M., Horiike, Y., and Baba, Y. (2011) Electroosmotic flow in microchannels with nanostructures, *ACS Nano 5*, 7775-7780.
21. King, S. B., and Dorfman, K. D. (2013) Role of order during Ogston sieving of DNA in colloidal crystals, *Anal Chem 85*, 7769-7776.
22. Dorfman, K. D., King, S. B., Olson, D. W., Thomas, J. D., and Tree, D. R. (2013) Beyond gel electrophoresis: microfluidic separations, fluorescence burst analysis, and DNA stretching, *Chem Rev 113*, 2584-2667.
23. Meistermann, L., and Tinland, B. (2000) DNA electrophoresis in a monodisperse porous medium, *Phys Rev E Stat Phys Plasmas Fluids Relat Interdiscip Topics 62*, 4014-4017.
24. Tinland, B., Meistermann, L., and Weill, G. (2000) Simultaneous measurements of mobility, dispersion, and orientation of DNA during steady-field gel electrophoresis coupling a fluorescence recovery after photobleaching apparatus with a fluorescence detected linear dichroism setup, *Phys Rev E Stat Phys Plasmas Fluids Relat Interdiscip Topics 61*, 6993-6998.

25. Jacobson, S. C., Ermakov, S. V., and Ramsey, J. M. (1999) Minimizing the number of voltage sources and fluid reservoirs for electrokinetic valving in microfluidic devices, *Anal Chem 71*, 3273-3276.
26. Alarie, J. P., Jacobson, S. C., and Ramsey, J. M. (2001) Electrophoretic injection bias in a microchip valving scheme, *Electrophoresis 22*, 312-317.
27. Shadpour, H., and Soper, S. A. (2006) Two-dimensional electrophoretic separation of proteins using poly(methyl methacrylate) microchips, *Anal Chem 78*, 3519-3527.
28. Jiang, G., Attiya, S., Ocvirk, G., Lee, W. E., and Harrison, D. J. (2000) Red diode laser induced fluorescence detection with a confocal microscope on a microchip for capillary electrophoresis, *Biosens Bioelectron 14*, 861-869.
29. Johnson, M. E., and Landers, J. P. (2004) Fundamentals and practice for ultrasensitive laser-induced fluorescence detection in microanalytical systems, *Electrophoresis 25*, 3513-3527.
30. Huang, B., Wu, H., Bhaya, D., Grossman, A., Granier, S., Kobilka, B. K., and Zare, R. N. (2007) Counting low-copy number proteins in a single cell, *Science 315*, 81-84.
31. Becker, H., and Locascio, L. E. (2002) Polymer microfluidic devices, *Talanta 56*, 267-287.
32. Duffy, D. C., McDonald, J. C., Schueller, O. J., and Whitesides, G. M. (1998) Rapid prototyping of microfluidic systems in Poly(dimethylsiloxane), *Anal Chem 70*, 4974-4984.
33. Heo, Y. S., Chung, S., Cho, K., Chung, C., Han, D.-C., and Chang, J. K. (2003) Effects of peak anomalies with the hydrophilic or hydrophobic properties of reservoirs during serial injection on a capillary electrophoresis microchip, *J Chromatogr A 1013*, 111-122.
34. Zhang, J., Chen, Y., and Brook, M. A. (2013) Facile functionalization of PDMS elastomer surfaces using thiol–ene click chemistry, *Langmuir 29*, 12432-12442.
35. Wong, I., and Ho, C.-M. (2009) Surface molecular property modifications for poly(dimethylsiloxane) (PDMS) based microfluidic devices, *Microfluid Nanofluid 7*, 291-306.
36. Fruetel, J. A., West, J. A., Debusschere, B. J., Hukari, K., Lane, T. W., Najm, H. N., Ortega, J., Renzi, R. F., Shokair, I., and VanderNoot, V. A. (2008) Identification of viruses using microfluidic protein profiling and Bayesian classification, *Anal Chem 80*,

9005-9012.

37. Fu, L. M., Yang, R. J., Lee, G. B., and Liu, H. H. (2002) Electrokinetic injection techniques in microfluidic chips, *Anal Chem 74*, 5084-5091.

38. Ermakov, S. V., Jacobson, S. C., and Ramsey, J. M. (1998) Computer simulations of electrokinetic transport in microfabricated channel structures, *Anal Chem 70*, 4494-4504.

39. Jacobson, S. C., Hergenroder, R., Moore, A. W., Jr., and Ramsey, J. M. (1994) Precolumn reactions with electrophoretic analysis integrated on a microchip, *Anal Chem 66*, 4127-4132.

40. Huang, X., Gordon, M. J., and Zare, R. N. (1988) Bias in quantitative capillary zone electrophoresis caused by electrokinetic sample injection, *Anal Chem 60*, 375-377.

41. Tsuda, T., Mizuno, T., and Akiyama, J. (1987) Rotary-type injector for capillary zone electrophoresis, *Anal Chem 59*, 799-800.

42. Slentz, B. E., Penner, N. A., and Regnier, F. (2002) Sampling BIAS at channel junctions in gated flow injection on chips, *Anal Chem74*, 4835-4840.

43. Gong, M., Wehmeyer, K. R., Stalcup, A. M., Limbach, P. A., and Heineman, W. R. (2007) Study of injection bias in a simple hydrodynamic injection in microchip CE, *Electrophoresis 28*, 1564-1571.

44. Roddy, E. S., Xu, H., and Ewing, A. G. (2004) Sample introduction techniques for microfabricated separation devices, *Electrophoresis 25*, 229-242.

Chapter Three

Development of Capillary Electrophoresis and Microchip Capillary Electrophoresis Methods for Protein Separation

3.1. Introduction

Electrophoresis-based separation and analysis techniques have been extensively used in proteomics, and among them capillary electrophoresis has proven to be one of the widely used methods for separation of proteins (*1-2*). Capillary electrophoresis uses high voltages, exhibits relatively short separation times and uses small sample volumes to attain very high separation efficiencies of up to millions of theoretical plates (*3*). Conventional electrophoresis methods, such as polyacrylamide gel electrophoresis present lower separation efficiencies than capillary electrophoresis (*4*). Other analytical methods such as 2-D gel electrophoresis with MS provide structural information and total analysis in proteomic studies (*4-6*). On the other hand, recent studies have revealed that both conventional capillary electrophoresis and MCE are adequate for total analysis in proteomics (*4, 7-9*). Capillary electrophoresis (CE) and MCE utilize the same electrophoretic separation modes for protein separation (*4, 9-12*).

CaM, bovine serum albumin (BSA), and concanavalin A (ConA) were selected as protein standards in this study. The goal of the work described in this chapter was to optimize the separation of AF647-labeled CaM, BSA, and ConA using HPCE and different microfluidic devices, such as glass, PDMS/glass, and Si-nanoparticle colloidal array chips under different separation modes and conditions (Scheme 1).

3.2. Materials and methods

Expression, purification, and labeling of a CaM mutant with AF647, T34C-CaM, were described in Chapter two. Commercially available BSA conjugated with AF647 and ConA (Life Technologies, Grand Island, New York) were used, and all protein samples were heat-denatured in the presence of SDS prior to the separation.

3.2.1. Materials

All reagents and samples were prepared with doubly-deionized water from an ultrapure water system (Barnstead, Dubuque, IA). Expression, purification, and AF647-labeling of CaM were described in Chapter two. AF647-labeled BSA and ConA were purchased from Molecular Probes (Eugene, OR). Fused silica capillaries (ID: 50μm and OD: 364 μm) were purchased from Polymicro Technology (Molex, Lisle, IL). Hydoxypropyl methylcelulose (HPMC) was purchased from Sigma-Aldrich (St. Louis, MO). n-Dodecyl-β-D-maltopyranoside (DDM) and HEPES were purchased from Fisher Scientific (Fair Lawn, NJ). Platinum (Pt) wire was purchased from TedPella (Redding, CA). HPMC and all other reagents, unless specified otherwise, were purchased from Sigma-Aldrich (St. Louis, MO).

3.2.2. Sample preparation

All samples were dissolved in the same run buffer (as an example BGE: 75 mM boric acid, pH 9.2) that was used for electrophoresis. Samples were heat-denatured in the presence of 3.5 mM SDS at 95°C for 5 min prior to the separation, and stock samples were stored at -20°C.

Final sample concentrations were adjusted using the same run buffer. Samples, reagents, and run buffers were filtered by 0.22 micrometer syringe filter before separations. Almost all run buffers, otherwise mentioned, in this dissertation work contained SDS. A sample of each protein (100 nM) was heat denatured (95 $^{\circ}$C for 5 min) in the presence of 3.5 mM SDS. Other specific details of sample preparation and buffer conditions will be discussed in relevant results sections.

3.2.3. Conventional capillary electrophoresis

All CE separations were performed in a Beckman P/ACE^{TM} MDQ instrument (Beckman, Fullerton, CA). A bare fused silica capillary (31.2 cm, ~21 cm to the detector window from the inlet) was used. The module used in LIF detection comprised a 635 nm laser, fiber-optic connector, and photomultiplier tube (PMT). Fluorescence emission was collected through a band pass filter, 705 nm, FWHM 72 nm, ET705/72, 12 mm diameter, mounted (Chroma, Bellows Falls, VT). New capillaries were conditioned prior to the separation for 20 min each with MeOH, 1 M NaOH, followed by 5 min with water using 10 psi pressure. Each separation was carried out at 20°C, and after each run, the capillary was washed in a sequential order with MeOH, 1M HCl, 1M NaOH, and water for 2 min each, followed by BGE (75 mM boric acid, pH 9.2) for 3 min before injecting the sample. All samples were injected into the capillary by pressure injections (0.5 psi for 10 s). All samples were dissolved in BGE containing 3.5 mM SDS. The samples were heat-denatured (95°C for 5 min) and the analysis was carried out under normal polarity. The control of instrument, data collection and analysis were done by 32 Karat software (Beckman, Fullerton, CA).

3.2.4. Microchip capillary electrophoresis

Glass chips were obtained from the Adams Micro-Fabrication facility (University of Kansas, KS) and Si-nanoparticle chips were obtained from Dr. Yong Zeng (University of Kansas, KS). PDMS/glass chips were fabricated according to the protocol described in chapter two.

3.2.4.1. Preparation of microfluidic devices for protein separation

Microfluidic channels in the device were checked using a microscope, and any particles were removed using 0.1 M NaOH or isopropyl alcohol with pressure. PDMS/glass and glass chips were conditioned with 0.1 M NaOH and nanopure water for 5 min each, followed by run buffer (which was specific to the experiment) for another 5 min. Before the separation, the device was checked again for any clogging. Similarly, after self-assembly of the colloidal array, Si-nanoparticle microfluidic devices were equilibrated with the run buffer for 20 min, and were not subjected to further conditioning prior to use.

3.2.4.2. Sample injection

Based on the separation mode and types of chip, two different electrokinetic injection methods were employed. A sample plug was introduced to the separation channel by manipulating the applied voltages in the reservoirs. Optimum applied voltages were determined using CaMAF647 injections. Injection mechanisms were described in detail in Chapter two. Specific details of injection time and voltages are discussed in the relevant sections.

3.2.4.3. Detection and data collection

As previously described in Chapter two, a semi-automated system was used to control the power supply, HV relay box, detection and data collection. The real-time electropherogram display and other functions were interfaced using in-house LabVIEW (National Instrument, TX) programs, which were kindly provided by Ryan Grigsby (Adams Micro-Fabrication facility, University of Kansas, KS).

3.3. Results

3.3.1. Separation of standard proteins by CE

An automated Beckman CE instrument was used to separate the three standard proteins, AF647-labeled CaM, BSA, and ConA. A red laser module (635 nm) with a fiber optic connecter was used as an excitation source, and sample injection, capillary washing and data collection were fully automated. As previously discussed, separation of proteins in bare capillaries by CZE was challenging. Surfaces of capillary walls adsorb proteins, and it is detrimental to the separation efficiency and reproducibility. The separation efficiency in CE is expressed as the number of theoretical plates, *N* for a given analyte *N*:

$$N = \frac{L^2}{\sigma_L^2} \qquad (1)$$

where L is the separation length and σ_L is variance of Gaussian distribution of an analyte band (*10*). Also, using the Einstein equation *N* can be described as follows (*10*):

$$N = \mu V / 2D \qquad (2)$$

where μ is the mobility of the individual analyte, D is its diffusion coefficient and V is the applied voltage across the capillary length. The separation efficiency can also be increased by increasing voltage. High voltages minimize the effect of diffusion, but this is limited by excess Joule heating and inadequate heat dissipation. Optimization of the field strength is required to maintain the balance between the separation efficiency and Joule heating. Also analytes with high mobility and low diffusion coefficients will give high plate counts due to relative low diffusion and band broadening (Equation 2). Equation 2, derived by Jorgenson and Lukacs assumes that diffusion is the only source for band broadening (*10*). But there are other sources of band broadening in CZE. The overall peak dispersion is a cumulative effect of analyte diffusion, injection, capillary wall effects, detection, and Joule heating (*10*).

The separation length plays a major role in both MCE and CE, and in this work, the minimum capillary length usable in the instrument was selected to minimize the band broadening from adsorption. Therefore, the optimum field strength and other separation conditions mentioned in the previous paragraph are essential to minimize band broadening and to obtain adequate peak capacity. In this study all protein molecules were negatively charged, and, therefore, large anions eluted first, followed by medium and small anions, respectively in CZE with cathodic EOF driven separations.

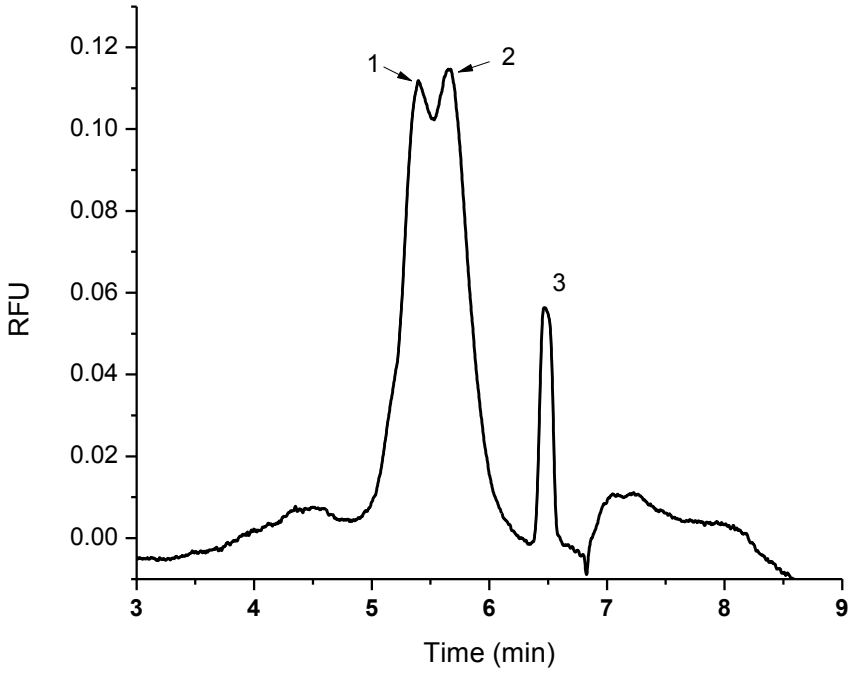

Figure 3.1. Separation of three standards with a bare silica capillary without HPMC modification. Separation conditions are as follows: length of the capillary: 31 cm, detection length: 21 cm, ID: 50 µm, BGE: 75 mM boric acid, pH 9.2, 3.5 mM SDS, and applied field strength was 193.5 V/cm. Concentration of each analyte CaM, BSA and ConA were ~40 nM, ~40 nM and ~20 nM, respectively. Peaks 1, 2, and 3 are ConA, BSA, and CaM, respectively.

Separation of SDS-protein complexes (proteins were heat denatured in the presence of SDS) with bare silica capillaries is depicted in Figure 3.1, and the capillary length of 31 cm was selected. The BGE used in Figure 3.1, 3.2 and 3.3 contained 75 mM boric acid, pH 9.2 and 3.5 mM SDS. According to the Equation 3, the increase of voltage, *V* should increase the resolution, *Rs*; however, *Rs* is also determined by other parameters, such as diffusion, EOF and electrophoretic mobility of analytes. In Equation 3, $\Delta\mu_{ep}$ is the difference in mobility between two analytes, μ_{ep} is the average mobility of the two analytes, μ_{eo} is the EOF, *E* is the field strength of separation and D_m is the average diffusion coefficient of the two analytes (*10*). Further, the voltage *V* is given by, $V = EL$, and for a given capillary length increasing *V* will

increase the resolution and this approach will be limited by excess production of heat inside the capillary.

$$R_s = 0.177\Delta\mu_{ep}\sqrt{\frac{EL}{(\mu_{ep} + \mu_{eo})D_m}} \qquad (3)$$

Another way to maximize the resolution is by reducing the EOF, and this will increase the migration time. Based on the Equation 3 improvement of resolution is directly proportional to the $\Delta\mu_{ep.}$of analytes. These relationships have been used to improve the resolution in different separations in this chapter.

According to Figure 3.1, the elution order is ConA, BSA and CaM, respectively, consistent with size-to-charge separation in CZE under cathodic-EOF driven conditions. Peaks of ConA and BSA were not fully resolved, and the CaM peak was baseline-resolved. From run to run, the resolution was reduced and alteration of migration time and brand broadening were observed. Therefore, it appears that relatively high and noisy background and partially resolved peaks were due to high adsorption of the proteins onto the capillary wall. These effects have been previously reported for bare capillaries (*13*). Further, the low separation efficiency and resolution might be due to the relatively high EOF generated from the bare capillary. CZE separations are significantly impaired by transient or permanent adsorption of proteins onto capillary walls (*14*). Even though the surface is negatively charged, anionic proteins can be adsorbed onto the channel wall by other interactions such as hydrophobic and hydrophilic interactions, van der Waals interactions, and H-bonding (*15-18*). One or more of these interactions can be present between a proteins and the surface (*18*). For example, negatively-charged BSA (above pH 5) has been used to coat negatively-charged glass and other polymeric

substrates (PMMA) to minimize nonspecific adsorption (*19*). Further, BSA shows both hydrophilic and hydrophobic interactions with a glass surfaces at physiological pH (*20-21*). This contamination of the capillary surface creates a non-uniform ζ-potential over the length of the capillary (*22*). The ζ-potential is responsible for generation of EOF, and this non-uniformity creates zonal variation of the EOF, and as a result, additional band broadening and poor reproducibility of migration times have been reported (*22-24*). To mitigate negative effects, it is necessary to deactivate the capillary surface by suppressing these undesirable wall interactions with charged or uncharged modifiers. To modify the capillary surface permanent or dynamic coating of walls can be done with nonionic molecules (*22*). Predominantly, they are water-soluble small molecules or nonionic and ionic polymers. Chemical bonding of small or large molecules or water-insoluble polymers were used in permanent coating (*22*). In this study, permanent coatings of capillary walls or microchip channel walls were not used. Buffer modifiers, such as n-dodecyl-β-D-maltopyranoside (DDM) and polymer-like cellulose derivatives, such as HPMC were used in this study (*18, 25*).

HPMC reduces EOF and thus allows adequate time for zone separation based on μ_{ep} of SDS-protein complexes before reaching the detection window (*18, 26*). Therefore, in the solution HPMC was used to coat capillary walls in CE and channel walls in MCE (*26*). A low concentration of HPMC reduces the EOF by reducing the ζ-potential and prevents interaction of SDS-protein complexes with the capillary wall (*26*). Higher concentrations of polymeric modifiers create variations in EOF, and reverse polarity analysis can be done under conditions that fully suppress EOF (*26*). First, separation was performed without HPMC (Figure 3.1), and then 0.01 and 0.05 % (w/v) HPMC were introduced in to BGE as separations were carried out (Figure 3.2 and 3.3).

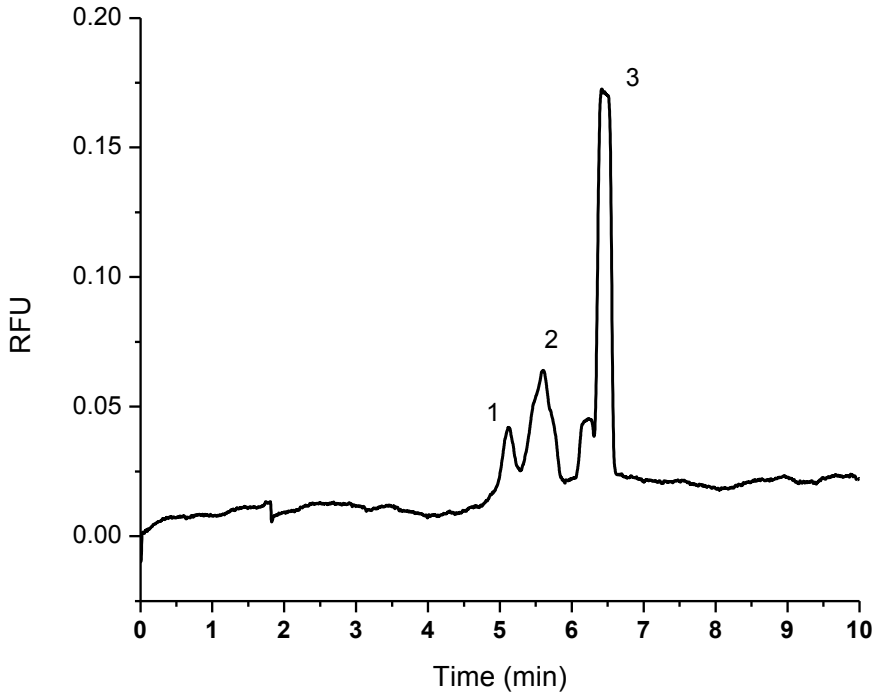

Figure 3.2. Separation of three standards with a bare silica capillary with 0.01% (w/v) HPMC. Capillary length: 31 cm, detection length: 21 cm, ID: 50 μm, BGE: 75 mM boric acid, pH 9.2, 3.5 mM SDS, 0.01% (w/v) HPMC, and applied field strength was 193.5 V/cm. Peaks 1, 2, and 3 are ConA, BSA, and CaM, respectively. Concentration of each analyte, CaM, BSA and ConA was ~40 nM, ~20 nM and ~10 nM, respectively.

In Figure 3.2, the three analytes were separated with good resolution and reproducibility. A small increase of migration times of analytes in the presence of HPMC was observed (Figure 3.1 and 3.2). This is due to the reduced EOF caused by the addition of HPMC.

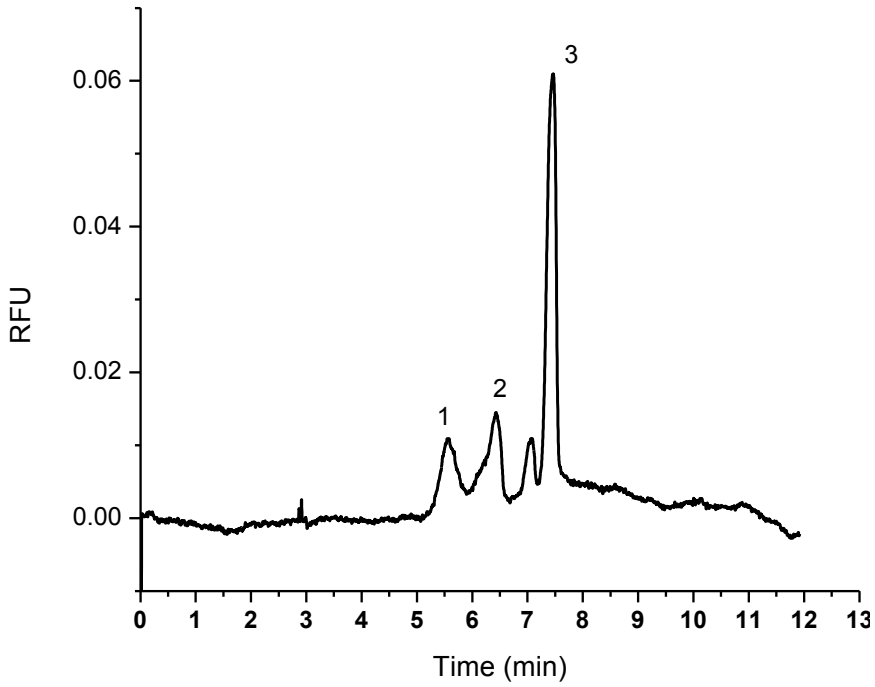

Figure 3.3. Separation of three standards with a bare silica capillary with 0.05% (w/v) HPMC. Capillary length: 31 cm, detection length: 21 cm, ID: 50 µm, BGE: 75 mM boric acid, pH 9.2, 3.5 mM SDS, 0.05% (w/v) HPMC, and applied field strength was 193.5 V/cm. Peaks 1, 2, and 3 are ConA, BSA, and CaM, respectively. Concentration of each analyte CaM, BSA and ConA were ~20 nM, ~10 nM and ~5 nM, respectively.

The effect of HPMC concentration was further investigated by increasing its concentration up to 0.05% (w/v). The background signal was reduced considerably, and this may be due to the minimized adsorption of SDS-protein complexes onto the capillary wall. At the same time, the three standards were baseline-separated (Figure 3.3). The standards were separated using CZE with HPMC as a dynamic modifier using a relatively short capillary (31 cm). The same length capillary was used for all CE separations. Higher amounts of HPMC [0.2-0.3% (w/v)] were tested to achieve conditions that totally suppress EOF. However, under reverse polarity conditions the standards could not be separated. Figure 3.4 shows detection of CaM with reverse polarity and unable to obtain any successful detection of CaM. The high viscosity of 0.2-

0.3% (w/v) HPMC created injection problems, and HPMC could not be dissolved completely in the run buffer that contained SDS. Further, high viscosity caused trapping of air bubbles in the run buffer and as a result, it was very difficult to obtain reproducible injections and separations.

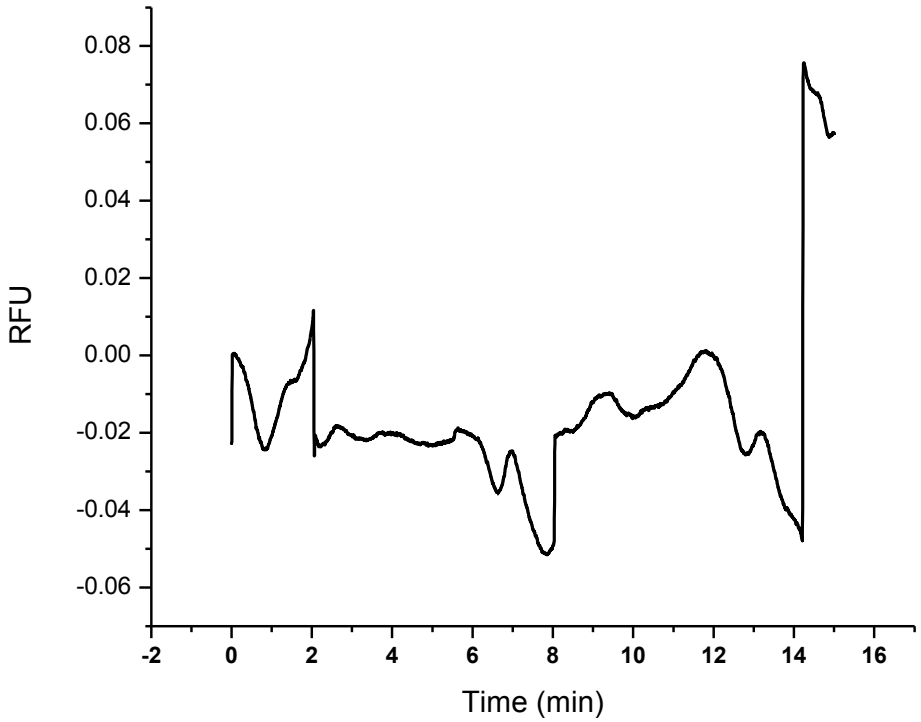

Figure 3.4. Detection of CaM with a bare silica capillary with 0.2% (w/v) HPMC and reverse polarity. Capillary length: 31 cm, detection length: 21 cm, ID: 50 µm, BGE: 4X TBE, pH 8.3, 3.5 mM SDS, 0.2% (w/v) HPMC, and applied field strength was 242 V/cm. Concentration of analyte CaM ~20 nM.

The effect of high HPMC concentration, 0.2% (w/v), with normal polarity on CaM detection is depicted in the Figure 3.5. For this injection, ~20 nM CaM was used. Reproducible injections could not be obtained in this CZE separation.

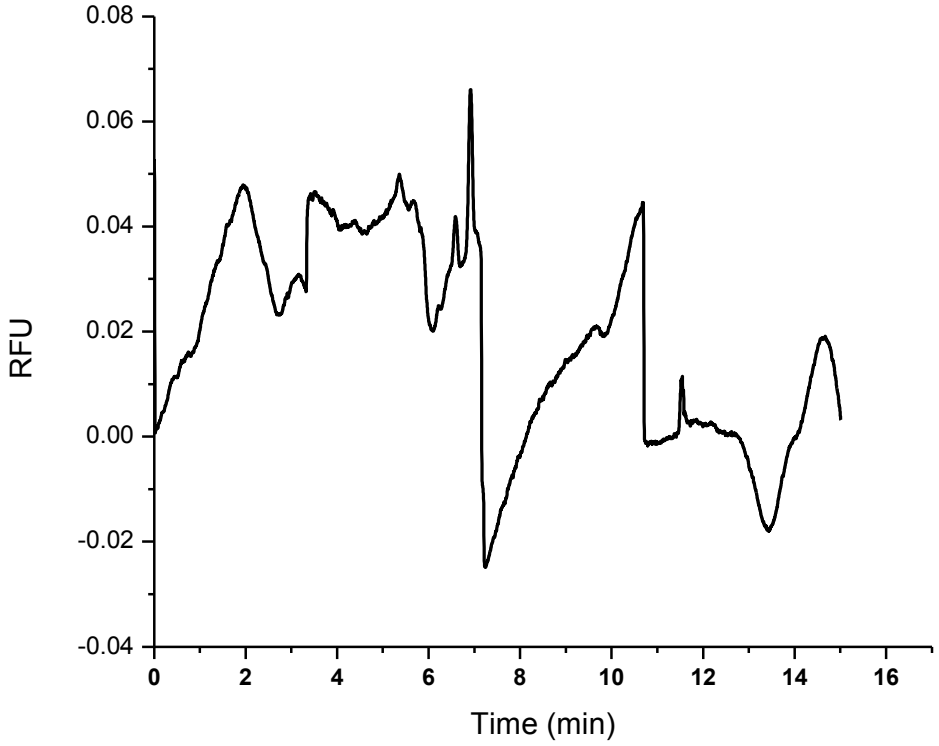

Figure 3.5. Detection of CaM with a bare silica capillary with 0.2% (w/v) HPMC and normal polarity. Capillary length: 31 cm, detection length: 21 cm, ID: 50 μm, BGE: 75 mM boric acid, pH 9.2, 3.5 mM SDS, 0.2% (w/v) HPMC, and applied field strength was 242 V/cm. Concentration of analyte CaM ~20 nM.

Separation parameters in Table 1.1 were calculated using the following equations. The peak-to-peak resolution, *R* was calculated by Equation 4:

$$R_{1,2} = \frac{2(t_2 - t_1)}{w_1 + w_2} \qquad (4)$$

where t_1 and t_2 are the migration times and w_1 and w_2 are the peak widths of adjacent peaks (*27*). The peak capacity, P_c is a separation performance measure of a capillary or a microfluidic separation channel with given conditions and was calculated using Equation 5:

$$P_c = 0.5887\left(\frac{t_r}{w_{1/2h}}\right) \quad (5)$$

where t_r is the time of migration of the peak and $w_{1/2h}$ is the full width at half maximum (FWHM) (*27-28*). The number of theoretical plates also known as the efficiency parameter of a microfluidic capillary, *N*, was calculated by Equation 6:

$$N = 5.545\left(\frac{t_R^2}{w_{1/2h}^2}\right) \quad (6)$$

where t_R is total time of separation and $w_{1/2h}$ is FWHM of a peak (*27, 29*). The height equivalent to a theoretical plate, *H* was calculated using Equation 6, where *L* is the length of the capillary or separation channel (*27, 30*).

$$H = \frac{L}{N} \quad (7)$$

Table 3.1. The calculated separation parameters for the standard proteins (Figure 3.3)

Parameter	**Values**			
Resolution (R)	$R_{1,2}$: 1.5, $R_{2,3}$: 2.9			
Peak capacity (Pc)	21			
Protein	*ConA (peak 1)*	*BSA (peak 2)*	*CaM (peak 3)*	*Average*
Number of theoretical plates, N/cm	2700	7800	12000	7500
Peak height, H(m)	1.2×10^{-4}	3.9×10^{-5}	2.6×10^{-5}	4.2×10^{-5}

Table 3.1 shows the separation parameters of the standard proteins in HPCE separation. Parameters were calculated using Figure 3.3 data (n=3). The peak-to-peak resolution of ConA

and BSA, and BSA and CaM was 1.5 and 2.9, respectively. The calculated peak capacity and the average number of theoretical plates of the capillary were 21 and 7500, respectively. The separation efficiency of the CE separation, the average of height equivalent to one theoretical plate, H was 4.2 x 10^{-5} m.

3.3.2. Microchip electrophoresis separation of protein standards

The standard proteins were then separated by microchip electrophoresis. The separation method was developed using the standard proteins with LIF detection as discussed in chapter two. Different microfluidic devices (glass, PDMS/glass, PDMS/PMMA), different injection mechanisms (gated and pinched), different run buffers (Tris, HEPES, phosphate, citric, and boric) were tested to obtain the highest possible resolution in the separation (Scheme 3.1 and Table 3.2). However, only the conditions that gave successful separation of the standard proteins are discussed in this chapter.

The gated injection needed only two positive high voltage leads to establish the gating, and the injection was predominantly based on EOF. It was necessary to use high field strengths and high pH run buffers to obtain strong EOF. The sample injection voltage and separation voltage were adjusted to obtain leak-free reproducible gating as described in Chapter two.

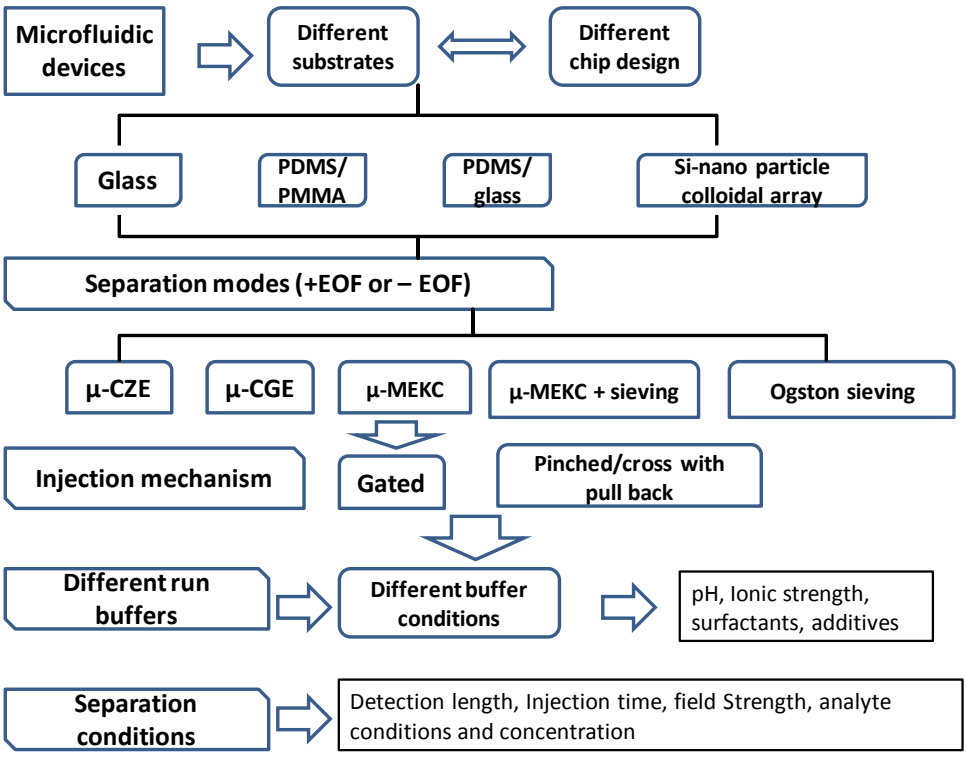

Scheme 3.1. Flow diagram showing different experimental conditions tested during separation of the standard proteins. Different chip substrates and different chip designs were tested under different separation modes. Two different electrokinetic injections, gated injection which was driven by EOF, and cross injection which was based on EOF or electrophoretic mobility of the run buffer, were employed.

Low pH buffers (citric acid and phosphate) were tested for gated injection in PDMS/glass and glass chips (Table 3.2). Low pH buffer (pH 4.0) alters the net charge of the standard proteins (average *pI* of the proteins are ~4.3, Table 3.5). With normal polarity proteins will migrate towards the cathode from anode irrespective to their charge (Figure 1.1). In Table 3.2, some of the conditions that did not provide successful separations are summarized, but successful separations are described in detail in the text. The low pH buffers generated low EOF. It was difficult to establish a fluidic gate under conditions that reduce EOF. As a result, using low pH buffers in the standard protein separation was not successful. HPMC was used with high pH run

buffers to reduce EOF in PDMS/glass and glass chips. However, it was difficult to get reproducible gating and the separation of the standard proteins was not successful.

Table 3.2. A short summary of buffers and buffer conditions used in MCE method development using the standard proteins

Separation mode	Buffer	pH	Modifiers/ additives	Conditions	Remarks
MCZE and MEKC 3.5 and 5-cm PDMS/glass chips	Boric acid	8.0, 8.5, and 9.2	SDS, HPMC SDS was added to reduce the adsorption (proteins with channel surface) and HPMC was used to reduce EOF. In MEKC a concentration of SDS above the CMC (critical micelle concentration = 8-9 mM) was used to form micelles and interactions of proteins with micelles determine the separation (*26*).	Buffer concentrations: 10, 25, 50, 100, and 150 mM, with the surfactant and the modifier, HPMC (0.01 – 0.05 % (w/v)) or without the surfactant and the modifier	* Could not separate a mixture of the three standards, but CaM and BSA were separated with 100 mM boric acid, pH 9.2, 3.5 mM SDS (Figure 3.6) * CaM and BSA were separated without SDS (Figure 3.7) * Unable to establish gating in the presence of HPMC. Changing voltages and injection times were not successful. * CaM and BSA were separated with 10 mM boric acid and 0.01% (w/v) HPMC. But it was difficult to reproduce the data (Figure 3.8). * MEKC-based separation (with 15 mM SDS) showed co-migration of the three standards.
MCZE and MEKC, 3.5 and 5-cm PDMS/glass chips	Tris-HCl	8.5	SDS/ HPMC SDS was added to form micelles and HPMC to reduce EOF.	12 mM, with 3.5/or10 mM SDS and with or without HPMC	Could not separate the three proteins in a mixture, Individual analytes had almost similar migration times. Could not establish gating in the presence of HPMC
MEKC, 5-cm PDMS/glass chip	Boric acid	9.2	SDS, ACN SDS was added to form micelles and ACN was added to increase the solubility.	25 mM boric acid, 25 mM SDS, and 20 % ACN	Could not separate the three proteins in a mixture. Individual analytes co-migrated
MCZE, 5- cm PDMS/glass	Phosphate /citric acid and phosphate	4.0 and 4.7	No additives or surfactants	Buffer concentrations are10, 20 mM	Unable to establish gating. Low pH buffer (below *pI*) combination was used to change the net charge (- to +) of the

chip					proteins. This reverses the direction of the mobility.
MCGE, 3.5- cm PDMS/glass chip	Bio-Rad CE-SDS run buffer	8.5	Sieving media and SDS	Use as it is	Unable to establish gating. The BGE suppresses EOF and polymeric substance acts as a sieving media to separate the proteins by size.
MCZE, 10- cm PDMS/glass serpentine chip	Boric acid	9.2	SDS	25, 50 mM boric acid and 3.5 mM SDS	Unable to establish gating. Longer separation channel allows high peak capacity and more time to separate based on μ with same E.
MCZE, 5- cm glass chip	MES, phosphate buffer	7.4, 4 and 4.7	SDS	10 mM MES buffer, 20 mM phosphate buffer, 3.5 mM SDS	Unable to establish reproducible gating. Low pH MES was used to reduce the EOF and phosphate buffer will change the net charge of the proteins.
MCZE 5 cm glass chip,reverse polarity separation	Boric acid	10	TTAB	25 mM boric acid and 2 mM TTAB	Unable to establish gating. Positively charged TTAB was used to reverse the charge of the channel surface and to separate the proteins with negative polarity.
MEKC, 5- cm glass chip	HEPES	7.5	DDM and SDS	20 mM HEPES, 0.1% (w/v) DDM, 3.5 mM SDS	Three proteins were separated (Figure 3.10). DDM was used to reduce the EOF, surface adsorption and micelles formation.
MCZE,10- cm glass chip	Boric acid	9.2	SDS	50 mM boric acid and 3.5 mM SDS	Three proteins were separated (Figure 3.9). Longer separation channel provides high peak capacity and allows more time to separate based on μ with same E.

3.3.2.1. Separation of the standard proteins by PDMS/glass microchips

Easy fabrication and low cost of production are positive attributes of PDMS/glass microfluidic devices (*31*). Strong adsorption, high Joule heating and frequent clogging are some of the drawbacks associated with PDMS/glass chips similar to other polymer-based devices (*31*). Different injection methods were selected based on the different separation modes. Different size PDMS/glass chips, such as 3.5-cm and 5-cm simple 'T' chips, and 10-cm long serpentine chips

were tested in the method development. Outcomes are discussed in Table 3.2.

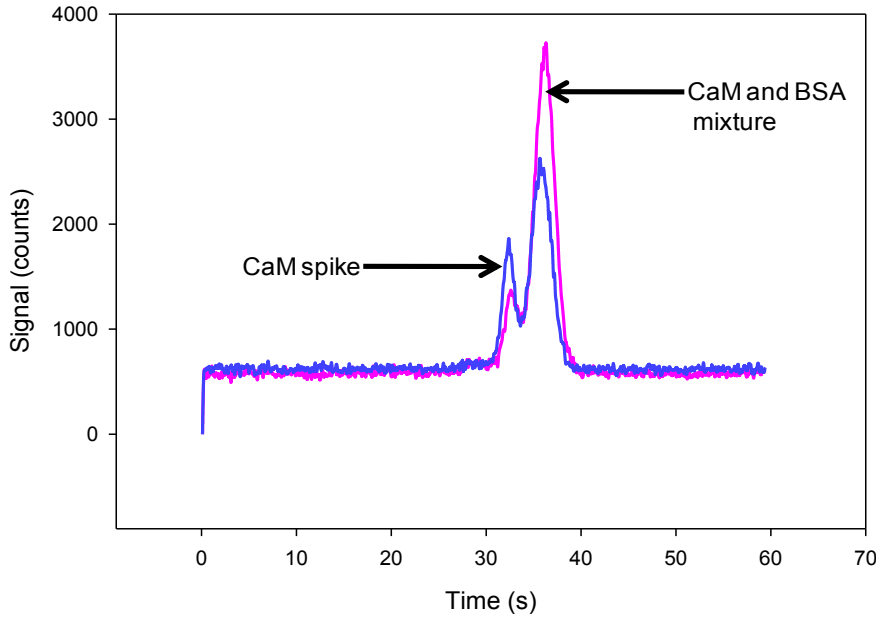

Figure 3.6. Separation of the standard SDS-protein mixture of CaM and BSA with 3.5 cm PDMS/glass chips by MCZE. The separation conditions were as follows: separation buffer composition was 100 mM boric acid, pH 9.2, 3.5 mM SDS, separation potential 1.4 kV (400 V/cm), injection time 0.3 s. The detection length was ~3 cm. Concentration of each analyte was ~50 nM. Two electropherograms were overlaid to identify the two peaks.

But the separation of a mixture of standards was unsuccessful in 3.5-cm and 5-cm long channels PDMS/glass chips with MCZE. This might be due to low peak capacity and low electrophoretic migration of analytes in a short separation distance.

Figure 3.6 shows the separation of two standards using a 3.5-cm long channel PDMS/glass chips with MCZE and gated injection. Only a mixture of CaM and BSA was injected, but it was difficult to achieve a baseline resolution of the two proteins. Peaks were assigned by spiking with CaM. All three standards (CaM, BSA and ConA) in a mixture co-migrated as a single peak in both 3.5-cm and 5-cm chips. Although different separation

conditions were tested (Table 3.2) it was still not possible to separate the three standards by PDMS/glass hybrid chips.

MCZE-based serpentine PDMS/glass chips with 10 cm separation channels were evaluated for standard protein separation. But the chip failed within a few minutes. A long separation channel in a microfluidic device with MCZE requires relatively high voltage to maintain the same field strength. High field strengths create high rates of Joule heating and electrolysis of the BGE (50 mM boric acid, pH 9.2 and 3.5 mM SDS). Also, longer separation channels are highly susceptible to clogging. A longer separation channel needs longer separation times with shallow and wide reservoirs (a relatively large volume is needed to reduce the effect of Joule heating), and it caused evaporation of buffers.

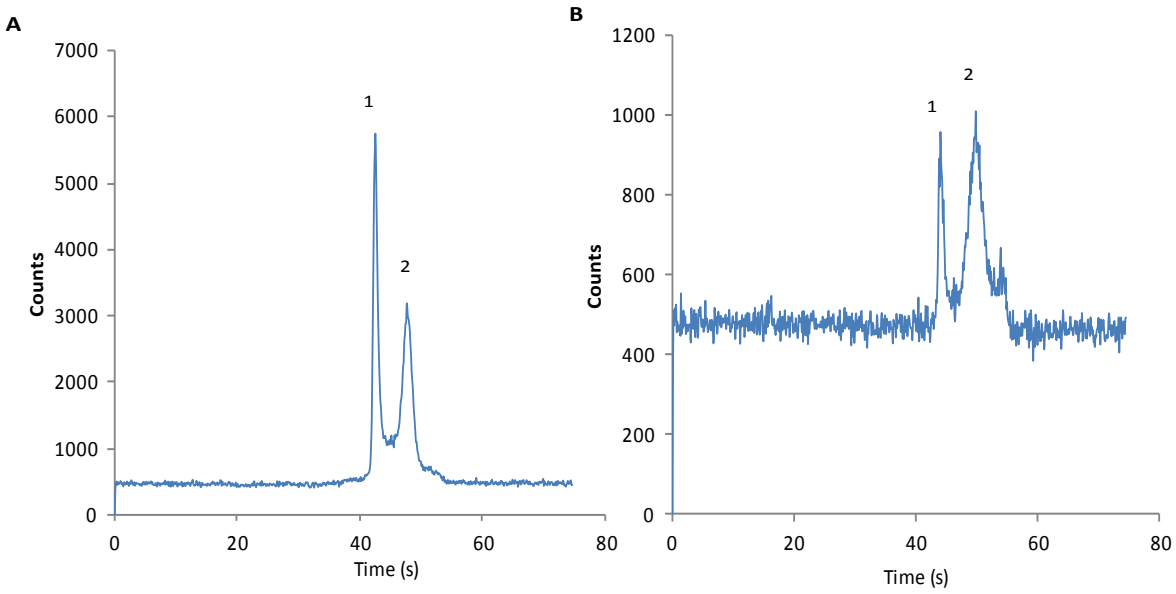

Figure 3.7. Separation of CaM and BSA without SDS in the BGE with MCZE. Chip: 5 cm PDMS/glass, BGE: 150 mM boric acid, pH 9.0. Separation and injection voltages were 2400 V and 2000 V, respectively. The separation field strength was 480 V/cm. Detection length and injection time was ~4 cm and 0.3 s, respectively. Peak 1 and peak 2 were CaM and BSA, respectively. (A) The electropherogram obtained for the first injection (B) The electropherogram obtained for the second injection.

The effect of protein adsorption onto the chip substrate in PDMS/glass chips is demonstrated in Figure 3.7. A relatively high ionic strength buffer (150 mM boric acid, pH 9.2) was used to reduce the EOF and only a mixture of two of the standard proteins (CaM and BSA) was used in this separation. Injection time, 0.3 s and the detection length (~4 cm) were kept constant for both runs. Panel A shows the first run of the MCZE separation with gated injection, and relatively a good resolution was obtained. Panel B shows the next run of the same sample, and the peak heights and peak shapes were changed. Further, the band broadening was increased and sensitivity was decreased likely due to the adsorption of protein into the surface.

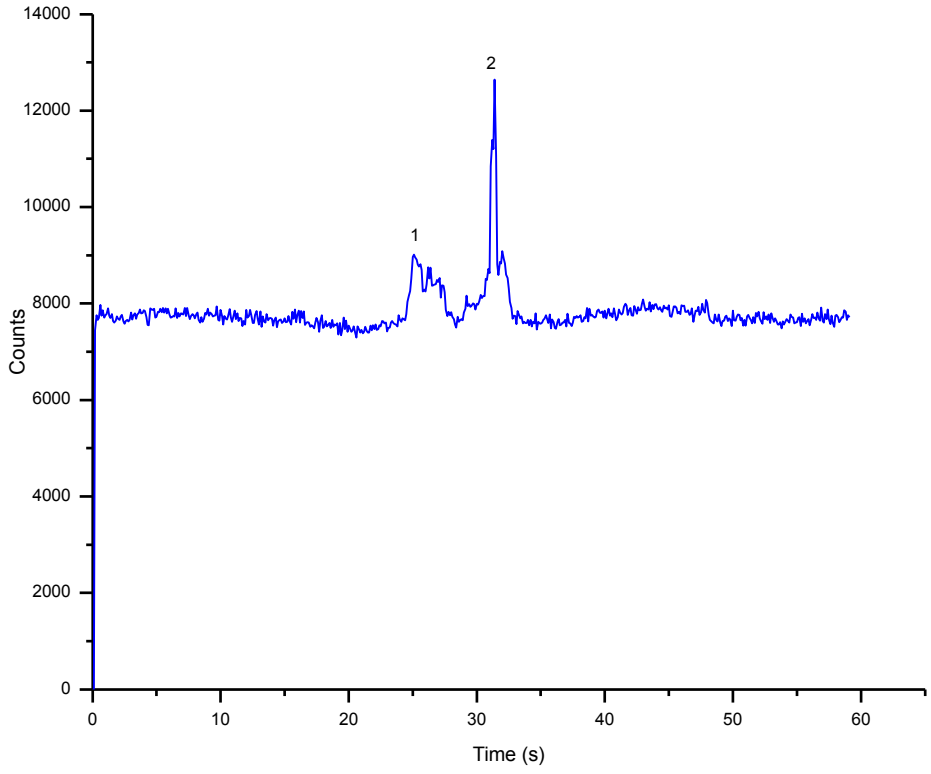

Figure 3.8. Separation of CaM and BSA with conditions that reduce EOF with MCZE. Chip: 3.5 cm PDMS/glass, BGE: 10 mM boric acid, pH 8.7, 0.01 % HPMC, and 3.5 mM SDS. Separation and injection voltages were 1400 V and 1200 V, respectively. The separation field strength was 400 V/cm. Detection length and injection time were ~3 cm and 0.3 s, respectively. Peak 1 and peak 2 were assigned as CaM and BSA, respectively.

Separation of CaM and BSA is depicted in Figure 3.8 and the EOF was reduced by HPMC. The BGE consisted of 10 mM boric acid, pH 8.7, 0.01 % HPMC, and 3.5 mM SDS. Deformed peak shapes were observed in this separation and the peak shape deformity was reported previously in HPMC-based separations (*18*). With gated injection, it was difficult to reproduce the data due to uneven injections and clogging of chips caused by HPMC. Uneven coating of HPMC creates uneven EOF and will result in different injection volumes.

3.3.2.2. Separation of protein standards by glass microchips

Because of operational problems such as high Joule heating, fluid evaporation, and clogging in the serpentine PDMS/glass chips, glass chips were selected. Glass chips are more stable to high voltages (7-8 kV), and large reservoirs can be cast around the reservoirs of the chip to increase the buffer and sample volume, and this would minimize effects of the Joule hating and buffer evaporation. Glass chips possess relatively rigid structure and a high heat capacity in comparison with the PDMS substrate.

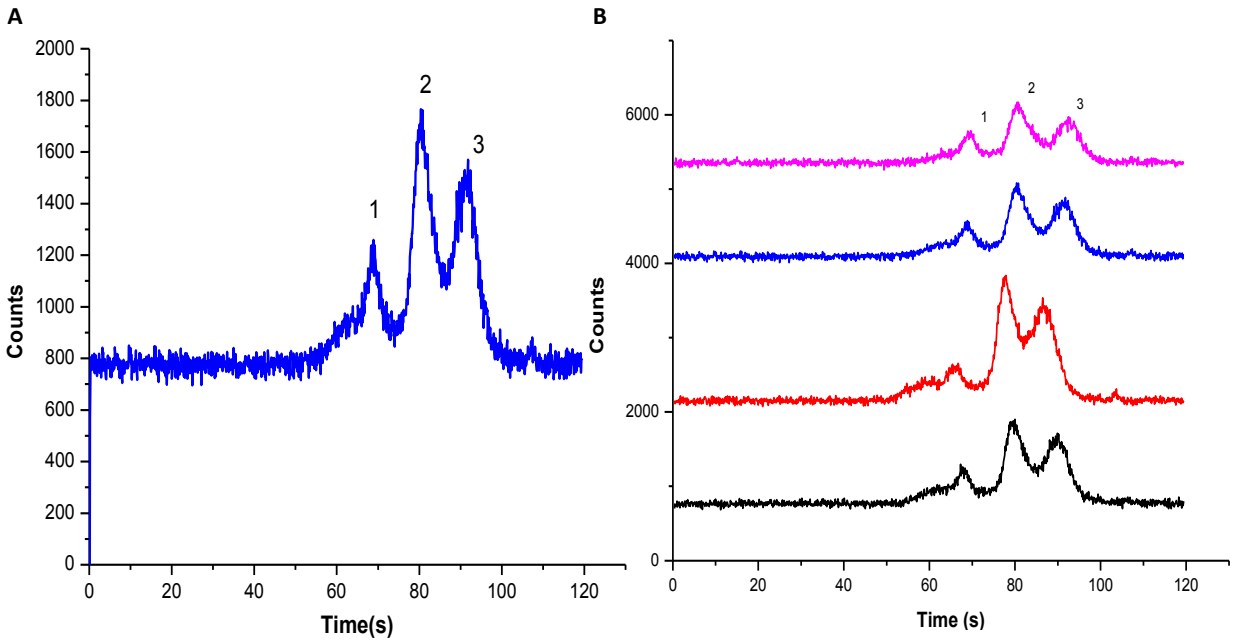

Figure 3.9. Separation of the standard proteins with MCZE by a serpentine glass chip (A). The separation conditions were as follows: separation buffer composition was 50 mM boric acid, pH 9.2, 3.5 mM SDS, separation potential 7.5 kV, field strength was ~750 V, and injection time 0.3 s. The detection length was ~9 cm. Peak 1, 2, and peaks 3 are ConA, CaM, and BSA, respectively. (B) Four consecutive runs showing reproducibility.

A serpentine glass chip with a 10 cm separation channel was used to separate the standards by MCZE with minimum modification (only 3.5 mM SDS used and it is below the CMC) to the channel wall or BGE. The run buffer contained 50 mM boric acid, pH 9.2 and 3.5 mM SDS. Three proteins were separated in under 100 s, and the elution order was ConA, CaM, and BSA respectively (Figure 3.9). The separation of the three proteins was based on size-to-charge ratio. The observed elution order contradicts the expected elution order of MCZE with normal polarity. According to the expected elution order, BSA should elute before CaM. However, CaM elutes before BSA under these experimental conditions. The addition of SDS into the run buffer did not change the order of elution (Figures 3.6 and 3.7). It is impossible to

explain the observed elution order using existing experimental conditions.

Figure 3.9.B shows four consecutive runs of the same separation, and the peak shape, peak width, peak height, and migration time varied from run to run. This may be due to varied surface adsorption of SDS-protein complexes onto the channel walls. Since the BGE did not contain any surface-specific modifiers other than SDS, the extent of adsorption of proteins was high. Further, glass substrates generate higher EOF in comparison to PDMS, and therefore controlling EOF with moderate velocity is essential for zone separation of analytes. Otherwise, it is necessary to have longer separation channels to allow adequate time for the zone separation. Hence, organic modifiers can be used to reduce EOF and thus allow shorter separation channels (*25*).

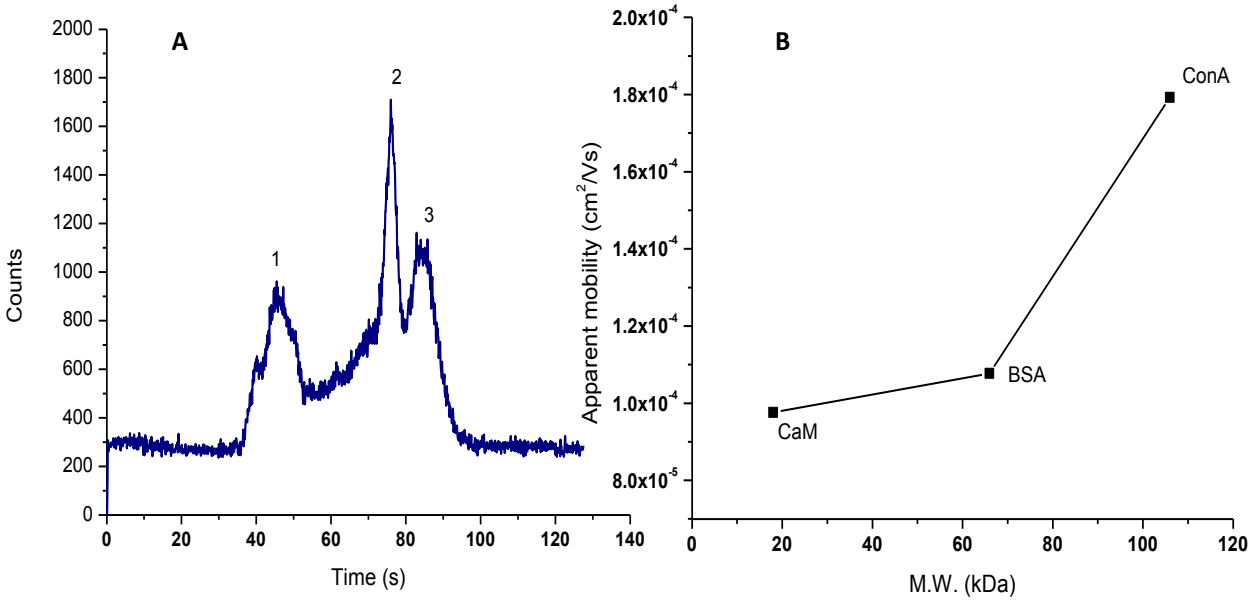

Figure 3.10. Separation of protein standards by MEKC with 5 cm glass chip. As BGE, 20 mM HEPES, pH 7.5, 0.1% (w/v) DDM, and 3.5 mM SDS were used. Separation voltage and detection length are 2500 V and ~4 cm, respectively. The separation field strength was 500 V/cm. Gated injection time is 0.5 s. (A) Peak 1, peak 2, peak 3 are ConA, BSA, and CaM, respectively. (B) Relationship between apparent mobility and the molecular weight of the standard proteins in panel A.

An organic modifier, DDM (a water-soluble, non-ionic disaccharide derivative with C_{10} linear hydrocarbon chain) was used as a dynamic coating in this experiment (*25*). A glass microchip with 5-cm long separation channel was used with a low conductive buffer, 20 mM HEPES, pH 7.5, 0.1% DDM, 3.5 mM SDS (Figure 3.10). The injection time and separation field strength were 0.5 s and 500 V/cm. Neutral DDM and SDS surfactants form negatively charge mixed micelles and interaction of the proteins with DDM-SDS micelles determines the separation. Addition of DDM into SDS reduces the CMC of SDS (0.26 mM) (*25*). The concentrations of surfactants used in this experiment were 10 fold above the CMC. Thus, the separation mechanism of proteins in the presence of DDM-SDS micelles is same as in MEKC. Further, adsorbed hydrophobic molecules (DDM) act as a coating, and that reduces the strength of the electrical bi-layer, which is essential for EOF generation (*22, 25*). Figure 3.10A shows separation of the three standard proteins in 100 s. The above mentioned separation conditions offered good reproducibility without changing migration times and peak shapes. This may be related to the reduced protein adsorption onto the channel walls in the presence of DDM.

The observed elution order was consistent with MEKC, first large ConA (106 kD), then relatively smaller BSA (66 kD), followed by CaM (18 kD) (Figure 3.10A). Apparent mobilities of the three proteins are illustrated in Figure 3.10 B. The partitioning of large molecules such as proteins inside micelles is impossible and thus the exact separation mechanism of large molecules under MEKC is yet to be defined (*26*). The number of micelles interacting with a protein depends on the protein size and number of hydrophobic residues. Hence, the interaction will increase the surface area. Further, the interaction of micelles with proteins may affect the frictional drag and alter the electrophoretic mobility of the proteins.

Irrespective of the separation mechanism the elution order of the proteins is compatible with the typical elution order of MCZE (from the largest negatively charge analytes to the smallest negatively charge analytes). The elution order of the three proteins with respect to apparent mobility and molecular weight of the proteins is illustrated in Figure 3.10B. Deviation in migration times and peak tailing in MEKC separations can occur as a result of high EOF and non specific adsorption of proteins to the channel wall (*19, 26*). The buffer recipe used in this experiments was initially reported by Zare and coworkers, and they used a 3-cm long PDMS chip (*25*). They have reported separation of immunocomplexes and photosynthetic protein-chromophore complexes in *Synechococus* cell lysate. In this experiment, a 5-cm long glass chip with DDM was used to reduce EOF and to minimize surface adsorption proteins. Further, the low conductive HEPES buffer at low pH created relatively lower EOF than the high pH boric acid buffer.

3.3.2.3. Separation of protein standards by Si-nanoparticle colloidal array microfluidic devices

Size-based separation methods have been popular in proteomics (*11*). Miniaturized systems like microchips still rely on gels or polymer-based solutions to separate large biomolecules, such as proteins (*32-34*). Non-conventional methods such as nano-structured molecule-sieving have received attention, and Zeng and Harrison introduced a sieving-based technique using self-assembled Si-nanoparticle colloidal arrays (*35-38*). In this work, the same method to separate the protein standards was applied. Sieving-based protein separation is challenging, and colloidal beds with very small pore sizes are needed to achieve separations with

high resolution (*36*).

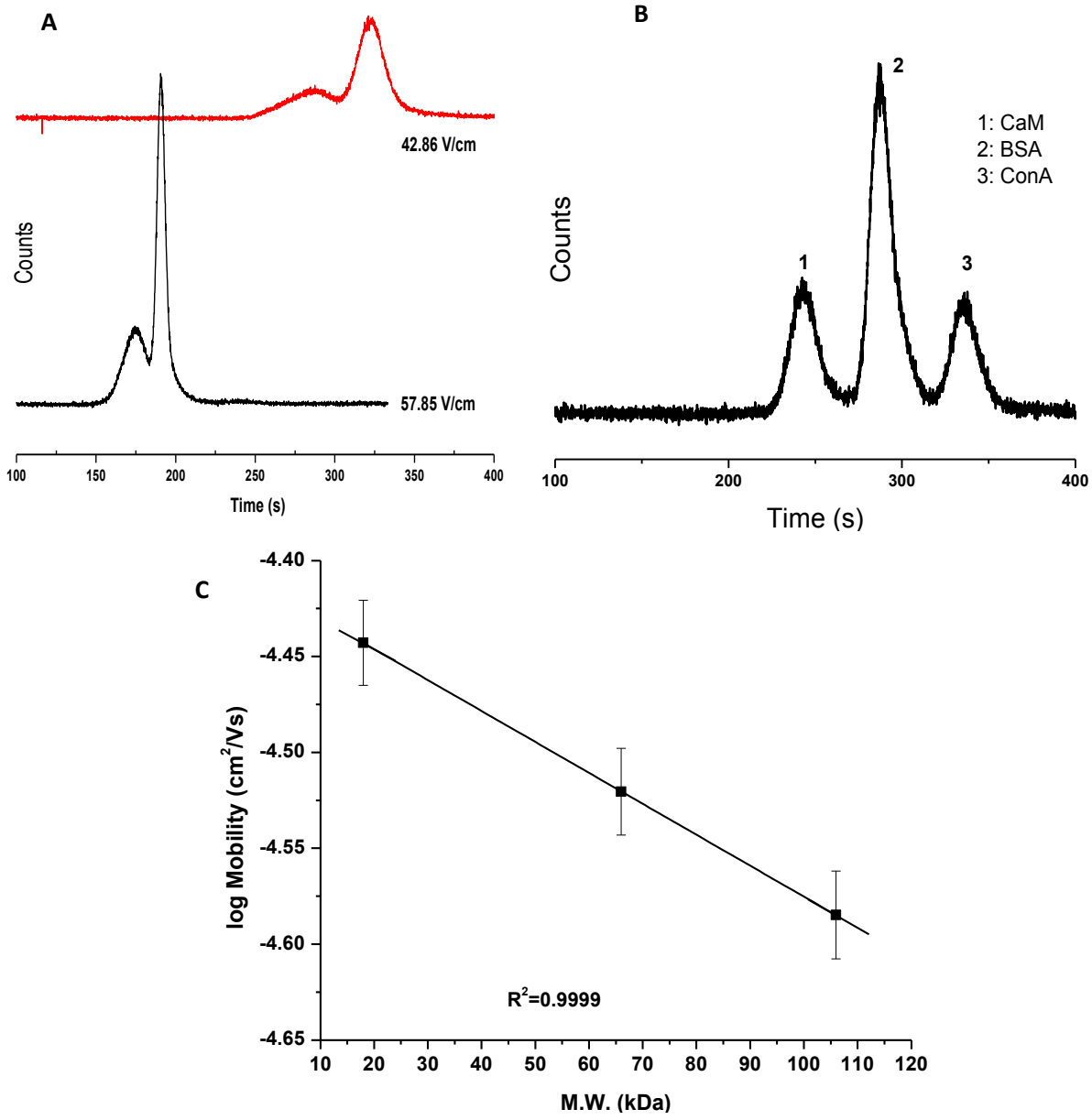

Figure 3.11. Separation of protein standards by Si-nanoparticle colloid array microfluidic devices. Separation length was 1 cm, detection length was ~5 mm. 4X TBE, pH 8.5, 3.5 mM SDS, was used as BGE (A) separation of a mixture of three protein standards using 400 nm array. (B) Separation of the same protein standards using 170 nm array. The separation field strength was 57.85 V/cm. (C) A semilog plot of the apparent mobilities of SDS-protein complexes vs protein molecular weights with a least-squares linear fit (n=7). Fit parameters are: R^2=0.9999 and log μ = -0.001MW - 4.413.

Further, it is important to note that this separation mechanism employs conditions that suppress EOF. BGE with high ionic strength, (4X TBE, pH 8.3) was used to obtain the conditions that suppress the EOF. High resistance of fluid flow in the sieving media also reduces the effect of EOF.

Figure 3.11A shows the separation of three standards with a 400 nm colloidal array. The BGE was 4X TBE, pH 8.3, 3.5 mM SDS and the detection length was ~5 mm. Two electropherograms were obtained with two different field strengths for the same sample. The standard proteins were partially resolved with the 400 nm Si-particles array. The pore size in the 400 nm bed was ~60 nm [~15 % of the diameter of a nanoparticle (*36, 38*)] and this may be too big for sieving-based separations of the proteins. The separation was greatly improved with a 170 nm Si-particle array (Figure 3.11B). The three proteins were baseline-resolved despite the shorter separation distance of ~5 mm (pore size, ~26 nm and field strength, 57.85 V/cm).

The sieving based separation of the standard proteins can be explained with the Ogston model. The model assumes that the ratio of electrophoretic mobility, μ, and free flow mobility, μ_o, is equal to the fractional gel (sieving media) volume, f, (volume that can be occupied by the analyte during migration) (*39-41*). Other parameters of the geometric model relating to f are the concentration of the gel, C, the particle (analyte) radius (radius-of-gyration), R_g, and the mean-pore-size of the sieving media, a. Also, in the random gels where $R_g < a$ and (*39-40, 42-43*):

$$\frac{\mu}{\mu_o} = f(C) = exp^{-KC} \qquad (8)$$

where, K is retardation factor and $K \sim R_g^2$ (*42*). Equation 8 can be rearranged with Equation 9:

$$R_g = R_o N^{\upsilon} \qquad (9)$$

The Equation 9 was proposed by Kohn et al. (*44*), and R_o is a constant and a prefactor for denatured proteins, N is the number of amino acids in the polypeptide chain, and υ is an exponential scaling factor where for an ideal random-coil in a solvent υ = ½ (*44*). Also $N = M/110$, where M is the molecular weight of protein and average molecular weight of an amino acid is 110 Da. Considering all above parameters and Equations 8 and 9, μ can be explained by:

$$\mu \sim \frac{\mu}{\mu_o} \sim exp^{-M} \qquad (10)$$

With the Equation 10, the logarithmic apparent mobility and the molecular weight of proteins will have a linear relationship with a negative slope. The apparent mobility of a protein was calculated by Equation 7 given in Chapter one.

Figure 3.11C depicts a plot of logarithmic electrophoretic mobility (apparent mobility) against molecular weight of the three standards. The average apparent mobility of each protein was determined from the separations performed under the same conditions as in Figure 3.11B. A linear least-squares fit to the variables shows good linearity (R^2=0.9999) that can be explained with the Ogston mechanism in 170 nm Si-colloidal arrays (*36, 38*). The sieving takes place in the colloidal array, and it provides the geometric and dynamic conditions necessary for the Ogston model (*36-39, 45-46*). The colloidal array offered the fractional volume needed to accommodate the standard proteins and it was assumed that the mobility of molecules was proportional to the fractional volume (*38, 47*). The array with a practical diameter of 170 nm (pore size ~26 nm) was used to separate the standard proteins used in this experiment (*36*). During the electrophoretic migration, smaller proteins traveled faster through the porous media, followed by the next largest protein (*37-38*). This separation encountered the Ogston mechanism requirements (static sieving

media, the radius of gyration of analytes smaller than the pore size) and it is indicated by the linear fit between the mobility and molecular weight of the proteins.

Table 3.3. The calculated separation parameters for the standard proteins by a Si-nanoparticle array (Figure 3.11B).

Parameter	**Values**			
Resolution (R)	$R_{1,2}$: 2.9, $R_{2,3}$: 2.6			
Peak capacity (Pc)	14			
Protein	*CaM (peak 1)*	*BSA (peak 2)*	*ConA (peak 3)*	*Average*
Number of theoretical plates, N/cm	1000	1900	1700	1500
Peak height ,H(m)	9.7×10^{-6}	5.3×10^{-6}	5.9×10^{-6}	6.5×10^{-6}

Table 3.3 shows the average separation parameters of the three standard proteins, and they were calculated using Figure 3.11B data (four electropherograms, n=4 was used to calculate the average apparent mobilities). The peak-to-peak resolution of CaM and BSA ($R_{1,2}$), and BSA and ConA ($R_{2,3}$) are 2.9 and 2.6, respectively. The calculated average peak capacity and the number of theoretical plates for the Si-nanoparticle colloidal array (1 cm) were 14 and 1500, respectively. The average separation efficiency of the Si-colloidal array, the height equivalent to the one theoretical plate (H), was 6.5×10^{-6} m. Accordingly, the Si-nanoparticle colloidal array provided the best separation of the standards.

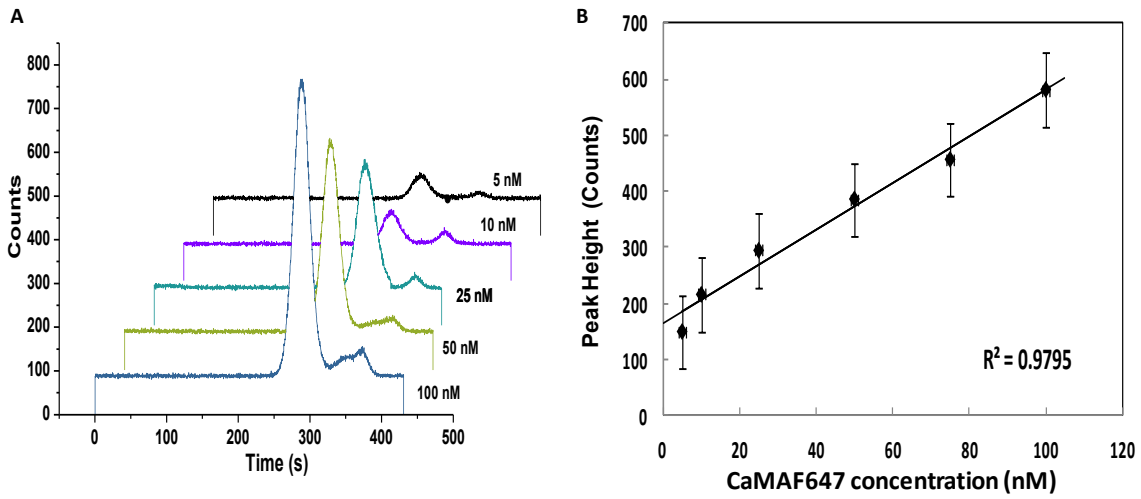

Figure 3.12. A calibration plot of CaMAF647 with a Si-nanoparticle array chip. The separation length was 1 cm and detection length was ~5 mm. BGE: 4X TBE, pH 8.5, 3.5 mM SDS ,and field strength was 57.85 V/cm. (A) An overlay of the electropherograms obtained for six AF647-labeled CaM standards ranging from 5 to 100 nM (B) A calibration curve of CaMAF647 standards with linear least-squares fit (n=4).

A calibration curve was generated to determine the concentration of AF647-labeled CaM, and estimate the limit of detection (LOD) and limit of quantitation (LOQ) using the Si nanoparticle chip (Figure 3.12). To mimic actual separation conditions with other proteins, 5 nM AF647-labeled BSA was also included in each sample. A linear least-squares fit of the data shows linearity (R^2=0.9797) for each electropherogram obtained. The LOD of this study was below 5 nM (S/N=5) and LOQ was within 5 nM (S/N=6) for these separation conditions.

3.4. Discussion

Capillary electrophoretic separation of proteins has been challenging due to several factors; ideally, the surface of the capillary does not interact with analytes under the electric

field, and the separation is governed by the mobility of analytes (*14, 48-49*). The main problem associated with CE separation is the non-specific adsorption of proteins, and the interaction between proteins and silanol groups at the inner capillary surface (*2, 4, 10-11*).

Table 3.4. A comparison of diffusion, mobility, and surface adsorption of small molecules and proteins

Analyte	Diffusion	Mobility	Adsorption
Small molecules	Rapid	High	Low
Proteins	Slow	Low	High

Macromolecules like proteins exhibit slow mobility under the electric field, relatively high non-specific adsorption (*15-19, 21, 26*), and interaction with the capillary wall or microchannel wall (Table 3.4). These unfavorable interactions are common in CE and MCE, often causing band broadening, asymmetric peaks, altered EOF, poor separation efficiency and irreproducibility (*4, 18*). Numerous approaches, such as modifying the capillary surface with coating have been proposed to improve the sensitivity and the separation efficiency. Dynamic and permanent coatings of channel walls not only suppress the adsorption but also enhance the separation efficiency (*22*). Other methods are focused on improving the BGE performance using extreme pH, high ionic strength, zwitterions, organic additives, and surfactants (*18, 22, 50*).

Dynamic coating and modification of run buffers are the two most common methods used for surface modification in both CE and MCE (*1, 4, 11*). In my method development, various buffers and modifiers were used in both CE and MCE, and the effect of these modifiers was discussed in the relevant sections. SDS (as an example in CZE, the SDS concentration was

3.5 mM and it is below the CMC (8-9 mM)) was added in all BGEs and sample reagents as a dynamic coater to reduce the adsorption (*51*), and to improve the separation efficiency and reproducibility. Similarly, samples were heat-denatured in the presence of SDS to reduce adsorption, and enhance the separation in both CE and MCE (*51*).

Table 3.5. A comparison of MW and *pI* of selected protein standards

Protein	**MW with AF647 (kDa)**	***pI*** *(52-54)*	**Grand average hydropathicity (GRAVY)** *(55-58)*
CaM	~18	3.9-4.3	~ - 0.649
BSA	~66	4.7	~ - 0.479
ConA	~106	4.5-5.5	~ - 0.208

As shown in the Table 3.5, the standard proteins have a wide range of molecular weights (MW), whereas their isoelectric points (*pI*) are very close to each other. Since the *pI* values are close to each other, separation with extreme pH might be unproductive due to their charge being the same (*4*). However, the masses of the proteins are very different and size-based separations were more successful than the charge-to-size separations. Because of close *pI* values, migration times would be close in all analytes, and consequently, CZE-based separation without modifying the BGE was poor (Figure 3.1). At pH>5, all three standards were negatively charged, and there is little difference in the electrophoretic mobilities of the SDS-protein complexes in open capillaries (*51*). Grand average of hydrophathicity (GRAVY) values of the standard proteins was calculated using ExPASy PortParam software (Table 3.5) (*55, 58*). The GRAVY value of a protein is an indicator of its solubility, and a protein with a negative GRAVY value was

described as hydrophilic. A protein with a positive GRAVY value was described as hydrophobic (*55*). Based on the GRAVY values, the standard proteins are negative and hydrophilic (Table 3.5). A separation of these analytes by CZE is challenging in both CE and MCE, unless modified separation conditions, such as modification of channel walls and changing the field strength, were used. (*59-60*). Changing the length of the capillary was not a limitation in CE; however, unmodified capillaries can cause surface adsorption and band broadening, and consequently sensitivity, reproducibility and separation efficiency were also diminished (*15*). Therefore, the shortest possible capillary length that could be used in the instrument was used. Further, surface modifications (HPMC) were introduced by HPMC in these separations as described in section 3.1.

Surface treatment in CE and MCE plays a significant role in achieving a high separation efficiency and resolution (*4*). Surface adsorption of biomolecules cannot be eliminated; however, it can be minimized by simple techniques, such as coating (*18*). Coating is an effective method to minimize non-specific adsorption of proteins onto capillaries. In this study, CE and MCE dynamic coating were used. Selection of buffers, additives and surfactants were based on the separation modes and injection methods. As an example, sieving-based separations use conditions that suppress EOF. Further, high ionic strength buffers were used to suppress EOF and samples were introduced by pinched injections. Hence, MCZE uses low ionic strength buffers with gated injection. Buffers with high buffer capacity, such as boric acid were selected, and their ionic strengths and pH values were adjusted depending on the separation modes and conditions.

The aim was to use a simple BGE (in CE) for separation of the standard proteins that could be used in MCE. Therefore, a minimum number of additives (SDS, HPMC) were used to

modify BGE and coat capillaries. It has been reported that surfactants such as SDS in BGE reduce interaction of proteins with the capillary wall and improve the separation efficiency (*51*). As a result, the proteins were heat-denatured in the presence of SDS in our experiments.

SDS and heat-denaturation alter the native conformation (*61*). Once all protein analytes are heat-denatured in the presence of a high concentration of SDS (10 mM), they have a uniform negative charge density and a spherical shape. In MCZE, the same shape but different size protein bands separate based on their electrophoretic mobility. Ultimately, the analytes are separated based on their size-to-charge ratio. On the other hand, hydrophobic moieties of SDS molecules in the run buffer, can interact with the microchannel wall (*62*). This interaction reduces adsorption of proteins onto the microchannel wall without changing the EOF (*62*). Using SDS, which acts as an additive and reduces surface adsorption of proteins, is an added advantage in the CE and MCE (*51, 62*).

3.5. Conclusion

In this chapter, the separation of SDS-protein complexes by capillary electrophoresis methods combined with LIF detection was demonstrated. Conventional CE was used to separate three protein standards with normal-polarity MCZE. The standards were successfully separated by HPCE using a relatively short capillary and dynamic coating with HPMC. Additionally, the three standards were separated in 100 s by MCE using glass chips. Si-nanoparticle colloidal array chips provided better resolution and separation in comparison with glass chips. The separation on glass chips is determined by the apparent electrophoretic mobility, whereas the separation on Si-nanoparticle chips is determined by the size (molecular weight). The EOF is

strong in glass chips and the baseline-resolution could not be obtained due to the inefficient zone-separation. Minimizing the surface adsorption and regulating the EOF are required to achieve high separation efficiency, high resolution, and sensitivity. The sieving-based separation mechanism offered better resolution and higher separation efficiency likely due to the conditions that suppress EOF, in comparison to MCZE. Conditions that suppress EOF promote electrophoretic migration of analytes, which results in better resolution and higher separation efficiency. Additionally, the sieving media reduce the diffusion and this also contributes to the better separation performance.

3.6. References

1. Jorgenson, J. W., and Lukacs, K. D. (1983) Capillary zone electrophoresis, *Science 222*, 266-272.
2. Gordon, M. J., Huang, X., Pentoney, S. L., Jr., and Zare, R. N. (1988) Capillary electrophoresis, *Science 242*, 224-228.
3. Hutterer, K. M., and Jorgenson, J. W. (1999) Ultrahigh-voltage capillary zone electrophoresis, *Anal Chem 71*, 1293-1297.
4. Manabe, T. (1999) Capillary electrophoresis of proteins for proteomic studies, *Electrophoresis 20*, 3116-3121.
5. Shevchenko, A., Tomas, H., Havlis, J., Olsen, J. V., and Mann, M. (2007) In-gel digestion for mass spectrometric characterization of proteins and proteomes, *Nat. Protocols 1*, 2856-2860.
6. Gygi, S. P., Corthals, G. L., Zhang, Y., Rochon, Y., and Aebersold, R. (2000) Evaluation of two-dimensional gel electrophoresis-based proteome analysis technology, *Proc Natl Acad Sci U S A 97*, 9390-9395.

7. Soga, T., Ohashi, Y., Ueno, Y., Naraoka, H., Tomita, M., and Nishioka, T. (2003) Quantitative metabolome analysis using capillary electrophoresis mass spectrometry, *Journal of Proteome Research 2*, 488-494.
8. Yan, X., Essaka, D. C., Sun, L., Zhu, G., and Dovichi, N. J. (2013) Bottom-up proteome analysis of E. coli using capillary zone electrophoresis-tandem mass spectrometry with an electrokinetic sheath-flow electrospray interface, *Proteomics 13*, 2546-2551.
9. Reyes, D. R., Iossifidis, D., Auroux, P.-A., and Manz, A. (2002) Micro total analysis systems. 1. Introduction, Theory, and Technology, *Anall Chem 74*, 2623-2636.
10. Weingerber. (1993) Practical capillary eletrophoresis, *2nd edition*.
11. Tran, N. T., Ayed, I., Pallandre, A., and Taverna, M. (2010) Recent innovations in protein separation on microchips by electrophoretic methods: an update, *Electrophoresis 31*, 147-173.
12. Lee, S. J., and Lee, S. Y. (2004) Micro total analysis system (μ-TAS) in biotechnology, *Appl Microbiol Biotechnol 64*, 289-299.
13. Verzola, B., Gelfi, C., and Righetti, P. G. (2000) Protein adsorption to the bare silica wall in capillary electrophoresis quantitative study on the chemical composition of the background electrolyte for minimising the phenomenon, *J Chromatogr A 868*, 85-99.
14. Dolnik, V. (2006) Capillary electrophoresis of proteins 2003-2005, *Electrophoresis 27*, 126-141.
15. Dolnik, V. (2004) Wall coating for capillary electrophoresis on microchips, *Electrophoresis 25*, 3589-3601.
16. Pallandre, A., de Lambert, B., Attia, R., Jonas, A. M., and Viovy, J. L. (2006) Surface treatment and characterization: perspectives to electrophoresis and lab-on-chips, *Electrophoresis 27*, 584-610.
17. Liu, J., and Lee, M. L. (2006) Permanent surface modification of polymeric capillary electrophoresis microchips for protein and peptide analysis, *Electrophoresis 27*, 3533-3546.
18. Doherty, E. A., Meagher, R. J., Albarghouthi, M. N., and Barron, A. E. (2003) Microchannel wall coatings for protein separations by capillary and chip electrophoresis, *Electrophoresis 24*, 34-54.

19. Shadpour, H., Musyimi, H., Chen, J., and Soper, S. A. (2006) Physiochemical properties of various polymer substrates and their effects on microchip electrophoresis performance, *J Chromatogr A 1111*, 238-251.
20. Larsericsdotter, H., Oscarsson, S., and Buijs, J. (2005) Structure, stability, and orientation of BSA adsorbed to silica, *J Colloid Interface Sci 289*, 26-35.
21. Jeyachandran, Y. L., Mielczarski, E., Rai, B., and Mielczarski, J. A. (2009) Quantitative and qualitative evaluation of adsorption/desorption of bovine serum albumin on hydrophilic and hydrophobic surfaces, *Langmuir 25*, 11614-11620.
22. Gilges M, K. M., and Schomburg G. (1994) Capillary zone electrophoresis separation of basic and acidic protiens using Poly(vinyl alcohol) coating in fused silica capillaries, *Anal Chem 66*, 2038-2046.
23. Hjertén, S., and Kubo, K. (1993) A new type of pH- and detergent-stable coating for elimination of electroendosmosis and adsorption in (capillary) electrophoresis, *Electrophoresis 14*, 390-395.
24. Towns, J. K., and Regnier, F. E. (1992) Impact of polycation adsorption on efficiency and electroosmotically driven transport in capillary electrophoresis, *Anal Chem 64*, 2473-2478.
25. Huang, B., Kim, S., Wu, H., and Zare, R. N. (2007) Use of a mixture of n-dodecyl-beta-D-maltoside and sodium dodecyl sulfate in poly(dimethylsiloxane) microchips to suppress adhesion and promote separation of proteins, *Anal Chem 79*, 9145-9149.
26. Shadpour, H., and Soper, S. A. (2006) Two-dimensional electrophoretic separation of proteins using poly(methyl methacrylate) microchips, *Anal Chem 78*, 3519-3527.
27. Giddings, J. C. (1991) *Unified Separation Science*.
28. Yan, X., and Gilman, S. D. (2010) Improved peak capacity for CE separations of enzyme inhibitors with activity-based detection using magnetic bead microreactors, *Electrophoresis 31*, 346-352.
29. Europe, C. (2004) *European Pharmacopoeia 5.0: Vol-2*, Council of Europe.
30. Yao, S., Anex, D. S., Caldwell, W. B., Arnold, D. W., Smith, K. B., and Schultz, P. G. (1999) SDS capillary gel electrophoresis of proteins in microfabricated channels, *Proc Natl Acad Sci U S A 96*, 5372-5377.

31. Henry, C. S. (2006) Microchip capillary electrophoresis: an introduction, *Methods Mol Biol 339*, 1-10.
32. Volkmuth, W. D., and Austin, R. H. (1992) DNA electrophoresis in microlithographic arrays, *Nature 358*, 600-602.
33. Han, J., and Craighead, H. G. (2000) Separation of long DNA molecules in a microfabricated entropic trap array, *Science 288*, 1026-1029.
34. Huang, L. R., Cox, E. C., Austin, R. H., and Sturm, J. C. (2004) Continuous particle separation through deterministic lateral displacement, *Science 304*, 987-990.
35. Wirth, M. J. (2007) Separation media for microchips, *Anal Chem 79*, 800-808.
36. Zeng, Y., and Harrison, D. J. (2007) Self-assembled colloidal arrays as three-dimensional nanofluidic sieves for separation of biomolecules on microchips, *Anal Chem 79*, 2289-2295.
37. Han, J., Fu, J., and Schoch, R. B. (2008) Molecular sieving using nanofilters: past, present and future, *Lab Chip 8*, 23-33.
38. Birdsall, R. E., Koshel, B. M., Hua, Y., Ratnayaka, S. N., and Wirth, M. J. (2013) Modeling of protein electrophoresis in silica colloidal crystals having brush layers of polyacrylamide, *Electrophoresis 34*, 753-760.
39. Ogston, A. G. (1958) The spaces in a uniform random suspension of fibres, *Trans Faraday Soc 54*, 1754-1757.
40. Rodbard, D., and Chrambach, A. (1970) Unified theory for gel electrophoresis and gel filtration, *Proc Natl Acad Sci U S A 65*, 970-977.
41. Morris, C. J., and Morris, P. (1971) Molecular-sieve chromatography and electrophoresis in polyacrylamide gels, *Biochem J 124*, 517-528.
42. Slater, G. W., Kenward, M., McCormick, L. C., and Gauthier, M. G. (2003) The theory of DNA separation by capillary electrophoresis, *Curr Opin Biotechnol 14*, 58-64.
43. Stellwagen, N. C., and Stellwagen, E. (2009) Effect of the matrix on DNA electrophoretic mobility, *J Chromatogra A 1216*, 1917-1929.
44. Kohn, J. E., Millett, I. S., Jacob, J., Zagrovic, B., Dillon, T. M., Cingel, N., Dothager, R. S., Seifert, S., Thiyagarajan, P., Sosnick, T. R., Hasan, M. Z., Pande, V. S., Ruczinski, I., Doniach, S., and Plaxco, K. W. (2004) Random-coil behavior and the dimensions of chemically unfolded proteins, *Proc Natl Acad Sci U S A 101*, 12491-12496.

45. King, S. B., and Dorfman, K. D. (2013) Role of order during Ogston sieving of DNA in colloidal crystals, *Anal Chem 85*, 7769-7776.
46. Rodbard, D., and Chrambach, A. (1970) Unified theory for gel electrophoresis and gel filtration, *Proc Natl Acad Sci U S A 65*, 970-977.
47. Narang, P., Bhushan, K., Bose, S., and Jayaram, B. (2005) A computational pathway for bracketing native-like structures fo small alpha helical globular proteins, *Phys Chem Chem Phys 7*, 2364-2375.
48. Cordova, E., Gao, J., and Whitesides, G. M. (1997) Noncovalent polycationic coatings for capillaries in capillary electrophoresis of proteins, *Anal Chem 69*, 1370-1379.
49. Dolnik, V. (1999) Recent developments in capillary zone electrophoresis of proteins, *Electrophoresis 20*, 3106-3115.
50. Schomburg, A., Kirchner, H., Lopez-Hanninen, E., Menzel, T., Rudolph, P., Korfer, A., Fenner, M., Poliwoda, H., and Atzpodien, J. (1994) Hepatic and serologic toxicity of systemic interleukin-2 and/or interferon-alpha. Evidence of a risk-benefit advantage of subcutaneous therapy, *Am J Clin Oncol 17*, 199-209.
51. Gudiksen, K. L., Gitlin, I., and Whitesides, G. M. (2006) Differentiation of proteins based on characteristic patterns of association and denaturation in solutions of SDS, *Proc Natl Acad Sci U S A 103*, 7968-7972.
52. Lin, Y. M., Liu, Y. P., and Cheung, W. Y. (1974) Cyclic 3':5'-nucleotide phosphodiesterase. Purification, characterization, and active form of the protein activator from bovine brain, *J Biol Chem 249*, 4943-4954.
53. Ge, S., Kojio, K., Takahara, A., and Kajiyama, T. (1998) Bovine serum albumin adsorption onto immobilized organotrichlorosilane surface: influence of the phase separation on protein adsorption patterns, *J Biomater Sci Polym Ed 9*, 131-150.
54. Entlicher, G., Kostir, J. V., and Kocourek, J. (1971) Studies on phytohemagglutinins. 8. Isoelectric point and multiplicity of purified concanavalin A, *Biochim Biophys Acta 236*, 795-797.
55. Kyte, J., and Doolittle, R. F. (1982) A simple method for displaying the hydropathic character of a protein, *J Mol Biol 157*, 105-132.
56. Bujacz, A. (2012) Structures of bovine, equine and leporine serum albumin, *Acta Crystallogr D Biol Crystallogr 68*, 1278-1289.

57. Mandal, D. K., and Brewer, C. F. (1993) Differences in the binding affinities of dimeric concanavalin A (including acetyl and succinyl derivatives) and tetrameric concanavalin A with large oligomannose-type glycopeptides, *Biochemistry 32*, 5116-5120.
58. Walker, J. M., (Ed.) (2005) *The proteomics Protocols Handbook*, Humana Press, Totowa, NJ.
59. Tachibana, Y., Otsuka, K., Terabe, S., Arai, A., Suzuki, K., and Nakamura, S. (2004) Effects of the length and modification of the separation channel on microchip electrophoresis-mass spectrometry for analysis of bioactive compounds, *J Chromatogr A 1025*, 287-296.
60. Huck, C. W., and Bonn, G. K. (2008) Analysis of proteins by capillary electrophoresis, *Methods Mol Biol 384*, 507-540.
61. Reynolds J., T. C. (1970) The gross conformation of protein-sodium dodecyl sulfate complexes, *J Biol Chem 245*, 5161-5165.
62. Nagata, H., Tabuchi, M., Hirano, K., and Baba, Y. (2005) Microchip electrophoretic protein separation using electroosmotic flow induced by dynamic sodium dodecyl sulfate-coating of uncoated plastic chips, *Electrophoresis 26*, 2247-2253.

Chapter Four

Photochemical Cross-linking of Calmodulin and Calmodulin-Binding Proteins

4.1. Introduction

Calmodulin binding proteins (CBPs) play a major role in regulating cellular functions through interacting with calmodulin (CaM) (*1-2*). The interaction of CaM and CBPs is determined by the cellular Ca^{2+} concentration. CBPs are associated with aging, and diseases like Alzheimer's, and cancer (*3-4*). Rapid and sensitive methods to analyze complex biological samples are required to identify and profile CBPs. The existing methods, such as the CaM-binding overly technique (CaMBOT), LC-MS, affinity chromatography, and SDS-PAGE, have limitations such as long analysis time and low sensitivity (*5-7*). Additionally, they require a considerable amount of sample which is a limiting factor in analyzing biological samples.

Here, a fast and sensitive method for studying CBPs is described. It utilizes a MCE protein separation assay with laser induced fluorescence detection (LIF), allowing us to use small sample volumes (*8*). Detection of CBPs was based on LIF detection of bound CaMAF647 in the CaM-CBP complex. The CaM binding affinity to CBPs is very strong: the K_d s are in the nanomolar to sub-nanomolar range with slow off-rates (*1, 9-10*) However, electrophoretic separation conditions, such as heat denaturation in the presence of SDS and high ionic-strength-buffers, could disrupt the CaM-CBP complex (*11-12*). Hence photo-chemical cross-linking to maintain the protein complexes was proposed. Endothelial nitric oxide synthase (eNOS) and calcineurin (CN) were selected as model proteins. eNOS has different isoforms, but the selected isoform had a MW of ~135 kD (*13-14*). CN is a heterodimer: the large subunit (calcineurin A, ~60 kD) binds to CaM, and the small sub unit (calcineurin B, ~19 kD) does not bind to CaM (*15-*

16). The *pI* values of the eNOS and CN are ~7 and ~6.7, respectively. In this chapter, photo-reactive cross-linking agents, methods of cross-linking, and analysis of the photo-chemically cross-linked proteins will be discussed.

4.2. Materials and methods

4.2.1. Materials

T34C-CaM was expressed and purified, followed by labeling with AF647. The CaM double mutant, T34-110C-CaM was available in the laboratory of Dr. Carey Johnson (University of Kansas, KS) (*17-18*). eNOS samples were kind gifts from Dr. David C. Arnett (Northwestern College, Orange City, Iowa) and Dr. Anthony Persechini (School of Biological Sciences, University of Missouri, Kansas City, MO). CN was kindly provided by Dr. Paul M. Stemmer (Wayne State University, Detroit, MI). Hetero bi-functional amine-reactive diazirine cross-linkers [succinimidyl 6-(4,4′-azipentanamido) hexanoate (NHS-LC-SDA), and succinimidyl 4,4-azipentanoate (NHS-SDA)], benzophenone-4-maleimide (BPM), and Zeba spin desalting columns were purchased from Pierce (Rockford, IL). Tris-HCl ready gels, Tris-Glycine buffer, and Precision Plus Protein dual color standards were purchased from Bio-Rad (Hercules, CA). PVDF membranes (0.45 μm) were purchased from Milliphore (Bedford, MA). Enhanced chemiluminiscence (ECL) detection kits were purchased from GE Healthcare, UK. CaM polyclonal and monoclonal antibodies were purchased from Santa Cruz (Paso Robels, CA).

4.2.2. Photochemical cross-linking of BPM-labeled CaM with eNOS

BPM labeling of CaM was carried out according to the double-labeling protocol published previously (*17-19*). The CaM mutant, T34-110C-CaM, which contains two Cys residues, was labeled in the presence of AF647 (1 mg) and BPM. BPM was dissolved (1mg /mL) in dimethylformamide (DMF). Unreacted AF647 and BPM were removed from the mixture of proteins as described in Chapter two. Double labeled T34-110C-CaM, which was labeled with two BPMs or two AF647 dyes or one BPM and one AF647, was separated from single labeled products (T34-110C-CaM containing one BPM and one AF647) by C18 reverse phase HPLC according to a previously published method (*17-18*). The concentration of recovered CaMAF647-labeled cross-linker (BPM-CaMAF647) was determined by UV-vis spectroscopy. BPM-CaMAF647 and eNOS were mixed in a molar ratio of 2:1 (2.6 μM of BPM-CaMAF647 was mixed with 1.3 μM eNOS) in 10 mM HEPES, pH 7.4 containing 2 mM Ca^{2+}. The mixture was incubated for 30 min at room temperature, followed by argon saturation for 30 min. The mixture was photo-irradiated at 350 nm for 30 min in a RAYONET photo-chemical reactor (Bradford, CT) with four bulbs (15 W each) (*20-21*).

4.2.3. Photochemical cross-linking of NHS-diazirine labeled CaM with CN and eNOS

CN and eNOS were cross-linked separately using NHS-diazirine according to the manufacture's protocol (*22-23*). Briefly, the ~50 μM CaMAF647 and the ~25 μM CBP were prepared in 2 mM Ca^{2+} containing 10 mM HEPES, pH 7.4, separately. 10 mM NHS-diazirine was prepared in DMSO. The cross-linker and CaMAF647 (50:1) were incubated for 30 min at room temperature. The reaction was quenched by adding Tris·HCl, pH 8 to obtain a final

concentration of 100 mM Tris, followed by incubation at room temperature for 5 min. Unreacted linker and salts were removed by Zeba desalting spin columns. The CaMAF647 labeled with cross-linker was mixed with a model CBP, 1:1 ratio (~10 μM each) in 2 mM Ca^{2+} containing 10 mM HEPES, pH 7.4 buffer. The mixture was incubated for 30 min at room temperature, followed by argon saturation for 30 min. The mixture was photo-irradiated at 350 nm for 15 min in a RAYONET photo-chemical reactor (Bradford, CT) with four bulbs (15 W each) (*21*). CN and eNOS were separately labeled with NHS-SDA and NHS-LC-SDA.

4.2.4. SDS-PAGE analysis of cross-linked CaM-CBP protein complexes

Protein samples (~1 μg from each sample) were reduced using β-mercaptoethanol, and heat-denatured in the presence of SDS (4 times the protein concentration). The samples were separated on 4-20% Tris-HCl ready gels using Tris-glycine-SDS as a run buffer. Protein Plus Dual Color standards were used as reference markers to estimate molecular weights of proteins. After the electrophoresis, gels were stained with Coomassie brilliant blue or used for Western blotting (WB).

4.2.5. Detection of photoproducts by Western blotting

Western blotting was carried out according to a previously published protocol (*24*). Following SDS-PAGE, photoproducts and proteins (control samples) were transferred onto a PVDF membrane by electrophoresis at 100 V for two hours using Tri-glycine buffer, pH 7.5. Non-specific absorption was blocked with 5% milk in 20 mM Tris, pH 7.5, 150 mM NaCl, 0.1%

(v/v) Tween 20, for one hour at room temperature, followed by treating with monoclonal CaM antibody for immunodetection. Enhanced chemiluminescence detection was used to visualize the bands of CaM and CaM-CBPs.

4.2.6. Intact protein analysis by LC-MS

Photo-chemically cross-linked CaM-CN and CaM-eNOS were analyzed by ESI-MS (Analytical Proteomics Laboratory, University of Kansas, KS) and LC-MS-TOF (Laboratory of Dr. David Weis, University of Kansas, KS). LC-MS-TOF analysis was performed in the laboratory of Dr. David Weis and briefly described in the following paragraphs. In this study, only CaM-CN was analyzed due to the higher purity of the CN sample than the eNOS sample before the cross-linking (Figure 4.8). Protein samples (0.4 μM) were prepared in 0.1% formic acid. In this analytical system, three units were incorporated, a robotic arm (LC-LEAP technologies), HPLC (Agilent 1200 series, Agilent Technologies, Santa Clara, CA) and MS-TOF (model 6220; Agilent technologies). Sample injections were performed using the robotic arm, and prior to introduction to the separation column (Jupiter 5uc4 300Ax50x1.00 mm, 5 micron, Phenomenex, Torrance, CA), the samples were desalted on a C4-trap (Jupiter C4-Trap, Phenomenex, CA). Desalting was performed by 0.1% formic acid for 3 min. The HPLC flow rate was 50 μL/min and gradient [with solvents A (0.1% formic acid) and B (acetonitrile: water: formic acid are 90%:10%:0.1%, respectively)], was programmed as follows: 15-60% B over 20 min, 60-95% B over 2 min, held at 95% B for 2 min, then brought back down to 5% B over 1 min then held at 5 % B for 3 min. Total time of the gradient elution was 28 min.

Masses of protein samples were measured by a TOF mass analyzer with an ESI source.

The mass spectra were collected in a positive ESI mode. Agilent MassHunter Acquisition was used to acquire mass spectra and Agilent MassHunter Qualitative Analysis software (version B.04.00) was used to analyze the spectra. Multiply charged ESI m/z spectra were converted by maximum entropy deconvolution algorithm and the parameters were: mass step 1 Da, mass range 40-100 kDa and calculated average mass was top 90 %.

4.2.7. In-gel tryptic digestion and MS analysis of CaM-CN and CaM-eNOS photoproducts

Around the target molecular weight area in a Coomassie blue-stained gel, a rectangular piece of gel was excised and digested using a previously published protocol (*25*). Briefly, the excised band was cut into pieces, and washed with a solution of 200 mM NH_4HCO_3/50% acetonitrile (ACN) (v/v) twice at 37°C. Gel pieces were treated with 100 mM DTT for 30 min at 60°C, followed by 100 mM iodoacetamide for 30 min at room temperature. Next, the gel pieces were re-swollen using 200 mM NH_4HCO_3 and 5 mM $CaCl_2$ buffer. Sequencing-grade modified trypsin was added at a 10:1 molar ratio of protein to trypsin and the sample was digested overnight at 37° C. The supernatant of the tryptic digested sample was drained and analyzed by ESI-LTQ-FT mass spectrometer (Analytical Proteomics Laboratory, University of Kansas, KS). In brief, UPLC (NanoAcquity chromatographic system, Waters Corp, Milford, MA) separation of peptides was performed on a reverse phase column, C18, 5 cm , 0.32 mm I.D , 5 µm, 300Å (VC-5-C18WSS-320EU, CVC-Micro Tech, Fontana, CA). A linear gradient was used from 1 to 40 % B in 50 min with a flow rate of 10 µL/min. Solvents A (99.9% H_2O, 0.1% formic acid) and B (99.9% acetonitrile, 0.1% formic acid) were used to establish the gradient. ESI (positive mode) spectra were acquired on the LTQ-FT mass spectrometer (ThermoFinnigan, Bremen, Germany)

and the instrument was set in the data-dependent acquisition mode before the data collection, and all lenses were optimized on the MH^+ ion obtained from leucine-enkephalin. The mass spectrometry data was analyzed using MassMatrix (version 2.3.6) software to identify CaM and CBP peptides in the excised gel band.

4.2.8. Analysis of CaM-CN photoproducts by microchip capillary electrophoresis

Separation of in-gel digested CaM-CN peptides by microchip electrophoresis (MCE) was performed using pinched injection as described in Chapter three. A PDMS/PMMA hybrid chip and 4X TBE, pH 8.3 were used. Other separation conditions were described in Figure 4.13.

4.3. Results and discussion

4.3.1. Protein-protein interactions and chemical cross-linking

As explained earlier, there are many methods available to investigate protein-protein interactions (PPIs) (*26-27*). These interactions can be investigated physically, genetically or computationally, and most methods rely on affinity-purification mass spectrometry (*26, 28-31*). Chemical cross-linking combined with mass spectrometry is a widely used technique in studying PPIs (*27-28*). Chemical cross-linking provides the identity of the interacting proteins and the structural information of the interaction site (*32*). It has been reported that chemical cross-linking can be effectively implemented to investigate two or a few proteins (*28*). Therefore, chemical cross-linking was selected to study CaM-CPB interactions.

PPIs can be persistent or transient (*28*). Proteins have different affinities toward

interacting partners, and the affinities are disrupted by post-transitional modifications (*28, 33*). Transient interactions such as hydrogen bonds, hydrophobic interactions and salt bridges are relatively weaker than persistent interactions (*28, 34*). Selecting a cross-linker depends on the analysis objective, but the amino acid composition of the interface also plays a major roll (*28, 35-36*).

Long-length cross-linkers might capture positions away from the PPI interface while shorter cross-linkers capture positions closer to the interface (*28*). Additionally, the selection of a cross-linker with a long and flexible linker creates a greater chance of coupling with partner proteins (*28, 37*). In my experiments, AF647-labeled CaM was labeled with a cross-linker, followed by binding with CBPs. Therefore, the selection of a cross-linker with long linker would be important.

A typical cross-linker in PPI studies has two functional groups, and they can be homo bi-functional or heterobifunctional (*38*). As depicted in Figure 4.1, each cross-linker has two reactions, and Reaction 1 is relatively more highly selective than the Reaction 2. In Reaction 1, A reacts with A′ and in the Reaction 2, B reacts with B′. Chemoselectivity can be different from Reaction 1 to Reaction 2 due to entropic loss (*28*). As a result, different products such as inter-protein and intra-protein cross-linking, can also be formed. This could be minimized by doing Reaction 1 and Reaction 2 separately, especially when using a heterobifunctional cross linker. In the CaM and CBP experiment, heterobifunctional cross-linkers were reacted separately to minimize the formation of side products.

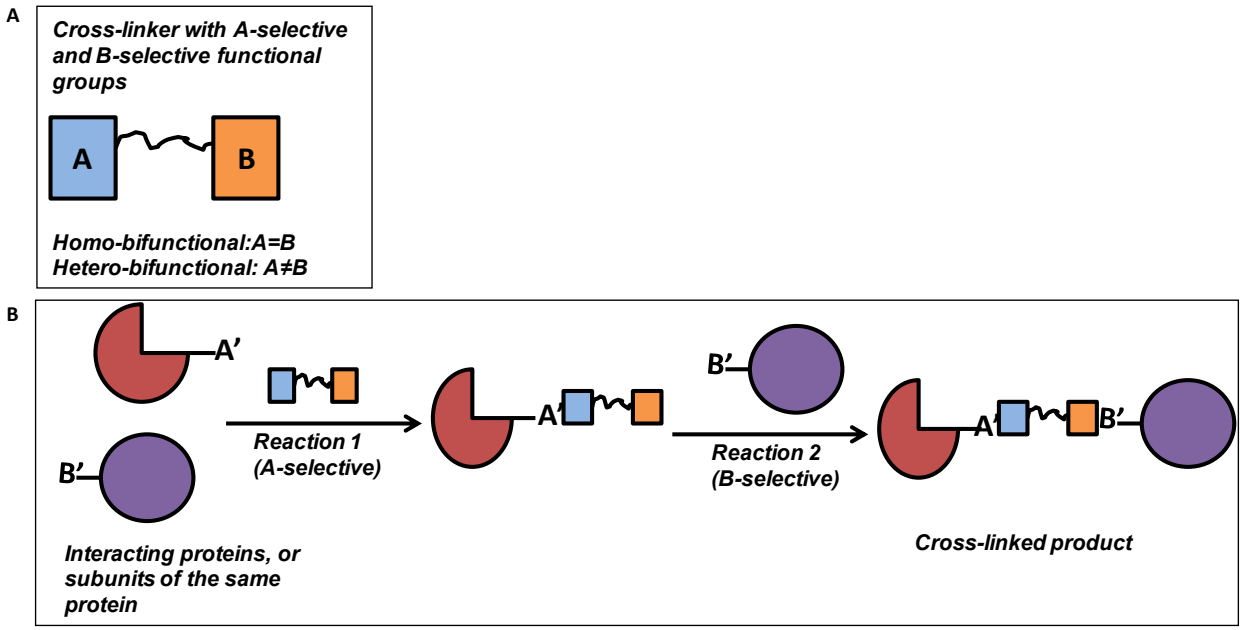

Figure 4.1. Inter-protein cross-linking. (A) Bifunctional chemical cross-linker (B) Two step procedure for chemical cross-linking: First step (Reaction 1) - labeling or activation of the first protein (CaM). Step two (Reaction 2) - the cross-linking with the second protein (CBP). A′ and B′ are reactive sites of the A and B functional groups, respectively (*28*).

Further, the choice of a cross-linker plays a crucial role in successful chemical crosslinking of two proteins. A cross-linker must provide a sufficient amount of cross-linked product to reach above the limit of detection (5 nM with the standard proteins). Mainly, it should have high affinity and chemoselectivity toward selected residues (*37, 39-40*). Also, the labeling of a cross-linker to the first protein should not interfere with its native conformation and binding. There are many cross-linking reagents reported in the literature and most of them are commercially available (*22*). Despite the large number of cross-linkers, proteins have a limited number of reactive amino acid side chains (*37*). Most cross linkers were developed to react with certain functional groups in amino acid side chains such as amines, carboxylic or thiols (*40*).

Careful control of reaction conditions including pH, which regulates the nucleophilicity of side chains, is required to obtain chemoselectivity (*27, 37*). Highly reactive nucleophiles such as sulfhydryl and amine groups are extensively used, and they target maleimides and imido esters, respectively (*28, 41*). Some cross-linkers are photoreactive such as benzophenone and diazirine; however, they are non selective when compared to maleimides and imido esters (*23, 42-44*). Photoreactive groups generate highly reactive free radicals and carbene species after photo-irradiation and thus they have low selectivity (*28, 42-43*). These functional groups are often used in heterobifunctional cross-linkers (*28*).

4.3.2. Photochemical cross-linkers

In these experiments heterobifunctional cross linkers, BPM, NHS-SDA and NHS-LC-SDA were evaluated. BPM has a thiol selective maleimide cross-linker and photoactive benzophenone. NHS-SDA and NHS-LC-SDA have an amine-reactive *N*- hydroxysuccinimide (NHS) ester group and photoreactive diazirine (Figure 4.2).

BPM: **Benzophenone-4-maleimide**
Molecular Weight: 277.28 g/mol

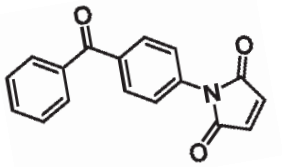

NHS-SDA: **NHS-Diazirine (SDA)** (succinimidyl 4,4-azipentanoate)
Molecular Weight: 225.20 g/mol
Spacer Arm: 3.9 Å

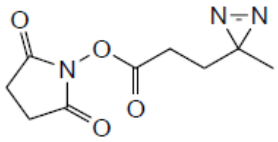

NHS-LC-SDA: **NHS-LC-Diazirine (LC-SDA)** (succinimidyl 6-(4,4-azipentanamido)hexanoate)
Molecular Weight: 338.36 g/mol
Spacer Arm: 12.5 Å

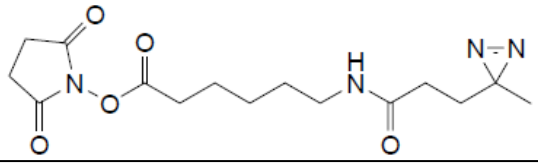

Figure 4.2. Photochemical cross-linkers used in this study

Two different photoreactive cross-linkers (BPM and NHS-diazirine) were used in these experiments, and based on the length of the linker between functional groups two diazirine compounds (NHS-SDA and NHS-LC-SDA) were used (Figure 4.2). The spacer, the distance between the two functional groups, of NHS-LC-SDA, is longer than that of BPM and NHS-SDA. The affinity labeling of CaMAF647 with the cross-linker (Reaction 1) was done first and photoactivation (Reaction 2) was done after the purification of unreacted cross-linker from Reaction 1. Photoreaction was done by UV irradiation.

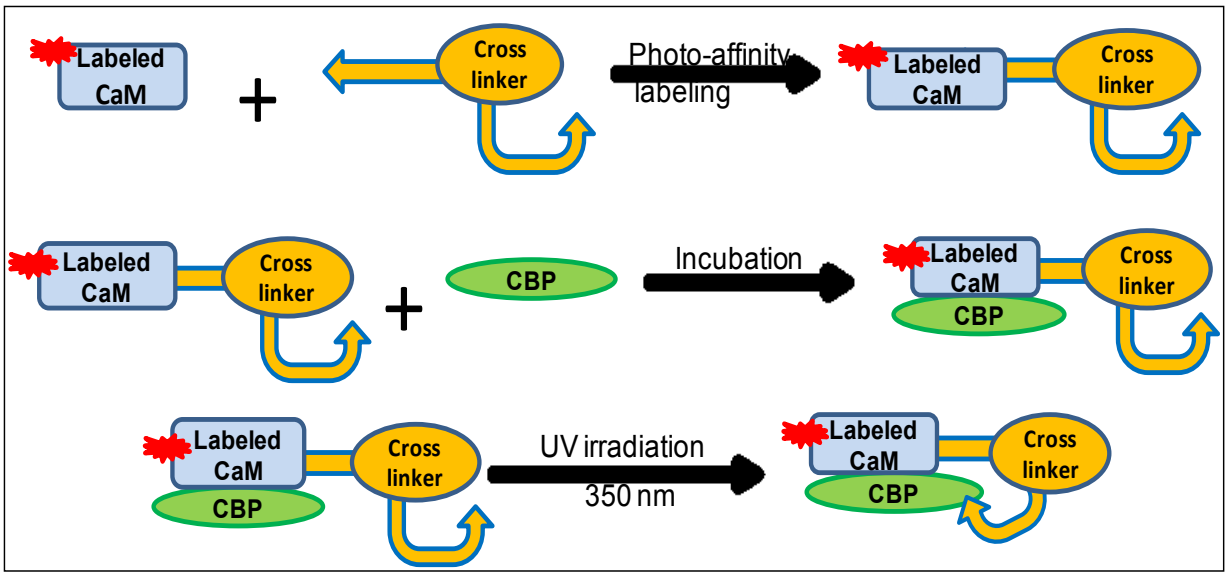

Figure 4.3. Flow diagram for photochemical cross-linking of CaM and CBPs

The detection of CaM after binding with CBPs was the goal of photochemical cross-linking. The fluorescence signal of CaMAF647 was detected in the CaM-CBP complexes during the MCE separation. The cross-linker (cl) labeled-CaMAF647 (CaMAF647-cl) was reacted with CN or eNOS in the presence of Ca^{2+}. The Ca^{2+}-loaded CaMAF647-cl binding with the model-CBP facilitates inter protein cross-linking as holo-CaM binds to the CBPs with high affinity. Photochemical cross-linking of CaM and CBP was performed in three main steps to increase the efficiency of inter-protein cross-linking (Figure 4.3). In the first step, photo-affinity labeling, CaMAF647 was reacted with the cross-linker. Excess cross-linker was removed after quenching. In the next step, CaMAF647-cl was incubated with CBP in high-Ca^{2+} HEPES, pH 7.4. In the final step, the incubated mixture of proteins was photo-irradiated by UV light at 350 nm. The same irradiation wavelength was used in BPM and NHS-SDA cross-linking (*23, 45*). Samples were placed in a rotating platform and kept in a fixed distance (5 cm) from the UV source during the irradiation to have uniform irradiation conditions.

4.3.3. Photochemical cross-linking of BPM labeled CaM and eNOS

The CaM-BPM double labeling method needed a relatively large amount of sample and the recovery percentage was relatively low (~2%). For example, ~125 µM (2.1 mg/mL) of CaMT34-110C was used as the starting concentration and the concentration of double-labeled product was ~2.6 µM. Further, the labeling and separation were time consuming.

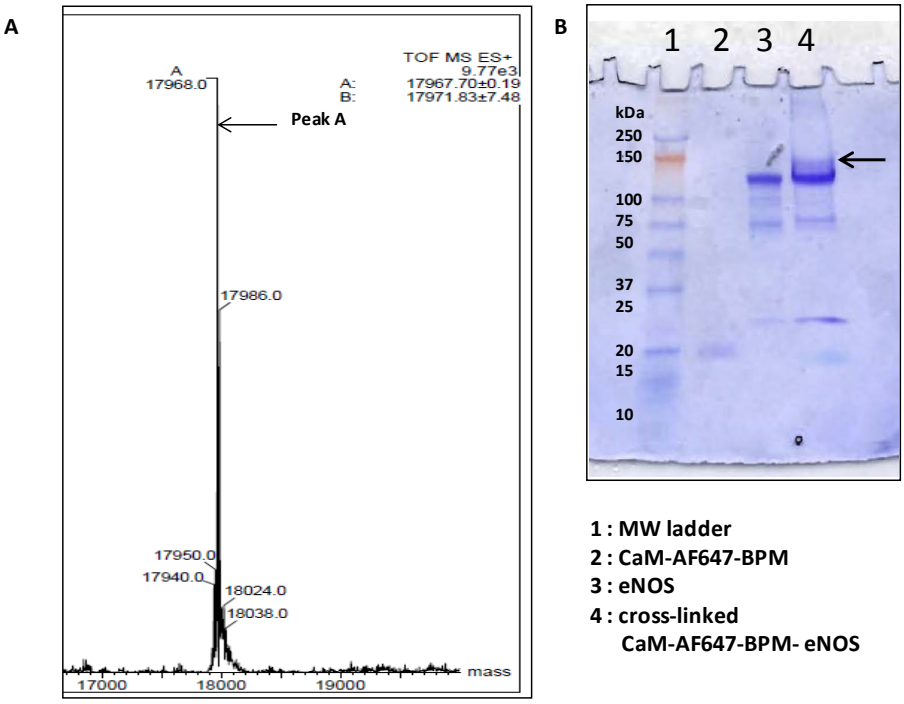

Figure 4.4. Photochemical cross-linking of BPM labeled CaMAF647 and eNOS. (A) MS analysis of AF647 and BPM labeled CaMT34-110C mutant. Peak A shows the double-labeled CaMT34-110C (17968.0 Da), which corresponds to the sum of masses of AF647, BPM and the mutant). (B) SDS-PAGE analysis of cross-linked double labeled CaM mutant with eNOS. The photoproduct is shown (arrow) with the MW of ~153 kDa.

First, BPM labeled CaMAF647 (BPM-CaMAF647) was analyzed by LC-MS (Figure 4. 4). The peak A corresponds to the double-labeled product (17968 Da). Panel B shows the SDS-PAGE analysis of photoproducts of BPM-CaMAF647 (~18 kDa) and eNOS (135 kDa).

Approximate expected mass of BPM-CaMAF647 and eNOS after cross-linking is ~153 kDa. The band corresponding to the photoproduct (pointed by an arrow) is less intense, which may be due to the low abundance of the photoproduct. Additionally, the low yield of photoproducts may be related to the low reaction efficiency of maleimide and CaMAF647, and the low recovery of double labeled product from the HPLC separation. Figure 4.5 shows the UV-vis spectrum of the product isolated form HPLC. The estimated concentration of BPM-CaMAF647 was 2.6 μM. Moreover, AF647 might be destroyed during the photo-irradiation, and it was observed that the blue color of AF647 completely disappeared after the irradiation.

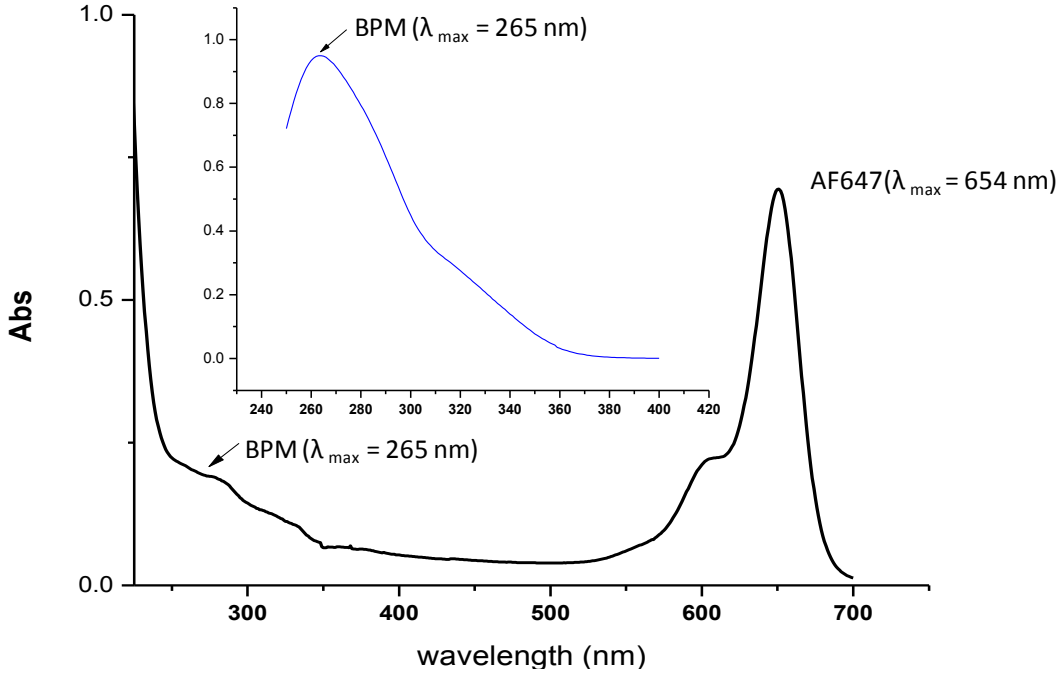

Figure 4.5. UV-vis spectrum of BPM-CaMAF647. Insert is UV-vis spectrum of BPM dissolved in methanol. BPM-CaMAF647 was dissolved in 10 mM HEPES, pH7.4, and 2 mM Ca^{2+} buffer. The molar absorptivity of AF647 and BPM are 265000 and 17000 $M^{-1}cm^{-1}$. The estimated concentration of BPM-CaMAF647 was 2.6 μM.

Figure 4.5 shows a prominent peak for AF647. A clear peak for BPM is not visible in the spectrum at λ_{max} 265 nm. Also, it was difficult to estimate the BPM concentration in the labeled protein sample.

4.3.4. Photochemical cross-linking of NHS-diazirine labeled CaM with CN and eNOS

To overcome the above discussed limitations, NHS-diazirine was selected as the cross-linker. NHS-SDA and NHS-LC-SDA, which contain an amine-reactive NHS moiety (Reaction 1, Figure 4.1) and photo-reactive diazirine ring (Reaction 2, Figure 4.1), were selected for photo affinity cross-linking. NHS-SDA has a shorter spacer, the distance between NHS and the diazirine ring, in comparison to NHS-LC-SDA (Figure 4.2). CaMAF647 was labeled with NHS-SDA, and it was photo-irradiated in the presence of CBP in a high Ca^{2+} buffer. The labeling efficiency of CaMAF647 with the cross-linker was determined by several factors, such as protein concentration, cross-linker concentration, and protein to cross-linker ratio.

4.3.4.1. NHS-SDA

CaMT34C has eight possible NHS-SDA reacting sites, including the N-terminal primary amine group, and NHS can react with any primary amine at physiological pH (pH 7-7.5). Figure 4.6 shows the amino acid sequence of CaM (obtained from PubMed-NCBI) and was color coded to demonstrate the possible reaction sites (K) for the NHS reaction. When the pH was increased, hydrolysis of NHS increased as well as the reaction with amines (*37, 46*). Under acidic pH such as pH 6, NHS preferentially reacts with the N-terminus and tyrosine hydroxyl groups; but in

alkaline pH, NHS reacts mainly with primary amines in lysine side chains and the N-terminus (*27, 32*).

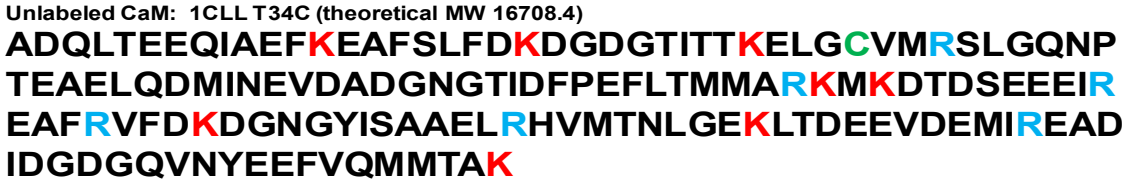

Figure 4.6. Amino acid sequence of CaMT34C mutant. Threonine at the 34th position was replaced with a cysteine (**C**). Amine-reactive lysines (**K**) are highlighted in red. **R** and **K** are also highlighted to identify the trypsin-cleavable sites (*47*).

The experiments were carried out at physiological pH, and the MS analysis of NHS-SDA labeled CaMAF647 is shown in Figure 4.7. Accordingly, multiple labeling of CaM with NHS-SDA can be seen. The NHS-SDA labeled CaMAF647 sample with CN and eNOS was photo-irradiated separately, and the photoproducts were analyzed by MCE. However, all products co-migrated and a single peak was observed in the separation. The migration times of photoproducts are similar to CaMAF647 migration times. Multiple labeling may disrupt the affinity of CaM to CBPs. Additionally, the short spacer of NHS-SDA might interfere with the inter-protein cross-linking. The theoretical mass of CaMAF647 is 17689.76 Da and the mass of the NHS-SDA linker after labeling is 111 Da. Multiple labeling of CaMAF647 with NHS-SDA linkers was observed (Figure 4.7). Peak A (18350.0 Da), B (18460.4 Da) and C (18239.6 Da) correspond to the labeling of CaMAF647 with six, seven and five NHS-SDA linkers, respectively.

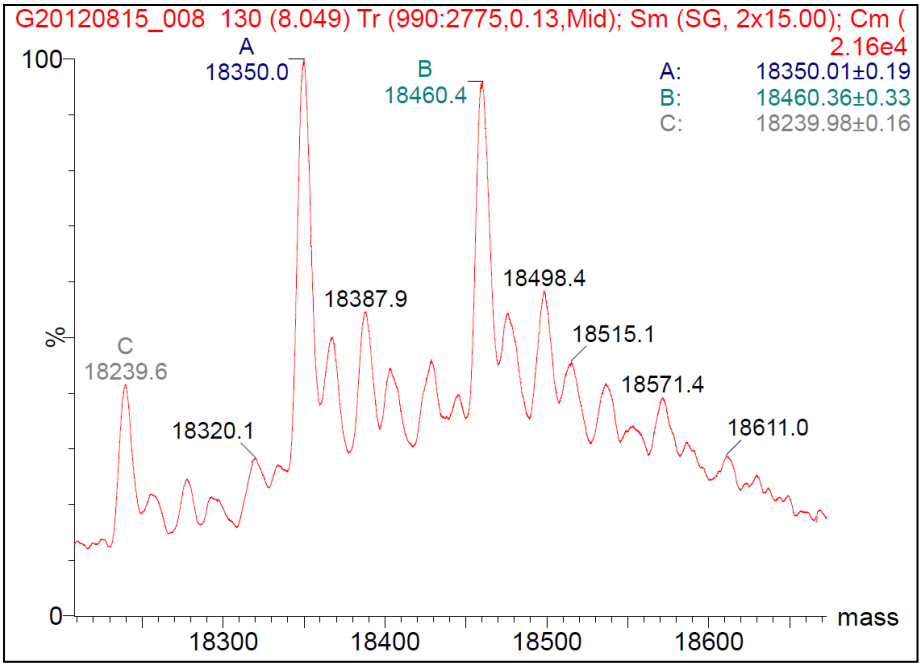

Figure 4.7. ESI-MS analysis of NHS-SDA labeled CaMAF647. Multiple labeling of the cross-linker with CaM was observed. Peak A, B and C show labeling of CaMAF647 with six, seven and five NHS-SDA, respectively.

4.3.4.2. NHS-LC-SDA

NHS-LC-SDA with a long spacer was selected to capture CBPs more efficiently during Reaction 2 (Figure 4.1). It has been reported that longer linkers have been successful in inter-protein cross linking (*28*). During the incubation, CaMAF647-cl bound to CBP in the presence of high Ca^{2+}. NHS-LC-SDA labeled CaMAF647 and eNOS were cross-linked, and the photoproduct was analyzed by Western blotting using a CaM polyclonal antibody (Figure 4.9). The CaM antibody identified a band at ~20 kDa corresponding to CaMAF647, which has a MW of ~17.8 kDa (Y in lane 1). The band corresponding to the CaM-eNOS photoproduct (expected MW of ~153 kDa) is marked (X) in lane 3. This data confirms the photo cross-linking of CaM and eNOS by NHS-LC-SDA. However, the low intensity of the band in the WB implies a low

amount of photoproducts generated from this experiment. To improve the reaction efficiency, reactions were performed by increasing concentration CaMAF647 before the labeling with NHS-LC-SDA. Higher concentration of the cross-linker-labeled-CaMAF647 was used (the concentration was increased from 0.2 to 10 µM) during the photo cross-inking and also different ratios of CaM-to-CBP were tested.

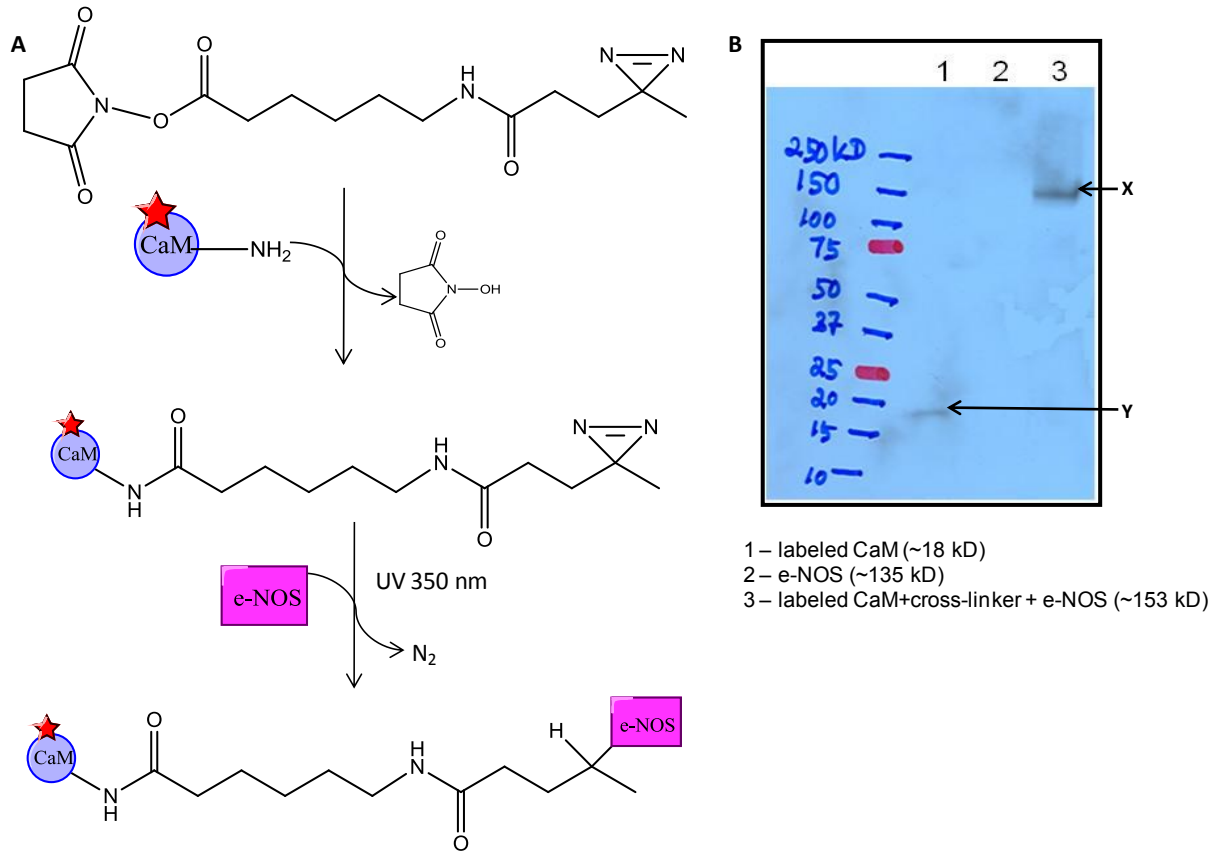

Figure 4.8. Photochemical cross-linking of NHS-LC-SDA labeled CaMAF647 and eNOS. (A) NHS-LC-SDA reacts with CaMAF647, followed by photo-irradiation in the presence of eNOS (B) Immunodetection of CaM-eNOS photoproduct. Bands corresponding to photoproduct (X, Lane 3) and CaMAF647 (Y, Lane 1) are indicated.

NHS-LC-SDA labeled CaM was successfully cross-linked with CN and eNOS separately. Figure 4.9 shows the SDS-PAGE and WB analysis of photo-chemically cross-linked samples. The monoclonal CaM antibody recognized a band corresponding to the CaM and CN photoproduct, which has an expected MW of ~77 kD (Lane 5), and the CaM and eNOS photoproduct, which has an expected MW of ~153 kD (Lane 6), respectively.

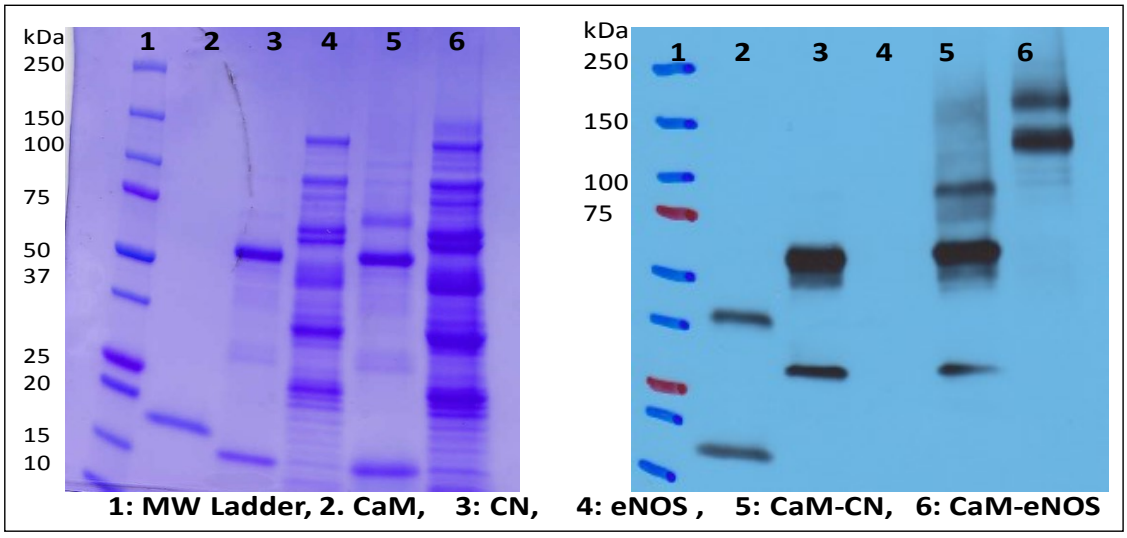

Figure 4.9. Detection of photochemically cross-linked CaM-CN and CaM-eNOS by NHS-LC-SDA. SDS-PAGE (left) and Western blotting (right) showing photoproducts of CaM-CN (~77 kDa) and CaM-eNOS (~153 kDa) in lane 5 and lane 6, respectively.

However, non-specific absorption of CaM monoclonal antibody, probably to the CN-A subunit (~60 kDa) and to the CN-B subunit (~15 kDa), was observed (Lane 3). Non specific adsorption of the monoclonal CaM antibody with CN subunits created some ambiguity in CaM-CN photoproduct identification while the CaM-eNOS photoproduct (~153 kDa) was confirmed by the WB (Lane 6).

Intact protein analysis of CaM-CN photoproducts

Next, we decided to analyze photoproducts by mass spectroscopy. The photo-irradiated CaM-CN sample was analyzed by LC-MS, but the data were inconclusive; however, the CN-A subunit and CN-B subunit were identified (separately) in the photo-irradiated sample, indicating unreacted CN in the sample (Figure 4.10). CaM-eNOS photoproducts were not subjected to LC-MS whole protein analysis due to the complexity of the sample.

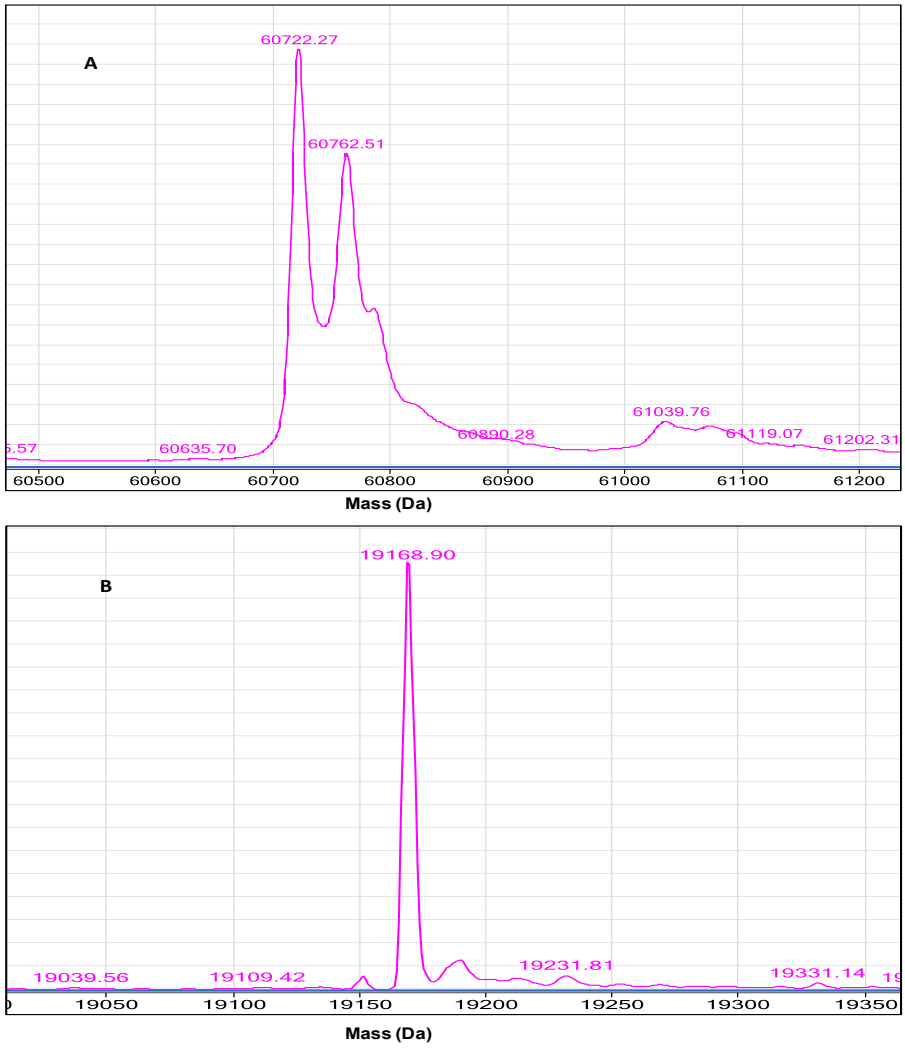

Figure 4.10. LC-MS-TOF detection of CN sub units in a CaM-CN photoproduct (A) CN-A subunit (MW=60722.27 Da) and (B) CN-B subunit (MW=19168.90 Da) were identified.

The theoretical average mass of the CN-A sub unit with the N-terminal polyhistidine tag is 60719.98 Da (*15-16*). The theoretical average mass of the CN-A sub unit with the N-terminal polyhistidine tag is 60719.98 Da. The observed average mass of CN-A sub unit was 60722.27 Da (Figure 4.10). In Figure 4.12, the CN-A sequence without the His-tag peptide segment (58687.8 Da, GI: 1352673) was used to MassMatrix search.

In-gel tryptic digestion and analysis of CaM-CN and CaM-eNOS photoproducts

Photoproducts were next analyzed by in-gel digestion, followed by MS analysis (Figure 4.11). Both CaM-CN and CaM-eNOS photoproducts were subjected to in-gel digestion with trypsin. Trypsin cleaves C-terminally to lysine or arginine. The tryptic digested samples were analyzed by ESI-MS analysis. The objective of the analysis was to identify CaM and CBP peptides in the digested samples. In this experiment, I did not focus on tandem-MS data analysis, which might reveal the crosslinking peptides from both proteins.

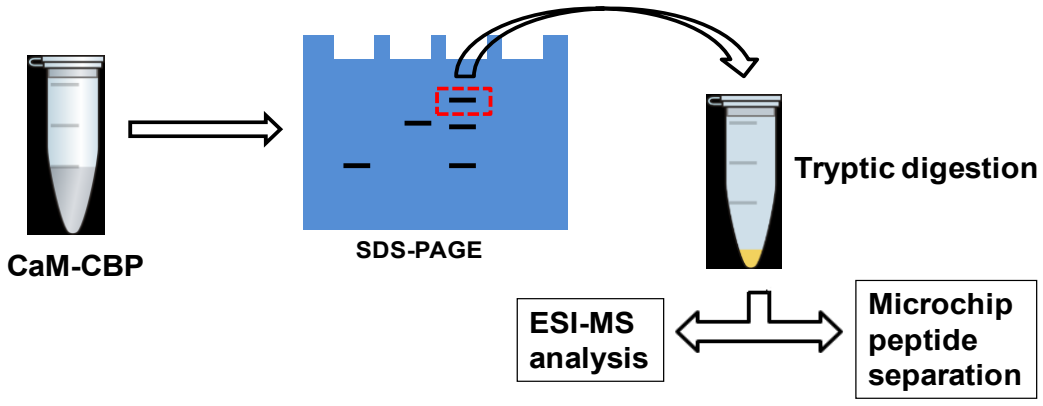

Figure 4.11. Detection of CaM-CN and CaM-eNOS photoproducts by in-gel tryptic digestion. After in-gel tryptic digestion, samples were analyzed by mass spectrometry and microchip peptide separation.

Detection of CaM and CN in the cross-linked CaM-CN sample

MassMatrix was used to analyze the MS data. The *Homo sapiens* CaM sequence (GI: 5542035) was used to obtain a FASTA file (where the text format of an amino acid sequence and the amino acids are represented by single-letter codes) file to use as the reference sequence. Tryptic digested peptides, which were obtained by MS analysis, were run against the reference sequence. CaM was identified with 30% sequence coverage (Figure 4.12, panel A) in the CaM-CN cross-linked sample. Also, the presence of a large number of unique peptides provides a strong indication of the presence of target protein in a cross-linked sample. Seven unique peptides of CaM were identified with good scores.

The cross-linked CaM-CN sample was further analyzed to check the presence of CN. A FASTA file of the *Homo sapiens* CN-A sequence (GI: 1352673) was obtained, and the MS data were run against it. CN-A was identified with 40% sequence coverage and 67 unique peptides (Figure 4.12 panel B). This proved the presence of the CN-A subunit in the cross-linked sample. This verified the presence of both CaM and CN-A in the cross-linked sample.

Panel (A)

HIT 1

Protein Mass: 16828.796 (monoisotopic) 16839.542(average) Protein Score: 113 Protein pp: 7992.0
gi|5542035|gb|AAD45181.1|AC006536_1 calmodulin [Homo sapiens]

Sequence:
001 MADQLTEEQI AEFKEAFSLF DKDGDGTITT KELGCVMRSL GQNPTEAELQ DMINEVDADG NGTIDFPEFL TMMARKMKDT DSEEEIREAF RVFDKDGNGY 100
101 ISAAELRHVM TNLGEKLTDE EVDEMIREAD IDGDGQVNYE EFVQMMTAK 149

Sequence Coverage: 30%
Sequence Tag Coverage: 26%

Index	scan#	charge	score	pp	pp2	ppTag	m/z	MW(obs)	MW	delta	miss	Unique	sequence + modifications [start:end]
904	924	+3	100	20.5	17.3	15.7	507.9256	1521.7622	1521.7431	0.0191	0	√	ADQLTEEQIAEFK
905	922	+2	175	20.5	19.5	10.2	761.3851	1521.7629	1521.7431	0.0197	0	√	ADQLTEEQIAEFK [2:14]
259	1001	+2	89	12.3	14.6	9.5	478.7457	956.4841	956.4724	0.0117	0	√	EAFSLFDK [15:22]
1052	1061	+3	11	6.0	3.2	2.8	615.6421	1844.9117	1844.8913	0.0205	1	√	EAFSLFDKDGDGTITTK
1053	1037	+3	36	8.7	7.5	5.1	615.6440	1844.9176	1844.8913	0.0263	1	√	EAFSLFDKDGDGTITTK [15:31]
978	911	+3	64	13.1	12.6	8.9	585.6382	1754.9002	1754.8708	0.0294	1	√	VFDKDGNGYISAAELR [92:107]
660	791	+2	10	5.1	3.6	2.8	633.3331	1265.6589	1265.6121	0.0468	0	√	DGNGYISAAELR [96:107]

Panel (B)

HIT 1

Protein Mass: 58650.304 (monoisotopic) 58687.479(average) Protein Score: 722 Protein pp: 20360.0
gi|1352673|sp|Q08209.1|PP2BA_HUMAN RecName: Full=Serine/threonine-protein phosphatase 2B catalytic subunit alpha isoform

Sequence:
001 MSEPKAIDPK LSTTDRVVKA VPFPPSHRLT AKEVFDNDGK PRVDILKAHL MKEGRLEESV ALRIITEGAS ILRQEKNLLD IDAPVTVCGD IHGQFFDLMK 100
101 LFEVGGSPAN TRYLFLGDYV DRGYFSIECV LYLWALKILY PKTLFLLRGN HECRHLTEYF TFKQECKIKY SERVYDACMD AFDCLPLAAL MNQQFLCVHG 200
201 GLSPEINTLD DIRKLDRFKE PPAYGPMCDI LWSDPLEDFG NEKTQEHFTH NTVRGCSYFY SYPAVCEFLQ HNNLLSILRA HEAQDAGYRM YRKSQTTGFP 300
301 SLITIFSAPN YLDVYNNKAA VLKYENNVMN IRQFNCSPHP YWLPNFMDVF TWSLPFVGEK VTEMLVNVLN ICSDDELGSE EDGFDGATAA ARKEVIRNKI 400
401 RAIGKMARVF SVLREESESV LTLKGLTPTG MLPSGVLSGG KQTLQSATVE AIEADEAIKG FSPQHKITSF EEAKGLDRIN ERMPPRRDAM PSDANLNSIN 500
501 KALTSETNGT DSNGSNSSNI Q 521

Sequence Coverage: 41%
Sequence Tag Coverage: 36%

Index	scan#	charge	score	pp	pp2	ppTag	m/z	MW(obs)	MW	delta	miss	Unique	sequence + modifications [start:end]
28	85	+2	12	14.4	5.2	8.2	346.6868	692.3664	692.3573	0.0090	0	√	LSTTDR
29	138	+2	13	16.0	4.7	10.1	346.6887	692.3700	692.3573	0.0127	0	√	LSTTDR [11:16]
317	605	+3	14	6.2	3.4	2.3	336.5211	1007.5489	1007.5421	0.0068	0	√	AVPFPPSHR
318	595	+2	27	6.0	4.6	7.8	504.2787	1007.5500	1007.5421	0.0079	0	√	AVPFPPSHR
319	446	+3	17	8.7	3.4	5.5	336.5223	1007.5524	1007.5421	0.0102	0	√	AVPFPPSHR
320	478	+3	16	6.0	3.6	5.5	336.5224	1007.5527	1007.5421	0.0106	0	√	AVPFPPSHR
321	568	+2	17	6.5	5.1	2.9	504.2803	1007.5533	1007.5421	0.0112	0	√	AVPFPPSHR
322	537	+3	15	8.1	3.6	5.5	336.5228	1007.5537	1007.5421	0.0116	0	√	AVPFPPSHR
323	479	+2	27	6.5	4.7	7.8	504.2816	1007.5560	1007.5421	0.0139	0	√	AVPFPPSHR
324	507	+3	16	12.5	3.6	9.1	336.5237	1007.5565	1007.5421	0.0144	0	√	AVPFPPSHR
325	447	+2	31	8.7	4.5	6.6	504.2820	1007.5567	1007.5421	0.0146	0	√	AVPFPPSHR
326	622	+2	29	11.2	4.5	4.6	504.2823	1007.5574	1007.5421	0.0152	0	√	AVPFPPSHR
327	509	+2	25	7.6	5.0	1.7	504.2848	1007.5623	1007.5421	0.0202	0	√	AVPFPPSHR
328	2378	+2	15	8.7	5.7	1.7	504.3018	1007.5964	1007.5421	0.0543	0	√	AVPFPPSHR [20:28]
556	279	+3	51	9.5	6.0	3.6	392.8677	1176.5885	1176.5644	0.0241	0	√	EVFDNDGKPR
557	308	+3	54	15.0	6.2	9.7	392.8677	1176.5885	1176.5644	0.0241	0	√	EVFDNDGKPR
558	284	+2	42	21.5	5.4	12.1	588.8015	1176.5958	1176.5644	0.0314	0	√	EVFDNDGKPR
559	309	+2	37	15.0	5.2	12.1	588.8043	1176.6014	1176.5644	0.0370	0	√	EVFDNDGKPR [33:42]
1	106	+2	54	11.6	13.8	4.6	300.1772	599.3470	599.3334	0.0137	0	√	AHLMK [48:52]
217	541	+2	52	13.5	9.7	4.0	458.7649	916.5225	916.5098	0.0127	0	√	LEESVALR
218	511	+2	55	14.9	9.7	4.9	458.7675	916.5278	916.5098	0.0179	0	√	LEESVALR [56:63]
435	793	+3	35	18.3	9.3	9.3	358.2207	1072.6476	1072.6361	0.0115	0	√	IITEGASILR
436	790	+2	74	25.5	8.4	10.6	536.8276	1072.6479	1072.6361	0.0118	0	√	IITEGASILR
437	821	+2	50	15.4	8.4	11.9	536.8293	1072.6514	1072.6361	0.0153	0	√	IITEGASILR [64:73]

Figure 4.12. Detection of CaM and CN in cross-linked CaM-CN sample by MS analysis. Panel (A) the sequence coverage of CaM and panel (B) the sequence coverage and a part of the identified CN peptides. Identifying both CaM and CN in the cross-linked sample suggested that the cross-linking reaction occurred.

Separation of in-gel digested CaM-CN peptides by microchip electrophoresis

In-gel digested CaM-CN sample and CaMAF647 sample were detected by a 3.5 cm PDMS/PMMA hybrid chip separately and detected by LIF of AF647. Pinched injection of the sample was performed with normal polarity, high ionic strength 4X TBE, and pH 8.3 to perform MCZE. Figure 4.13 shows an overlay of two electropherograms of CaM-CN peptides and CaMAF647 peptides. Detection of AF647 conjugated peptides in the CaM-CN sample indicates the successful cross-linking of CaM and CN.

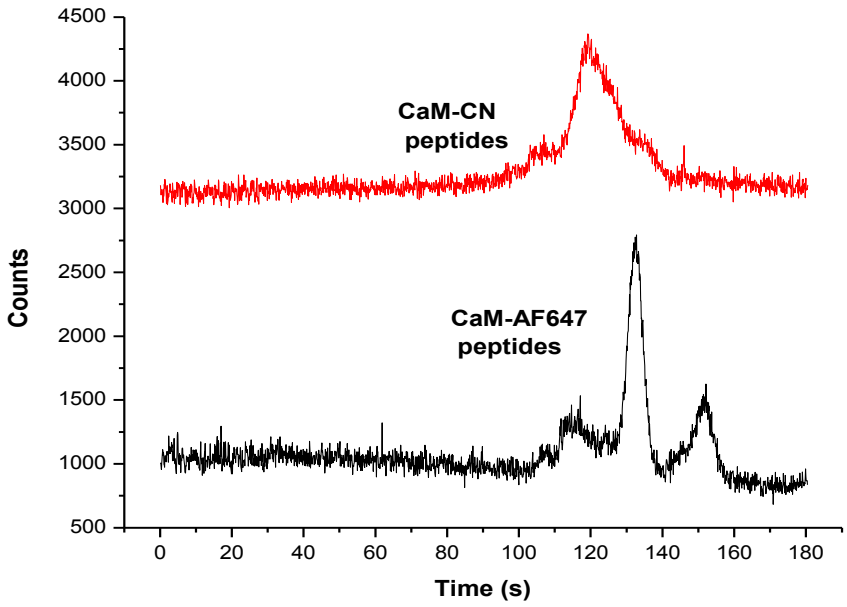

Figure 4.13. Detection of in-gel digested peptides of CaM-CN and CaMAF647 on a microchip. Separation conditions are: 3.5cm PDMS/PMMA chip and detection length ~3 cm. Separation buffer, 4X TBE, pH 8.3, 3.5 mM SDS. Separation was performed with pinched injection and the field strength was 170 V/cm.

Detection of CaM and eNOS in the cross-linked CaM-eNOS sample

Wild type eNOS was a gift from a collaborator and the exact amino acid sequence could not be verified. Hence an isoform of *Homo sapiens* eNOS amino acid sequence was selected in MS analysis. The *Homo sapiens* eNOS sequence (GI: 266648) was used to obtain a FASTA file to use as a reference sequence for CaM. Tryptic digested peptides, which were obtained by MS analysis, were run against reference sequences. CaM was identified with 46% sequence coverage and total of 13 unique peptides (Figure 4.14, panel A) in the CaM-eNOS cross-linked sample. Similarly, eNOS was identified with 20% sequence coverage and a total of 80 unique peptides (Figure 4.14, panel B). This suggests that the cross-linked sample contained both CaM and eNOS. Cumulatively, the MS data verifies the cross-linking of CaM and eNOS.

Panel (A)

HIT 1

Protein Mass: 16828.796 (monoisotopic) 16839.542(average) Protein Score: 60 Protein pp: 498.4
gi|5542035|gb|AAD45181.1|AC006536_1 calmodulin [Homo sapiens]

Sequence:
001 MADQLTEEQI AEFKEAFSLF DKDGDGTITT KELGCVMRSL GQNPTEAELQ DMINEVDADG NGTIDFPEFL TMMARKMKDT DSEEEIREAF RVFDKDGNGY 100
101 ISAAELRHVM TNLGEKLTDE EVDEMIREAD IDGDGQVNYE EFVQMMTAK 149

Sequence Coverage: 46%
Sequence Tag Coverage: 39%

Index	scan#	charge	score	pp	pp2	pptag	m/z	MW(obs)	MW	delta	miss	Unique	sequence + modifications [start:end]
1639	929	+10	45	5.2	5.3	1.7	414.1743	4132.6774	4132.0002	0.6772	0	√	EQIAEFKEAFSLFDKDGDGTITTKELGCVMRSLG
491	871	+4	26	11.8	5.9	4.6	321.4506	1282.7807	1282.6161	0.1645	0	√	LFDKDGDGTITT [19:30]
144	148	+2	50	9.1	9.3	1.7	461.2816	921.5560	921.4524	0.1036	0	√	GDGTITTKE [24:32]
130	140	+2	19	6.1	6.8	1.3	454.2747	907.5420	907.4553	0.0867	0	√	TTKELGCV + CAMC(7) [29:36]
213	514	+2	12	5.6	3.3	2.7	501.2507	1001.4941	1001.5010	-0.0069	0	√	RSLGQNPTE [38:46]
584	569	+2	63	13.7	14.0	3.2	701.3329	1401.6585	1401.6492	0.0093	0	√	SLGQNPTEAELQD [39:51]
72	242	+2	10	6.8	4.5	1.9	423.2010	845.3948	845.3636	0.0313	0	√	GQNPTEAE [41:48]
45	581	+2	12	6.9	6.6	2.0	394.2097	787.4122	787.3832	0.0289	0	√	PTEAELQ [44:50]
104	477	+2	16	4.0	6.9	1.5	440.2112	879.4151	879.4539	-0.0388	0	√	MARKMKD [73:79]
965	983	+4	12	8.3	2.4	4.4	498.7893	1992.1354	1991.9590	0.1764	0	√	TNLGEKLTDEEVDEMIR [111:127]
35	923	+2	22	4.6	6.1	1.8	381.7484	762.4895	762.3815	0.1081	0	√	VDEMIR
36	951	+2	26	9.9	6.1	5.4	381.7488	762.4904	762.3815	0.1090	0	√	VDEMIR [122:127]
170	200	+3	20	8.5	5.0	1.3	321.5078	962.5090	962.4612	0.0478	0	√	VDEMIREA [122:129]

Panel (B)

HIT 1

Protein Mass: 133204.598 (monoisotopic) 133287.907(average) Protein Score: 743 Protein pp: 17246.4
gi|266648|sp|P29474.3|NOS3_HUMAN RecName: Full=Nitric oxide synthase, endothelial; AltName: Full=Constitutive NOS; Short=cNOS

Sequence:
001 MGNLKSVAQE PGPPCGLGLG LGLGLCGKQG PATPAPEPSR APASLLPPAP EHSPPSSPLT QPPEGPKFPR VKNWEVGSIT YDTLSAQAQQ DGPCTPRRCL 100
101 GSLVFPRKLQ GRPSPGPPAP EQLLSQARDF INQYYSSIKR SGSQAHEQRL QEVEAEVAAT GTYQLRESEL VFGAKQAWRN APRCVGRIQW GKLQVFDARD 200
201 CRSAQEMFTY ICNHIKYATN RGNLRSAITV FPQRCPGRGD FRIWNSQLVR YAGYRQQDGS VRGDPANVEI TELCIQHGWT PGNGRFDVLP LLLQAPDEPP 300
301 ELFLLPPELV LEVPLEHPTL EWFAALGLRW YALPAVSNML LEIGGLEFPA APFSGWYMST EIGTRNLCDP HRYNILEDVA VCMDLDTRTT SSLWKDKAAV 400
401 EINVAVLHSY QLAKVTIVDH HAATASFMKH LENEQKARGG CPADWAWIVP PISGSLTPVF HQEMVNYFLS PAFRYQPDPW KGSAAKGTGI TRKKTFKEVA 500
501 NAVKISASLM GTVMAKRVKA TILYGSETGR AQSYAQQLGR LFRKAFDPRV LCMDEYDVVS LEHETLVLVV TSTFGNGDPP ENGESFAAAL MEMSGPYNSS 600
601 PRPEQHKSYK IRFNSISCSD PLVSSWRRKR KESSNTDSAG ALGTLRFCVF GLGSRAYPHF CAFARAVDTR LEELGGERLL QLGQGDELCG QEEAFRGWAQ 700
701 AAFQAACETF CVGEDAKAAA RDIFSPKRSW KRQRYRLSAQ AEGLQLLPGL IHVHRRKMFQ ATIRSVENLQ SSKSTRATIL VRLDTGGQEG LQYQPGDHIG 800
801 VCPPNRPGLV EALLSRVEDP PAPTEPVAVE QLEKGSPGGP PPGWVRDPRL PPCTLRQALT FFLDITSPPS PQLLRLLSTL AEEPREQQEL EALSQDPRRY 900
901 EEWKWFRCPT LLEVLEQFPS VALPAPLLLT QLPLLQPRYY SVSSAPSTHP GEIHLTVAVL AYRTQDGLGP LHYGVCSTWL SQLKPGDPVP CFIRGAPSFR 1000
1001 LPPDPSLPCI LVGPGTGIAP FRGFWQERLH DIESKGLQPT PMTLVFGCRC SQLDHLYRDE VQNAQQRGVF GRVLTAFSRE PDNPKTYVQD ILRTELAAEV 1100
1101 HRVLCLERGH MFVCGDVTMA TNVLQTVQRI LATEGDMELD EAGDVIGVLR DQQRYHEDIF GLTLRTQEVT SRIRTQSFSL QERQLRGAVP WAFDPPGSDT 1200
1201 NSP 1203

Sequence Coverage: 20%
Sequence Tag Coverage: 18%

Index	scan#	charge	score	pp	pp2	pptag	m/z	MW(obs)	MW	delta	miss	Unique	sequence + modifications [start:end]
411	256	+2	10	8.2	3.3	3.4	604.3090	1207.6106	1207.6066	0.0041	0	√	QGPATPAPEPSR [29:40]
722	861	+3	83	19.7	13.5	14.1	548.9644	1644.8785	1644.8704	0.0081	0	√	PSPGPPAPEQLLSQAR
723	891	+3	112	23.4	14.0	18.8	548.9644	1644.8785	1644.8704	0.0081	0	√	PSPGPPAPEQLLSQAR
724	858	+2	27	12.6	3.4	9.3	822.9449	1644.8825	1644.8704	0.0121	0	√	PSPGPPAPEQLLSQAR
725	898	+2	26	11.4	3.3	9.3	822.9474	1644.8875	1644.8704	0.0171	0	√	PSPGPPAPEQLLSQAR [113:128]
563	999	+2	82	16.2	16.2	11.0	689.3424	1377.6775	1377.6685	0.0090	0	√	DFINQYYSSIK
564	1032	+2	41	9.3	13.1	7.1	689.3439	1377.6805	1377.6685	0.0120	0	√	DFINQYYSSIK [129:139]
187	563	+2	42	7.6	10.6	4.1	490.2593	979.5113	979.5095	0.0019	0	√	ESELVFGAK
188	527	+2	62	13.4	9.8	10.4	490.2598	979.5123	979.5095	0.0028	0	√	ESELVFGAK
189	496	+2	58	12.0	10.2	9.1	490.2607	979.5140	979.5095	0.0045	0	√	ESELVFGAK
190	577	+2	31	7.1	10.1	2.7	490.2619	979.5165	979.5095	0.0070	0	√	ESELVFGAK [167:175]

Figure 4.14. Detection of CaM and eNOS in the cross-linked CaM-eNOS sample. Panel (A) sequence coverage of CaM (B) a part of the identified eNOS peptides by MS analysis.

4. 4. Conclusion

Photo-chemical cross-linking of an active protein and its binding enzyme was a challenging task. Even though the CaM binding affinities to CBPs are high, cross-linker modified CaM may present altered affinities toward CBPs. The cross-linking of BPM labeled CaM and eNOS shows low efficiency probably due to the low concentration of BPM labeled CaM in the mixture. NHS-SDA with a short spacer did not yield inter-protein cross-linking in our experimental conditions. NHS-LC-SDA with a long spacer did yield inter-protein cross-linking, and SDS-PAGE and Western blotting revealed the formation of photoproducts. Further, mass spectrometric analysis of the in-gel digested cross-linked sample revealed the presence of both CaM and CBPs in the sample. CaMAF647 (~18 kD) was detected in gel bands which were excised from high MW regions (~75 and ~150 kD) of the gel and this confirms the crosslinking of CaMAF647 with the CBPs. CaMAF647 was successfully cross-linked with CN and eNOS, separately. Multiple labeling of CaMAF647 with the photo-cross-linker was observed. Therefore, a mixture of AF647-labeled species might be formed by the photo cross-linking reaction.

4. 5. References

1. Chin, D., and Means, A. R. (2000) Calmodulin: a prototypical calcium sensor, *Trends Cell Biol 10*, 322-328.
2. Means, A. R. (2004) Calmodulin-mediated signaling. Handbook of Cell Signaling, *2*, 83-85.
3. Mons, N., Enderlin, V., Jaffard, R., and Higueret, P. (2001) Selective age-related changes in the PKC-sensitive, calmodulin-binding protein, neurogranin, in the mouse brain, *J Neurochem 79*, 859-867.

4. O'Day, D. H., and Myre, M. A. (2004) Calmodulin-binding domains in Alzheimer's disease proteins: extending the calcium hypothesis, *Biochem Biophys Res Commun 320*, 1051-1054.
5. O'Day, D. H. (2003) CaMBOT: profiling and characterizing calmodulin-binding proteins, *Cell Signal 15*, 347-354.
6. Berggard, T., Arrigoni, G., Olsson, O., Fex, M., Linse, S., and James, P. (2006) 140 mouse brain proteins identified by Ca2+-calmodulin affinity chromatography and tandem mass spectrometry, *J Proteome Res 5*, 669-687.
7. Jang, D. J., Guo, M., and Wang, D. (2007) Proteomic and biochemical studies of calcium- and phosphorylation-dependent calmodulin complexes in Mammalian cells, *J Proteome Res 6*, 3718-3728.
8. Huang, B., Wu, H., Bhaya, D., Grossman, A., Granier, S., Kobilka, B. K., and Zare, R. N. (2007) Counting low-copy number proteins in a single cell, *Science 315*, 81-84.
9. Quintana, A. R., Wang, D., Forbes, J. E., and Waxham, M. N. (2005) Kinetics of calmodulin binding to calcineurin, *Biochem Biophys Res Commun 334*, 674-680.
10. McMurry, J. L., Chrestensen, C. A., Scott, I. M., Lee, E. W., Rahn, A. M., Johansen, A. M., Forsberg, B. J., Harris, K. D., and Salerno, J. C. (2011) Rate, affinity and calcium dependence of nitric oxide synthase isoform binding to the primary physiological regulator calmodulin, *FEBS J 278*, 4943-4954.
11. Rath, A., Glibowicka, M., Nadeau, V. G., Chen, G., and Deber, C. M. (2009) Detergent binding explains anomalous SDS-PAGE migration of membrane proteins, *Proc Natl Acad Sci U.S.A 106*, 1760-1765.
12. Cho, H. J., Xie, Q. W., Calaycay, J., Mumford, R. A., Swiderek, K. M., Lee, T. D., and Nathan, C. (1992) Calmodulin is a subunit of nitric oxide synthase from macrophages, *J Exp Med 176*, 599-604.
13. Rafikov, R., Fonseca, F. V., Kumar, S., Pardo, D., Darragh, C., Elms, S., Fulton, D., and Black, S. M. (2011) eNOS activation and NO function: structural motifs responsible for the posttranslational control of endothelial nitric oxide synthase activity, *J Endocrinol 210*, 271-284.
14. Tesauro, M., Thompson, W. C., Rogliani, P., Qi, L., Chaudhary, P. P., and Moss, J. (2000) Intracellular processing of endothelial nitric oxide synthase isoforms associated

with differences in severity of cardiopulmonary diseases: cleavage of proteins with aspartate vs. glutamate at position 298, *Proc Natl Acad Sci U S A 97*, 2832-2835.

15. Mondragon, A., Griffith, E. C., Sun, L., Xiong, F., Armstrong, C., and Liu, J. O. (1997) Overexpression and purification of human calcineurin α from Escherichia coli and assessment of catalytic functions of residues surrounding the binuclear metal center, *Biochemistry 36*, 4934-4942.
16. Carruthers, N. J., and Stemmer, P. M. (2008) Methionine oxidation in the calmodulin-binding domain of calcineurin disrupts calmodulin binding and calcineurin activation, *Biochemistry 47*, 3085-3095.
17. Devore, M. S., Gull, S. F., and Johnson, C. K. (2013) Reconstruction of calmodulin single-molecule FRET states, dye-interactions, and CaMKII peptide binding by MultiNest and classic maximum entropy, *Chem Phys 422*.
18. Allen, M. W., Urbauer, R. J., Zaidi, A., Williams, T. D., Urbauer, J. L., and Johnson, C. K. (2004) Fluorescence labeling, purification, and immobilization of a double cysteine mutant calmodulin fusion protein for single-molecule experiments, *Anal Biochem 325*, 273-284.
19. Allen, M. W., Urbauer, R. J., and Johnson, C. K. (2004) Single-molecule assays of calmodulin target binding detected with a calmodulin energy-transfer construct, *Anal Chem 76*, 3630-3637.
20. Farrell, I. S., Toroney, R., Hazen, J. L., Mehl, R. A., and Chin, J. W. (2005) Photo-cross-linking interacting proteins with a genetically encoded benzophenone, *Nat Meth 2*, 377-384.
21. Haywood, J., Mozziconacci, O., Allegre, K. M., Kerwin, B. A., and Schoneich, C. (2013) Light-induced conversion of Trp to Gly and Gly hydroperoxide in IgG1, *Mol Pharm 10*, 1146-1150.
22. http://www.piercenet.com/instructions/2162067.pdf.
23. Gomes, A. F., and Gozzo, F. C. (2010) Chemical cross-linking with a diazirine photoactivatable cross-linker investigated by MALDI- and ESI-MS/MS, *J Mass Spectrom 45*, 892-899.
24. Dremina, E. S., Sharov, V. S., Kumar, K., Zaidi, A., Michaelis, E. K., and Schoneich, C. (2004) Anti-apoptotic protein Bcl-2 interacts with and destabilizes the

sarcoplasmic/endoplasmic reticulum Ca2+-ATPase (SERCA), *Biochem J 383*, 361-370.

25. Tang, X., Sayre, L. M., and Tochtrop, G. P. (2011) A mass spectrometric analysis of 4-hydroxy-2-(E)-nonenal modification of cytochrome c, *J Mass Spectrom 46*, 290-297.
26. Gavin, A.-C., Bosche, M., Krause, R., Grandi, P., Marzioch, M., Bauer, A., Schultz, J., Rick, J. M., Michon, A.-M., Cruciat, C.-M., Remor, M., Hofert, C., Schelder, M., Brajenovic, M., Ruffner, H., Merino, A., Klein, K., Hudak, M., Dickson, D., Rudi, T., Gnau, V., Bauch, A., Bastuck, S., Huhse, B., Leutwein, C., Heurtier, M.-A., Copley, R. R., Edelmann, A., Querfurth, E., Rybin, V., Drewes, G., Raida, M., Bouwmeester, T., Bork, P., Seraphin, B., Kuster, B., Neubauer, G., and Superti-Furga, G. (2002) Functional organization of the yeast proteome by systematic analysis of protein complexes, *Nature 415*, 141-147.
27. Sinz, A. (2010) Investigation of protein–protein interactions in living cells by chemical crosslinking and mass spectrometry, *Anal Bioanal Chem 397*, 3433-3440.
28. Zybailov, B. L., Glazko, G. V., Jaiswal, M., and Raney, K. D. (2013) Large Scale Chemical Cross-linking Mass Spectrometry Perspectives, *J Proteomics Bioinform 6*, 001.
29. Huynen, M. A., Snel, B., von Mering, C., and Bork, P. (2003) Function prediction and protein networks, *Curr Opin Cell Biol 15*, 191-198.
30. Marcotte, E. M., Pellegrini, M., Ng, H.-L., Rice, D. W., Yeates, T. O., and Eisenberg, D. (1999) Detecting Protein Function and Protein-Protein Interactions from Genome Sequences, *Science 285*, 751-753.
31. Rain, J.-C., Selig, L., De Reuse, H., Battaglia, V., Reverdy, C., Simon, S., Lenzen, G., Petel, F., Wojcik, J., Schachter, V., Chemama, Y., Labigne, A., and Legrain, P. (2001) The protein-protein interaction map of Helicobacter pylori, *Nature 409*, 211-215.
32. Sinz, A. (2006) Chemical cross-linking and mass spectrometry to map three-dimensional protein structures and protein–protein interactions, *Mass Spectrom Rev 25*, 663-682.
33. Cho, K. I., Lee, K., Lee, K. H., Kim, D., and Lee, D. (2006) Specificity of molecular interactions in transient protein-protein interaction interfaces, *Proteins 65*, 593-606.
34. Xu, D., Tsai, C. J., and Nussinov, R. (1997) Hydrogen bonds and salt bridges across protein-protein interfaces, *Protein Eng 10*, 999-1012.
35. Moreira, I. S., Fernandes, P. A., and Ramos, M. J. (2007) Hot spots--a review of the protein-protein interface determinant amino-acid residues, *Proteins 68*, 803-812.

36. Chakrabarti, P., and Janin, J. (2002) Dissecting protein-protein recognition sites, *Proteins 47*, 334-343.
37. Paramelle, D., Miralles, G., Subra, G., and Martinez, J. (2013) Chemical cross-linkers for protein structure studies by mass spectrometry, *Proteomics 13*, 438-456.
38. Sinz, A. (2003) Chemical cross-linking and mass spectrometry for mapping three-dimensional structures of proteins and protein complexes, *J Mass Spectrom 38*, 1225-1237.
39. Kent, S. B. H. (2009) Total chemical synthesis of proteins, *Chem Soc Rev 38*, 338-351.
40. Grimsley, G. R., Scholtz, J. M., and Pace, C. N. (2009) A summary of the measured pK values of the ionizable groups in folded proteins, *Protein Sci 18*, 247-251.
41. Madler, S., Seitz, M., Robinson, J., and Zenobi, R. (2010) Does chemical cross-linking with NHS esters reflect the chemical equilibrium of protein-protein noncovalent interactions in solution?, *J Am Soc Mass Spectrom 21*, 1775-1783.
42. Brunner, J. (1993) New photolabeling and crosslinking methods, *Annu Rev Biochem 62*, 483-514.
43. Blencowe, A., and Hayes, W. (2005) Development and application of diazirines in biological and synthetic macromolecular systems, *Soft Matter 1*, 178-205.
44. Hurst, G. B., Lankford, T. K., and Kennel, S. J. (2004) Mass spectrometric detection of affinity purified crosslinked peptides, *J Am Soc Mass Spectrom 15*, 832-839.
45. Clerico, E. M., Szymanska, A., and Gierasch, L. M. (2009) Exploring the interactions between signal sequences and E. coli SRP by two distinct and complementary crosslinking methods, *Biopolymers 92*, 201-211.
46. Besselink, G., and de Korte, D. (2002) Sephadex-based cell-affinity adsorbents: preparation and performance, *Biotechnol Appl Biochem 35*, 55-60.
47. Chattopadhyaya, R., Meador, W. E., Means, A. R., and Quiocho, F. A. (1992) Calmodulin structure refined at 1.7 A resolution, *J Mol Biol 228*, 1177-1192.

Chapter Five

Separation of Calmodulin, Calcineurin and Endothelial Nitric Oxide Synthase using Microfluidic Capillary Electrophoresis

5.1. Introduction

CaM acts as a Ca^{2+} triggered molecular switch, and in response, it regulates more than 100 enzymes in many biological pathways (*1-2*). The development of sensitive and rapid analytical methods is necessary to profile this CBP "interactome." In this present work, a MCE-based method coupled with highly sensitive fluorescence detection was developed to study CBPs. Both the separation and detection were carried out on the same platform and this multi-functionality was utilized in separating CaM-CBP complexes.

We selected CN and eNOS as CaM-binding model proteins in this study. The approach was to separate model proteins in a CaM-CBP interactive state. The separation of intact CaM-CBP complexes was not possible under the denaturing separation conditions of MCE. Consequently, CN and eNOS were photo-cross-linked with CaM as described in Chapter four. AF647-labeled CaM and two standard proteins (BSA and concanavalin A) were used to test the microchip platform as discussed in the Chapter three. A photochemical bi-functional cross-linker (NHS-LC-diazirine) was used to make a covalent link between CaMAF647 and CBP to allow separations under denaturing conditions. The photoproducts of cross-linked CaM-CBP were separated individually and as a mixture. Overall, the goal of this Chapter was to separate photo-cross-linked CaM-CN and CaM-eNOS using different microfluidic devices, such as glass, PDMS/glass, PDMS/PMMA and a Si-nanoparticle colloidal array under different separation modes and conditions. CaM-CN and CaM-eNOS were also separated using CE.

5.2. Materials and methods

All reagents and samples were prepared with doubly-deionized water from an ultrapure water system (Barnstead, Dubuque, IA). Single mutated CaM (T34C-CaM) was obtained from the laboratory of Dr. Carey Johnson (University of Kansas, KS), and was expressed in *E. coli* and purified by a phenyl sepharose column (GE Heathcare, Pittsburg, PA) according to a previously published method (*3*). T34C-CaM was conjugated with AF647 C_2-malemide (Molecular Probes, Eugene, OR). Purified eNOS was kindly provided by Dr. David C. Arnett (Northwestern College, Orange City, IA) and Dr. Anthony Persechini (School of Biological Sciences, University of Missouri, Kansas City, MO). Wild type CN was a kind gift of Dr. Paul M. Stemmer (Wayne State University, Detroit, MI). An amine-reactive diazirine photo-cross-linker, NHS-LC-SDA, and Zeba spin desalting columns were purchased from Pierce, Rockford, IL. SU-8 10 negative photoresist, SU-8 developer and silicon wafers were purchased from Micro-chem, (Newton, MA) and Silicon (Boise, ID). PDMS elastomer and curing agent were purchased from Ellsworth Adhesive (Minneapolis, MN). DDM, Tris base and Tris hydrochloride were purchased from Fisher Scientific (Fair Lawn, NJ). Pt wire was purchased from TedPella (Redding, CA). All the other reagents, unless specified otherwise were purchased from Sigma-Aldrich (St. Louis, MO).

5.2.1. Fabrication of PDMS/glass microfluidic chips.

PDMS microchips were fabricated using standard soft lithography as described previously in Chapter two (*4*). PDMS chips were cast using a 10:1 mixture of the elastomer and the curing agent. In this study, different simple “T” devices and a serpentine device were used.

The fabrication of PDMS/glass hybrid chips was performed in Adams Micro-Fabrication facility (University of Kansas, Kansas). The fabrication process was described in detail in Chapter two.

5.2.2. Fabrication of glass microfluidic chips

Glass microchips with different channel structures were fabricated in the Adams Micro-Fabrication facility, University of Kansas, Kansas.

5.2.3. Fabrication of Si-nanoparticle microfluidic devices

Si-nanoparticle chips were kindly provided by Dr. Yong Zeng (University of Kansas, Kansas). Briefly, a chip with 10 mm separation channel and 4 mm long side arms in a simple "T" format was made. The separation devices were assembled by sealing the replicas to clean glass slides with oxygen plasma oxidation, and the process of colloidal self-assembly was explained previously (*5*). The fabrication process and assembly were described in Chapter two.

5.2.4. Sample preparation

The sample preparation procedure was described in Chapter three. All protein (photo-cross-linked) samples were dissolved in the same run buffer (100 nM), which was used for electrophoresis at a given time. All samples that contained 3.5 mM SDS (unless otherwise specified in the separation conditions) were heat-denatured at 95°C for 5 min before the separation. Stock sample solutions were stored at -20°C and final sample concentrations were

adjusted using the same run buffer as needed. Protein samples and run buffers were filtered using a 0.22 μm syringe filter prior to separations.

5.2.5. Separation of CBPs by CE

The separation conditions that were used in the standard protein separation (Chapter three) were utilized for the separation of CBPs (if otherwise is mentioned). All CE separations were performed in a Beckman P/ACE^{TM} MDQ instrument as described in Chapter three (Beckman, Fullerton, CA). Bare fused-silica capillaries (ID: 50 μm) were used. A module contained a 635 nm laser, fiber optic connector, and photomultiplier tube (PMT) was used in LIF detection.

5.2.6. Preparation of microfluidic devices for separations

The preparation of microfluidic devices was described in Chapter three and four. Briefly, microfluidic device channels were checked using a microscope and any particles in the channels were removed using NaOH or isopropyl alcohol. Usually, all PDMS/glass, PDMS/PMMA and glass chips were conditioned with 0.1 M NaOH, nano pure water, and the run buffer for 5 min each, respectively. Before the separation, the device was checked again for any clogging in the channels. Conversely, Si-nanoparticle microfluidic devices were not subjected to any conditioning. After self-assembly of the colloidal array, the chip was equilibrated with a run buffer for 20 min.

5.2.7. Sample injection

Based on separation modes and types of chips, two electrokinetic injection methods were employed. A sample plug was introduced into the separation channel by manipulating the applied voltages in the reservoirs of the device. Optimum applied voltages were obtained using CaMAF647 injections. Detailed descriptions of sample injection methods were included in Chapter two. Specific voltages, injection times, and other separation conditions were included in relevant figure captions.

5.2.8. Detection and data collection

A semi-automated system was used to control the power supply, HV relay box, detection and data collection as described in Chapter two. Real-time electropherograms and other functions were interfaced using LabVIEW (National Instrument, TX) programs, which were kindly provided by Ryan Grigsby (Adams Micro-Fabrication facility, University of Kansas, KS).

5.3. Results and discussion

5.3.1 Separation of CaM-CBP photoproducts by CE

CaM-CBP complexes were separated by CE using the same capillary and experimental conditions that were used in the standard protein separation (Chapter three, section 3.3.1). Figure 5.1A shows electropherograms obtained for the separation of CaM-eNOS (top) and CaM-CN (bottom) photoproducts separately. In this analysis, HPMC was added to the BGE (75 mM boric acid, pH 9.2, 3.5 mM SDS, and 0.05 % HPMC), and a field strength of 241.9 V/cm was used.

HPMC reduced the EOF and non-specific surface adsorption of analytes onto the capillary wall by coating the capillary surface.

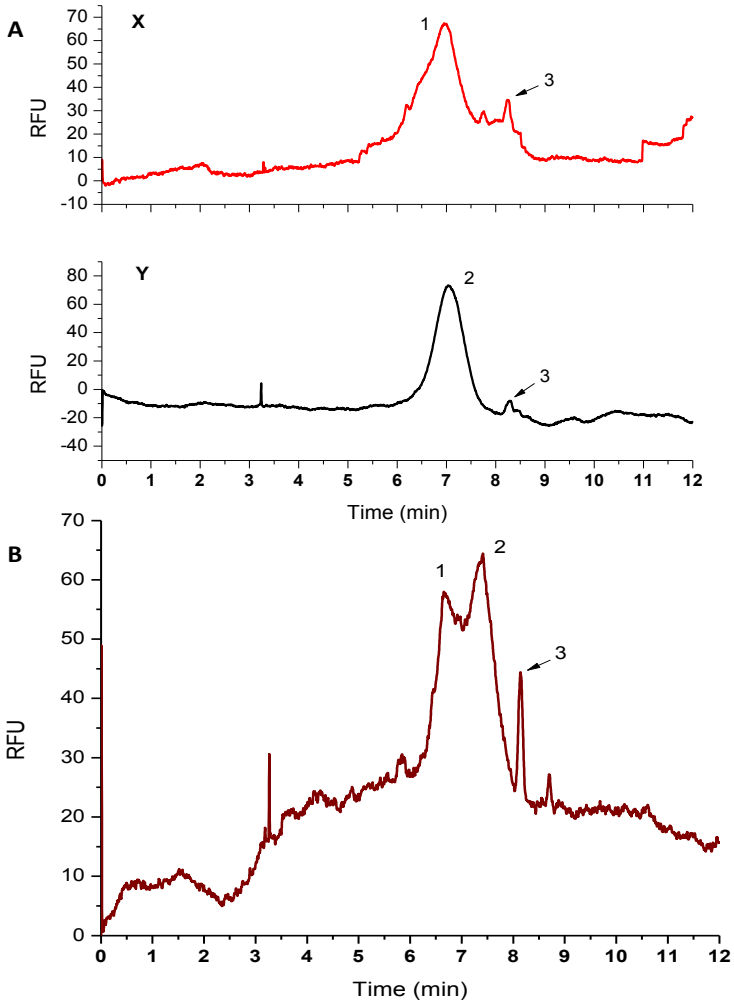

Figure 5.1. Separation of CaM-CBP complexes by CZE. (A) Electropherograms of CaM-eNOS and CaMAF647 (top) and CaM-CN and CaMAF647 (bottom). Peak 1 is CaM-eNOS, peak 2 CaM-CN, and peak 3 is CaMAF647. The separation field strength was 241.9 V/cm. (B) Separation of a mixture of CaM-eNOS and CaM-CN. Peaks 1, 2, and 3 are CaM-eNOS, CaM-CN, and CaMAF647, respectively. The field strength was 241.9 V/cm. Other separation conditions were the same for both panels: 31 cm bare silica capillary (ID: 50 µm), BGE: 75 mM boric acid, pH 9.2, 3.5 mM SDS, 0.05% (w/v) HPMC.

The peaks 1, 2 and 3 in Figure 5.1A were assigned to CaM-eNOS, CaM-CN and CaMAF647, respectively using migration times of individual samples of CaM-CN and CaM-eNOS, respectively (Figure 5.1A). The same separation conditions were used to separate a mixture of CaM-CN and CaM-eNOS (Figure 5.1B). However, a mixture of CaM-CN and CaM-eNOS photoproducts could not be fully resolved using the same experimental conditions.

5.3.2. Separation of CaM-CBP photoproducts by gated injection with MCZE

MCE separation of CBPs was carried out by the microchip platform. CaM-CBP complexes used in this study were obtained by cross-linking CaMAF647 with CN and eNOS using NHS-LC-SDA. For the CBP separation, different microfluidic devices (glass, PDMS/glass, PMMA/glass, Si-nanoparticle array), different injection methods (gated and pinched), and different run buffers (Tris, HEPES, TBE and boric) were tested to achieve the highest possible resolution. Gated injection was driven by EOF, and cross injection was based on the electrophoretic mobility of run buffers. MCZE was achieved only under gated injection in our experimental conditions. Different separation conditions and modes were tested for the standards proteins and only successful methods were used for CBPs separations. The different separation conditions and modes tested for the standard proteins were summarized in Chapter three, Table 3.2.

5.3.2.1. Separation of CaM-CBP photoproducts with gated injection using PDMS/glass chips

PDMS/glass hybrid chips were employed for the separation of CBP photoproducts under the MCZE mode, and 3.5, 5-cm channel simple "T" chips and 10-cm channel serpentine chips were used.

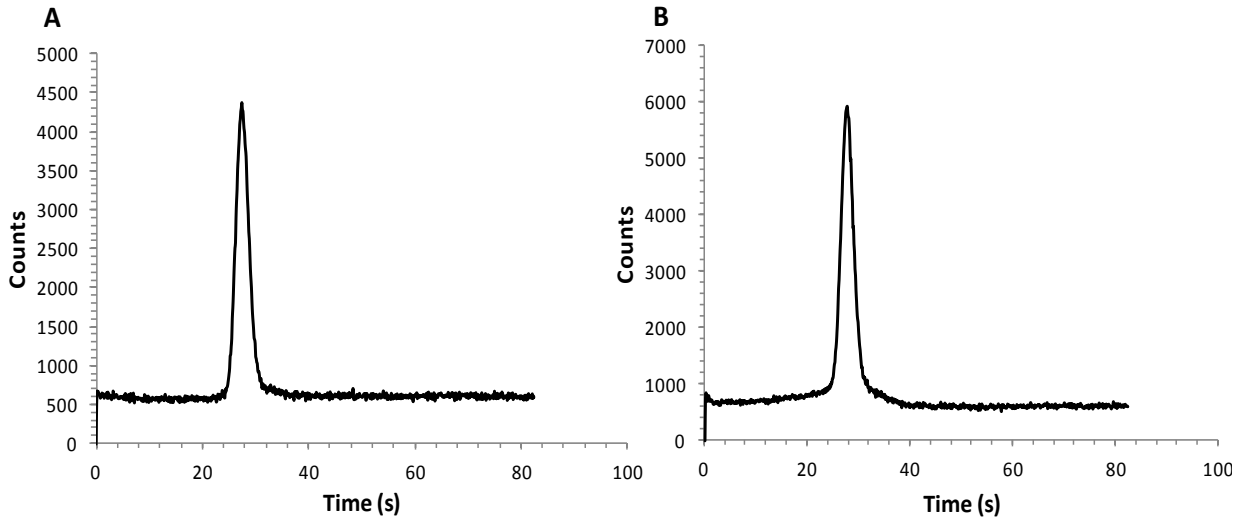

Figure 5.2. Electropherograms of photo-cross-linked CaM and eNOS photoproducts with a 3.5 cm PDMS/glass microchip. (A) Electropherogram shows the photoproducts of CaM-eNOS. (B) Electropherogram shows the co-migration of CaMAF647 and CaM-eNOS photoproducts in a mixture of CaM-eNOS photoproducts with externally added CaMAF647, which was labeled with the cross-linker. The analyte concentration was ~100 nM. BGE: 100 mM boric acid, pH 9.2, and 3.5 mM SDS. The detection length was ~3 cm from the place of injection. An applied separation voltage of 2.0 kV (~570 V/cm) and gated injection were used with 0.4 s injection times.

An electropherogram obtained for the separation of CaM-eNOS photoproducts is shown in Figure 5.2A. The composition of BGE was 100 mM boric acid, pH 9.2 and 3.5 mM SDS. The separation length of PDMS/glass chip was 3.5 cm and detection length was ~3 cm. The applied separation voltage was 2.0 kV (~570 V/cm) and gated injection was used with a 0.4 s injection

time. A sample of CaMAF647, which was labeled with the cross-linker, was added to a sample of CaM-eNOS photoproducts and the obtained electropherogram is shown in Figure 5.2B. Both electropherograms show only one peak and it represents at least two analytes, unreacted cross-linker labeled CaMAF647 and CaM-eNOS photoproduct.

This co-migration might be due to the small difference in electrophoretic mobilities of two analytes. A high field strength in the separation channel created relatively high cathodic EOF and it caused fast movement of analyte ions. These fast moving negatively-charged analytes had an inadequate time for zone separation before they reached to the detection point. As a result of high field strengths in the separation channel, relatively high cathodic EOF was created, and it caused fast bulk flow. The fast moving analytes created a low peak capacity and less time for electrophoretic separation of analyte bands. Thus, the photoproducts co-migrated with unreacted CaMAF647 (Figure 5.2). This observation was consistent for both 3.5 and 5 cm PDMS/glass chips.

Since the PDMS/glass substrate has a relatively low number of negatively-charged silanol groups compared to glass, a relatively low EOF can be obtained with low pH run buffers. In low pH buffers obtaining reproducible gating was difficult under conditions that suppress EOF, especially when BGE was modified with additives, such as DDM or HPMC (Chapter three, Table 3.2).

High pH and low pH buffers were tested in these separation conditions, and it was difficult to gain a reproducible gating in those chips when run buffers with pH<7.8 were used. Lower pH in BGE created relatively low EOF, and it was difficult to establish gating under conditions of low EOF. Even with high pH buffer (boric acid), relatively high voltages at the

sample reservoir and buffer reservoir leads were required to establish an effective and efficient gating.

Next, the separation length was increased to improve the peak capacity and separation. In order to increase the separation length, serpentine PDMS/glass chips (10 cm) were designed and fabricated; high voltages, such as 5 and 7.5 kV were placed in the buffer and sample reservoir, respectively to obtain leak-free reproducible injections. High field strength (750-1000 V/cm) increased the Joule heating and reagents were quickly heated. This led to chip failure within a short period of time. Therefore, 10 cm serpentine PDMS/glass chips could not be utilized in gated injections under my experimental conditions.

5.3.2.2. Separation of CaM-CBP photoproducts using glass microfluidic devices

Next, 10 cm serpentine glass chips were tested to get better separations of CBPs. As discussed earlier, long separation channels were introduced to promote the electrophoretic mobility of individual analytes against the dispersive EOF. Glass chips contained cast reservoirs and thus larger solution reservoirs compared to PDMS/glass chips. Large volumes of BGE reduced the effect of Joule heating, and also glass has better thermal conductivity than PDMS (*6*). As a result, glass chips could be continuously used in multiple runs without changing reagents. Since glass is more tolerant to high separation fields than PDMS, a glass chip with a longer separation channels was selected as an alternative to PDMS/glass chips.

Figure 5.3 shows the separation of CaM-CN photoproducts in a 10 cm glass serpentine chip. The sample was dissolved in the same run buffer for this MCZE analysis. In this separation, the detection length was ~8 cm and BGE was 50 mM boric acid, pH 9.2 containing

3.5 mM SDS. These separation conditions provided the best separation in this analysis. Higher pH and higher field strengths generated relatively high EOF. EOF was adjusted by changing BGE conditions (pH and ionic strength), but some of the low abundant photoproducts could not be detected likely due to the band broadening and co-migration. Low ionic strength buffers reduced the resolution whereas high ionic strength buffers such as 150 mM boric acid, pH 9.2 resulted in inconsistent gating due to high Joule heating and electrolysis.

The photoproducts of CaM-CN were assigned to peak 1 and peak 3 and their signal-to-noise ratio (S/N) was above 5 for peak 1 (Figure 5.3A, bottom panel). The unassigned small peak that has the lowest migration time is less intense with respect to other two peaks (peak 1and 3). A sample of CaMAF647 was added into a sample of CaM-CN photoproduct, and the mixture was analyzed using the same conditions discussed above. AF647 was also included in the mixture as a positive marker during this separation. Figure 5.3A (top) shows the separation of a mixture of AF647, CaMAF647 and CaM-CN photoproducts; peak 1and 3 were assigned to CaM-CN photoproducts, and peak 2 and 4 were assigned to CaMAF647 and AF647, respectively. The total protein concentration used in Figure 5.3B (bottom) was ~100 nM, and a mixture of CaMAF647 (~150 nM) and AF647 (10 nM) was added to the sample of CaM-CN photoproducts. Panel B shows the separation of CaMAF647 and AF647, and the identity of the AF647 peak was confirmed by spiking with AF647 (Figure 5.3B). The same separation conditions used in panel A except the separation length (~7 cm) was used for the separation of a mixture. This data was obtained in a separate experiment to determine the migration times of CaMAF647 and AF647. CaMAF647 was assigned by the peak shape, peak intensity and migration time, and CaMAF647 eluted first, followed by AF647.

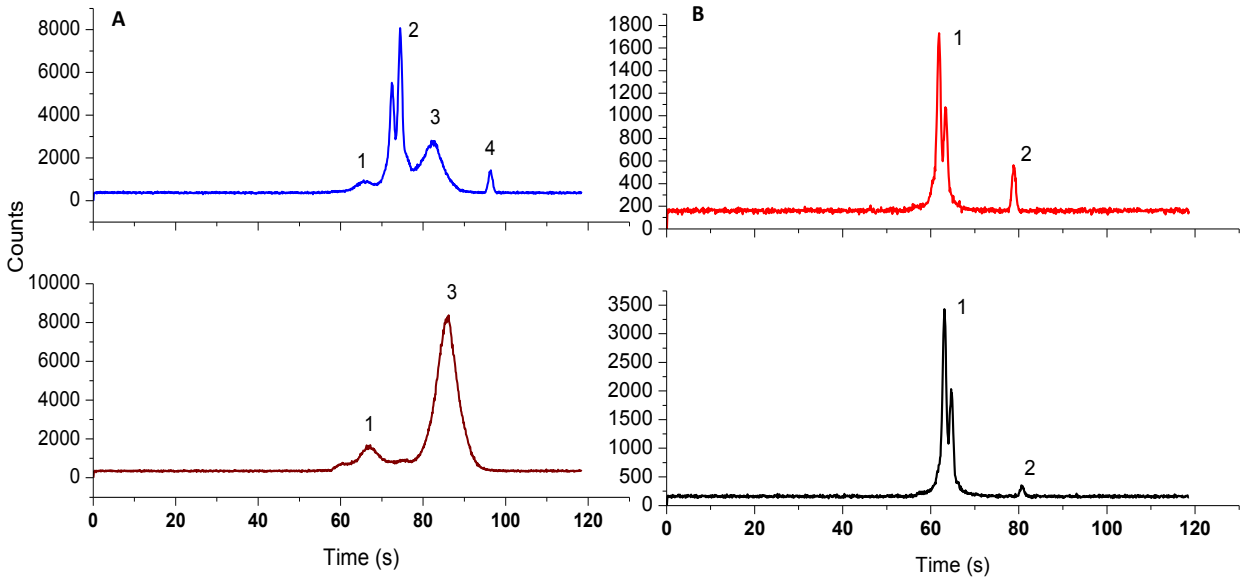

Figure 5.3. Separation of CaM-CN photoproducts using a 10 cm serpentine glass chip. Panel A: the cross-linking concentration ratio of CaM-AF 647 and CN was 1:1**.** The separation conditions were as follows: separation buffer composition was 50 mM boric acid, pH 9.2 3.5 mM SDS, separation potential 7.5 kV, injection time 0.3 s. The detection length was ~8 cm. Top: separation of CaM-CN photoproducts, CaMAF647, and AF647. Bottom: separation of CaM-CN photoproducts. A mixture of CaMAF647 and AF647 was added to the sample of CaM-CN photoproducts, relative concentration of CaMAF647 and AF647 was ~150 nM and ~10 nM, respectively. After adding the mixture of CaMAF647 and AF647 the top electropherogram was obtained. Peak 1 and 3 are assigned to CaM-CN photoproducts. Peak 2 and 4 are CaMAF647 and AF647. Panel B: separation of CaMAF647 and AF647 (a lower concentration sample than the added sample of CaMAF647 and AF647 in panel A) using the same separation conditions except the detection length (~7 cm) on a different day. Bottom: a mixture of CaMAF647 and AF647. Top: a sample of AF647 was spiked to the sample used to take the bottom electropherogram. Peak 1 and 2 were identified as CaMAF647 and AF647, respectively.

Under MCZE with normal polarity, the net flow of negatively charged proteins was towards the cathodic lead and the separation was based on the size-to-charge ratio. Both sample and run buffer contained SDS and therefore, all analytes had the same charge density. As a result, proteins should separate based on the size (large proteins should elute first and small proteins last).

According to the migration times, the photoproduct that eluted at ~65 s (peak 1) should be larger than the photoproduct that eluted at ~85 s (peak 3) (Figure 5.3A, top panel). However, the addition of CaMAF647 into the separation mixture showed the photoproduct that corresponds to peak 3 should be smaller than the CaMAF647, and this determination was based on the expected elution order of cathodic EOF-based MCZE. The deviation of migration time may be due to relatively low mobility of the photoproduct (peak 3), and thus may tend to interact with the channel surface. It is also possible that peak 3 corresponds to a CaM-CaM cross-linked product. This had been observed with the standard protein separation under the same conditions (CaM eluted before BSA, Chapter three, Figure 3.9). The interactions of proteins with the channel surface affected the migration time. Also, changing buffer condition and thus the mobility of proteins may alter migration times. Non specific interactions of proteins with unmodified surface channels were reported in the literature (*7-9*). The interactions are detrimental to the resolution and sensitivity of the separation.

Figure 5.4 shows the separation of CaM-eNOS photoproducts in a 10 cm glass serpentine chip. The sample was dissolved in the same run buffer for this MCZE analysis. In this separation, the detection length was ~8 cm and BGE was 50 mM boric acid, pH 9.2 containing 3.5 mM SDS. In this separation, CaMAF647 (peak 1) was eluted before CaM-eNOS photoproduct (peak 2).

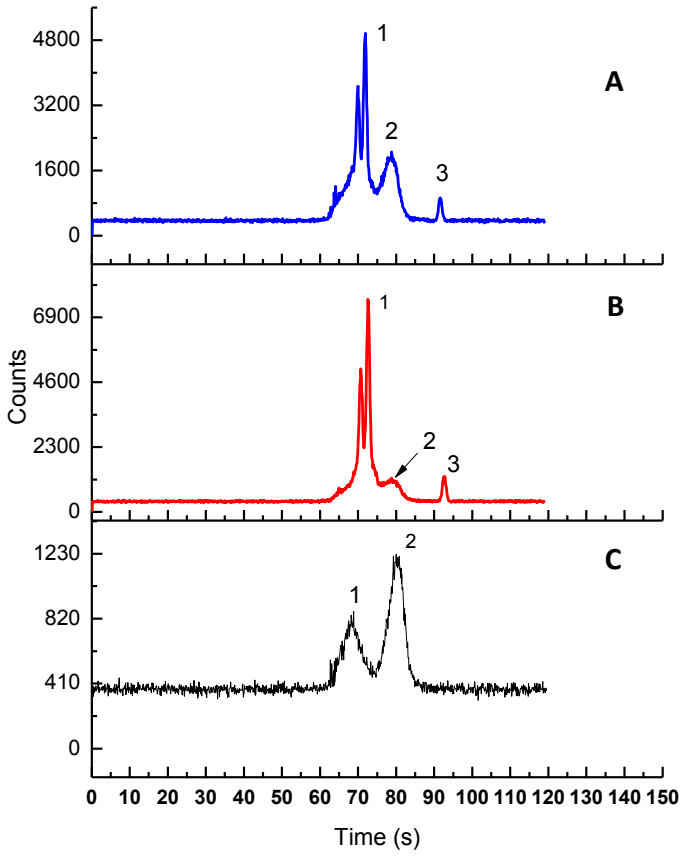

Figure 5.4. Separation of CaM-eNOS photoproducts using a 10 cm glass serpentine microchip. The cross-linking concentration ratio of CaMAF647 and eNOS was 1:1**.** The separation conditions were as follows: separation buffer composition was 50 mM boric acid, pH 9.2, 3.5 mM SDS, separation potential 7.5 kV, injection time 0.3 s, detection length ~8 cm. (A) The electropherogram was obtained by spiking a sample of CaM-eNOS into the sample that gave the electropherogram in Figure 5.4B. Figure 5.4A shows CaMAF647 (peak1), CaM-eNOS (peak 2), and AF647 (peak 3). (B) Addition of CaMAF647 addition into the sample that gave the electropherogram in 5.4C (C) Separation of CaM-eNOS photoproducts.

The electropherogram in Figure 5.4C shows the separation of CaM-eNOS photoproducts. The same separation conditions which were used to obtain the electropherogram in Figure 5.3 were also used in this experiment. A sample of CaMAF647 was added to the mixture of CaM-eNOS, followed by electrophoretic separation, and the obtained electropherogram shows three major peaks (Figure 5.4B). Increasing the concentration of CaM-eNOS in the sample by spiking

a sample of CaM-eNOS resolved the peak 2 (Figure 5.4A). Peak 1, peak 2, and peak 3 were assigned as CaMAF647, CaM-eNOS photoproducts and AF647, respectively. CaM eluted first, followed by CaM-eNOS photoproducts and AF647 (Figure 5.4A).

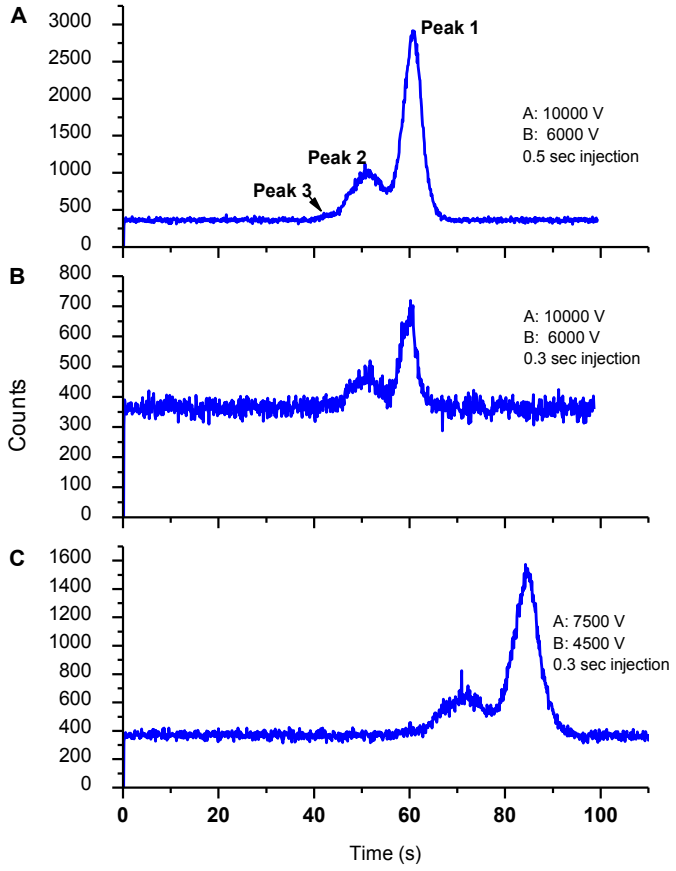

Figure 5.5. Separation of a mixture of photoproducts of CaM-CN and CaM-eNOS by a 10 cm glass serpentine microchip. The cross-linking concentration ratio of CaMAF647 and CBP (CN and eNOS) was 1:1**.** The separation conditions were as follows: separation buffer composition is 50 mM boric acid, 3.5 mM SDS, pH 9.2, separation potential 7.5 kV, injection time 0.3 and 0.5 s. The detection length was ~8 cm. Panels (A), (B), and (C) show the effects of field strengths and injection times.

A mixture of CaM-CN and CaM-eNOS photoproducts was separated by a 10 cm glass serpentine microchip under the same conditions described in the previous section. The

electropherogram in Figure 5.5C shows the separation of a mixture of CaM-CN and CaM-eNOS photoproducts. An increase of injection time from 0.3 to 0.5 s increased peak heights (Figure 5.5A and B). In contrast, the increase of field strength decreased the peak height under the same injection time (Figure 5.5B and C). The increase of field strength increased the velocity of the fluid flow. Therefore, the available volume of sample for injection at the channel cross-junction (where fluidic gate establish in gated injection) was smaller in comparison to a fluid flow with a lower velocity. As a result, the volume of the sample plug injected into the separation channel under a relatively high voltage (Figure 5.5B) was smaller than that of a low voltage (Figure 5.5C) and the smaller injection volume caused smaller peaks (Figure 5.5B). In contrast, relatively a long injection time (0.5 s) applied under the same high field strength gave relatively a large injection volume and resulted relatively large peaks (Figure 5.5A).

Sampling biases in electrokinetic injections and such electropherograms that do not represent actual concentrations of analytes, were observed in my experiments and also were reported in the literature (*10-13*). Analytes that have different electrophoretic mobilities enter microchannels at different rates and this leads to sampling bias. Further, it was very difficult to maintain high voltages due to Joule heating and electrolysis and generated air bubbles caused chip failure. Peak 1 was common to both CaM-CN and CaM-eNOS photoproducts and difficult to separate further in these experimental conditions (Figure 5.5A). Applying different field strengths (5-10 kV), ionic strengths (10-150 mM boric acid) and separation lengths (4-9.5 cm) did not improve the resolution of co-migrating peaks. Also, BGE with different pH (pH 8.2-10, boric acid) was tested to improve the resolution of the co-migrating peaks. To obtain conditions that minimize EOF, a polymer additive, HPMC was used. Even with very low concentrations of HPMC (0.01% w/v) it was impossible to obtain reproducible gated injections. This might be due

to coating of channel surfaces by HPMC, and this dynamic coating might reduce not only the adsorption of proteins but also EOF. The reduction of EOF decreased the ability to establish the fluidic gate and hence the reproducibility of gated injections.

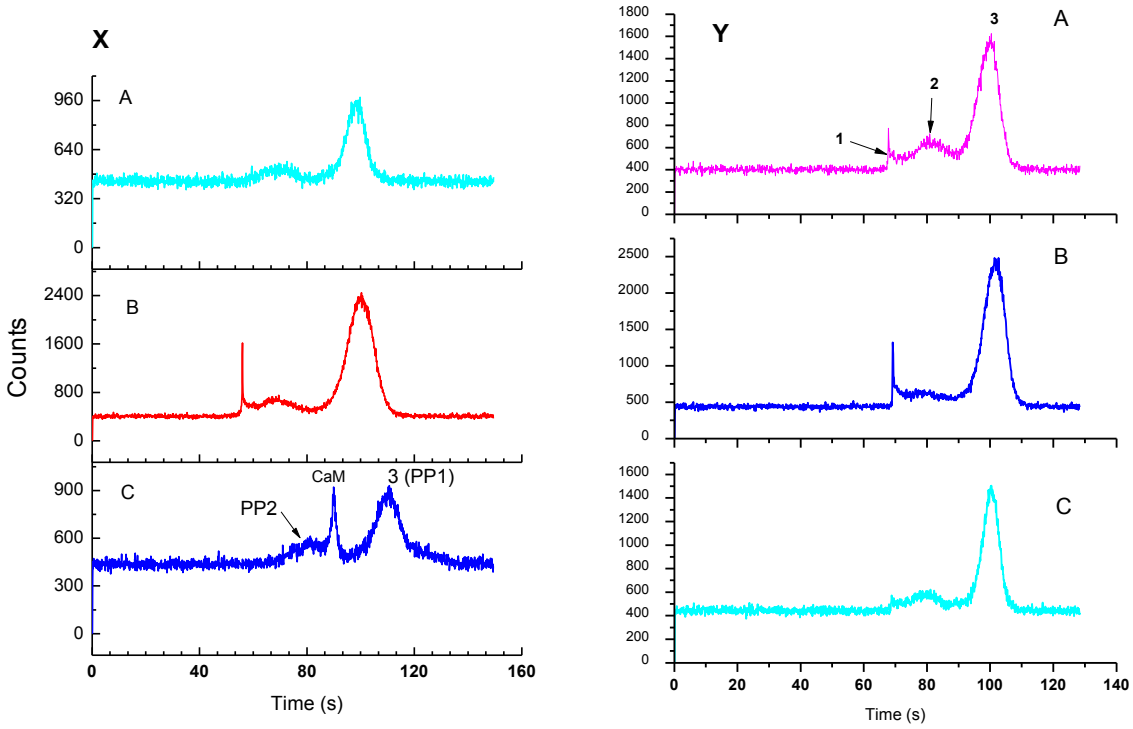

Figure 5.6. Separation of CaM-CN and CaM-eNOS photoproducts using a 10 cm glass serpentine microchip with Tris buffer. The cross-linking concentration ratio of CaM-AF647 and CBP (CN and eNOS) was 1:1. The separation conditions were as follows: separation buffer composition was 12 mM Tris, pH 8.5, 3.5 mM SDS, separation potential 9.0 kV, gated injection time was 0.5 s. The detection length was ~8 cm. Panel X shows the electropherograms of a mixture of CaM-CN, CaM-eNOS, and CaMAF647. Panel XA shows the electropherogram of a mixture of CaM-CN and CaM-eNOS. Panel XB shows spiking of CaM-CN into the sample of panel XA. Panel XC shows the spiking of CaMAF647 to the sample of panel XB. CaM AF647 was in between peak 3 and PP2, but the identity of PP2 could not be verified. Peak 3 is the common peak for both CaM-CN and CaM-eNOS. Panel Y shows the electropherograms of a mixture of CaM-CN, and CaM-eNOS. Panel YC shows an electropherogram of CaM-CN and CaM-eNOS. Panel YB shows an electropherogram obtained after adding a sample of CaM-CN to the sample that gave YC. Panel YA shows an electropherogram obtained after adding a sample of CaM-eNOS to the sample that gave YB. Peak 3 is common for both CaM-CN and CaM-eNOS samples, and peak 1 was assigned to CaM-CN and the identity of peak 2 could not be verified (Peak 2 could be CaMAF647 or a photoproduct of CaM-eNOS).

To overcome the limitations discussed so far, another run buffer was tested to gain better separation conditions. A low conductive Tris buffer was introduced to reduce the EOF and lower Joule heating without adding BGE modifiers. Here, a 10 cm glass chip was used and the detection length was kept ~8 cm. With the separation voltage of 9.0 kV, 12 mM Tris, pH 8.5 containing 3.5 mM SDS was used as the run buffer. Reduction of ionic strength further decreased the Joule heating. Figure 5.6X shows the detection of CaM-CN, CaM-eNOS and CaMAF647 in a mixture. Spiking data of CaMAF647 is shown in the Figure 5.6XC. Detection of a mixture of CaM-CN and CaM-eNOS photoproducts, in a different experiment is shown in Figure 5.6Y. The total analyte concentration of the mixture was ~60 nM and two distinct peaks were identified (peak 1 and peak 3). The Peak 3 is common for both CaM-CN and CaM-eNOS, and it is possible that peak 3 corresponds to a CaM-CaM cross-linked product. Peak 1 and 2 were assigned as CaM-CN and CaMAF647, respectively using spiking with CaM-CN and CaMAF647, respectively (Figure 5.6XC). However, other peaks could not be assigned. The low abundance of photoproducts (for example PP2) made it difficult to identify the individual photoproducts. The Joule heating and high surface adsorption of analytes onto the channel surface caused an adverse effect during the chip operation. This caused unsuccessful gating and led to chip failure. High surface adsorption can be related to variations of peak heights, migration times, and band broadening from run-to-run.

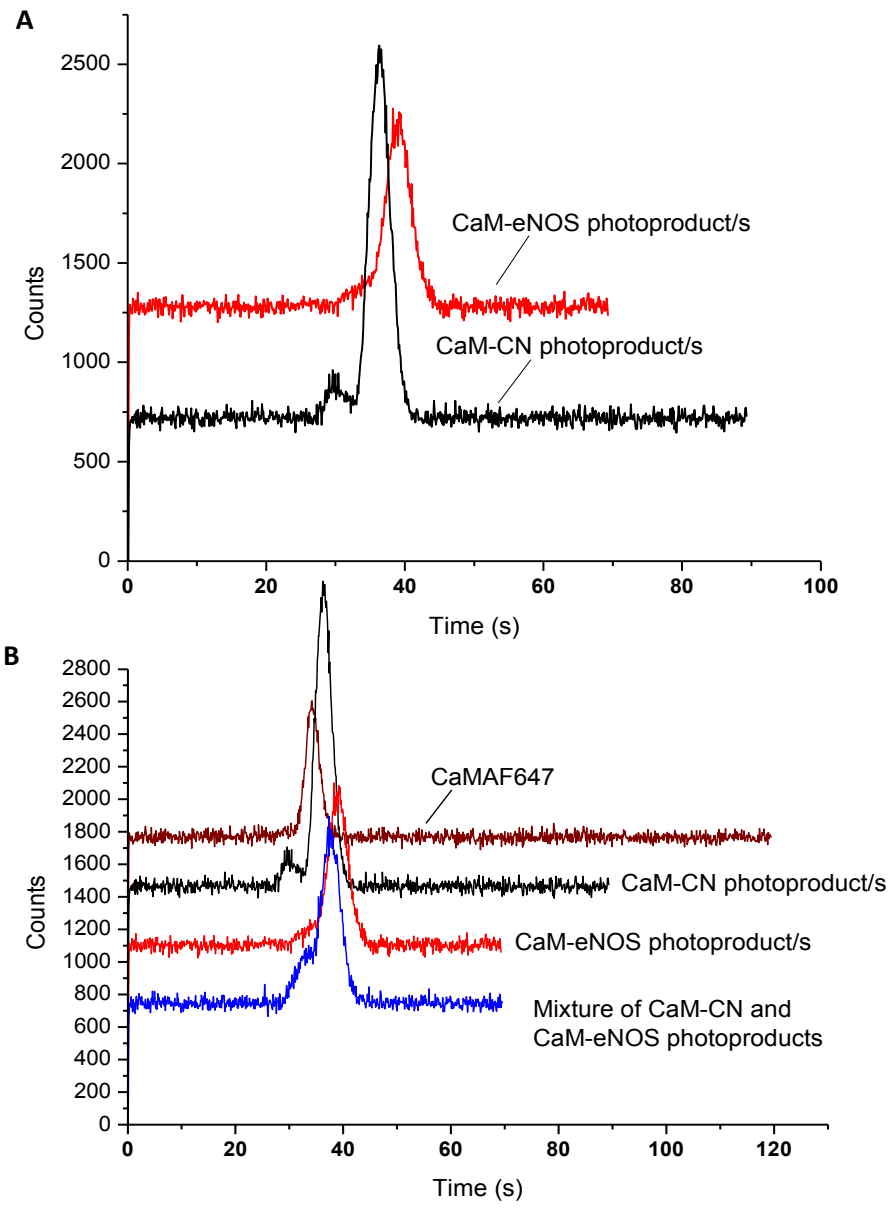

Figure 5.7. MEKC separation of CaM-CN and CaM-eNOS photoproducts using a 5 cm simple "T" glass chip. The cross-linking concentration ratio of CaMAF647 and CBP (CN and eNOS) was 1:1**.** The separation conditions were as follows: separation buffer composition was 20 mM HEPES, pH 7.9, 0.1% DDM (w/v), 3.5 mM SDS, separation potential 2.5 kV, gated injection time 0.3 s, detection length ~3 cm. (A) An overlay of electropherograms obtained for the detection of CaM-CN and CaM-eNOS photoproducts, separately. Time offset is 0% and counts offset is 20%. (B) An overlay of electropherograms for the detection of a mixture of CaM-CN and CaM-eNOS photoproducts, individual CaM-CPB photoproducts, and CaMAF647. Time offset is 0% and counts offset is 40%.

To minimize the above mentioned drawbacks, a different glass chip design, simple "T" was introduced. In this analysis, the separation mode was MEKC and DDM was used to reduce the EOF. Hydrophobic DDM dynamically coats the glass surface and reduces EOF. To further reduce EOF and Joule heating, 20 mM HEPES, pH 7.9 was used under lower pH conditions than boric acid (*14*). Interaction of the proteins with DDM-SDS micelles determines the separation (as described in the Chapter three, Figure 3.10). Two different migration times were observed for CaM-CN, when it was separated individually and in a mixture of photoproducts (Figure 5.7.A and B). But it was difficult to separate CaM-CBP photoproducts in a mixture with different separation conditions such as changing field strength, and the BGE conditions. To increase the resolution, surface coating was required to reduce EOF, which would increase apparent mobility of protein-micellar complexes. But gated injection requires higher field strength and conditions that create strong EOF; therefore, the electrophoretic migration could not be improved under these conditions. It was difficult to carry out separations with gated injection and CZE or MEKC under conditions that suppress EOF.

5.3.3. Separation of CaM-CBP photoproducts by pinched injection

Next, other separation modes, such as microchip MEKC and microchip-based sieving methods were considered. These separation modes required a different injection mechanism and were performed under conditions that suppress EOF. Gated injection is not efficient with low EOF and thus it was essential to have a different injection mechanism. For that pinched injection with "pull back" mechanism was utilized. As explained in Chapter two, three leads of the high voltage power supply were manipulated using a high voltage relay box to perform injections and

separations. Additives, such as HPMC and a high ionic strength buffer, 4X Tris-borate EDTA, pH 8.3, were used. All separations were based on the electrophoretic mobility of negatively-charged analytes.

Different chips such as PDMS/glass PDMS/PMMA and Si-nanoparticle colloidal array microchips were used for CaM-CBP photoproduct separation with this injection method. Promising results obtained from those methods are discussed in the following paragraphs.

5.3.3.1. Separation of the CaM-CBP photoproducts with PDMS/glass microchip

Figure 5.8 shows the separation of a mixture of CaM-CN and CaM-eNOS using cross-injection. A sample plug was introduced into the separation channel of a 3.5 cm PDMS/glass chip. The detection length was ~1.5 cm and the run buffer was 4X TBE (356 mM Tris-borate, 8 mM EDTA), pH 8.3. This low conductive, high ionic strength run buffer maintained low EOF. Additionally, 0.05% (w/v) HPMC (~90 kDa) was used to obtain conditions that suppress EOF. To promote the formation of micelles 10 mM SDS was used in both sample and run buffer.

Figure 5.8 shows four distinct peaks, but the peak that represents CaM-eNOS photoproduct (in between peak 2 and peak 3) was not prominent due to band broadening, and it was difficult to increase its peak height by changing the sample concentration without compromising the resolution of the other three peaks. The peaks were identified using migration times. Figure 5.9 shows the verification of CaM-CN and CaM-eNOS peaks. Multiple runs of the above analysis are shown in Figure 5.8A, and consistent gated-injections and migration times were maintained throughout the analysis. The observed deformed peak shapes were related to the presence of HPMC in the run buffer, as reported in previous studies (*15*).

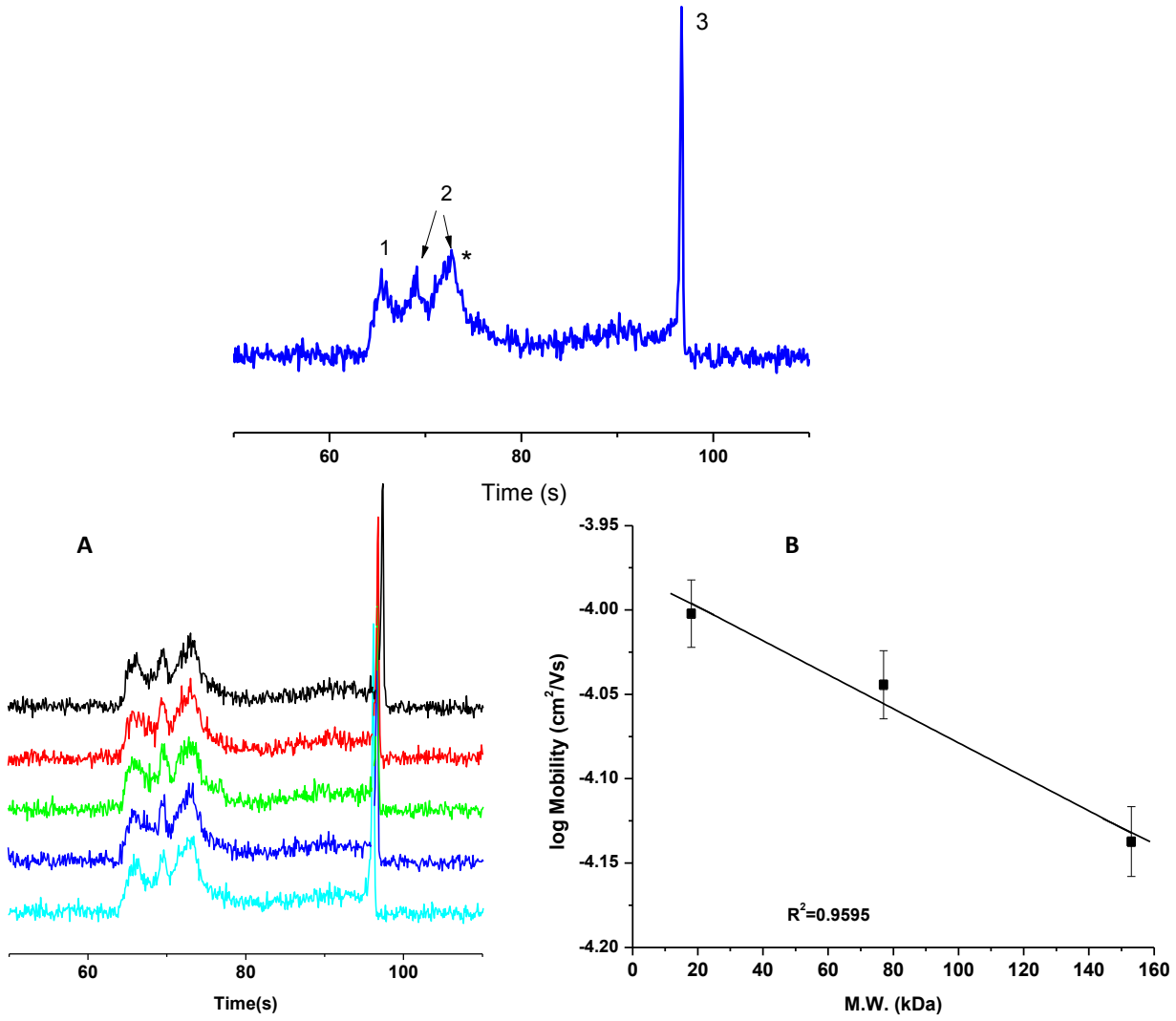

Figure 5.8. Separation of CaM-CN and CaM-eNOS photoproducts using conditions that suppress EOF with a PDMS-glass chip. Simple "T" PDMS/glass chip with a 3.5 cm separation channel was used and the separation conditions as follows: 4X TBE, pH 8.3, 0.05% (w/v) HPMC, 10 mM SDS, separation potential 800 V and detection length ~1.5 cm. Peak 1 represents CaM and peak(s) 2 represents CaM-CN photoproducts, and peak 3 was assigned to CaM-eNOS photoproducts. **(**A) Consecutive multiple runs (n=5) show consistent migration times (B) Apparent mobility vs. molecular weight of analytes and the least square linear fit of the two parameters, R^2=0.9595 and $\log \mu = -0.001MW - 3.978$. Peak (CaM-CN) labeled with * used for mobility calculation (top panel) and calculation of mobility is described in Chapter three.

To demonstrate the observed elution order with respect to molecular weights of proteins and their mobilities, a semi-empirical model was tested and the relationship between the log of apparent mobility, log μ, and the molecular weight, MW, was studied. The relationship between log μ and MW (M) was derived using the Ogston sieving model (Chapter three, Equation 10). The log of apparent mobility of the analytes and their molecular weights were fitted using a least square linear fit model with R^2=0.9595 (Figure 5.8B). The linearity shows the separation is consistent with the Ogston sieving model. The model explained the relationship between molecular weight and mobility in a sieving media; it predicts that the largest molecule has the lowest mobility and the fastest molecule has the lowest molecular weight. This deviation might be explained by the presence of HPMC in the run buffer. HPMC, which was used to suppress EOF, might also act as a sieving matrix inside the separation channel, causing large molecular-weight analytes to elute at higher migration times. The run buffer contained HPMC (viscous polymer) acted as "polymeric gel" in this analysis giving an elution order, which is similar to microchip gel electrophoresis (*16-17*).

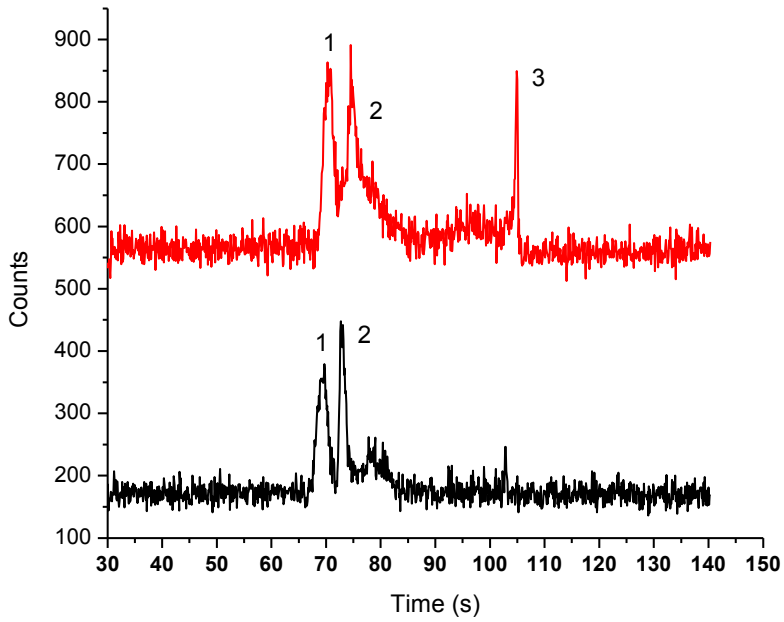

Figure 5.9. Identification of CaM-CN, CaM-eNOS photoproducts using conditions that suppress EOF and PDMS-glass chip. Separation conditions were as same as Figure 5.8. Only the chip and sample concentrations were different. Top: separation of CaM-CN and CaM-eNOS in a mixture. Bottom: separation of CaM-CN. Peak 1 is CaM and 2 represent CaM-CN photoproducts. Peak 3 represents CaM-eNOS photoproducts.

The separation mode in this analysis was MEKC and the elution order was from larger molecules to smaller molecules. The observed elution order of this analysis contradicts with the theoretical elution order explained by Shadphour et.al. (*18*). They reported typical MEKC elution order, in which large analytes elute first followed by the smaller analytes. In my experimental conditions smaller molecules eluted first, followed by larger molecules (Figure 5.9). Migration time comparisons with individual separations confirmed CaM-eNOS photoproducts (~153 kDa) as the largest analyte, and it eluted after the smaller CaM-CN photoproducts (~77 kDa) (Figure 5.9).

5.3.3.2. Separation of CaM-CBP photoproducts with a PDMS/PMMA microfluidic device

To achieve conditions that further suppress EOF, PDMS/PMMA chips were introduced (*16*). With the same separation conditions and the run buffer, a mixture of CBPs were separated using a PDMS/PMMA chip, and the obtained electropherogram shows four distinct peaks (Figure 5.10). According to migration time and spiking, peak 1 is CaM and peak 2 represents CaM-CN photoproducts, and peak 3 represents CaM-eNOS photoproducts.

Identification of CaM-eNOS photoproducts with spiking shows in Figure 5.11. The elution order was the same as in Figure 5.8. The relationship between log μ and MW (M) was derived by the Ogston sieving model (Chapter three, Equation 10). Further, based on the analyte mobilities, the linear least-squares fit between the molecular weight and log of apparent mobility showed in Figure 5.10B shows a linear relationship (R^2=0.9897), and it was consistent with the theoretical elution order of microchip gel electrophoresis which can be explained by the Ogston sieving model (*16*).

However, the adjustment of analyte concentrations, field strengths, and run buffer conditions did not improve the resolution in PDMS/glass or PDMS /PMMA chips. Getting reproducible gating became very challenging due to viscous HPMC in the run buffer, which created plaque buildup on the channel wall. Highly viscous and hydrophobic HPMC adsorbed onto the PDMS channel wall and the buildup was detected through a microscope.

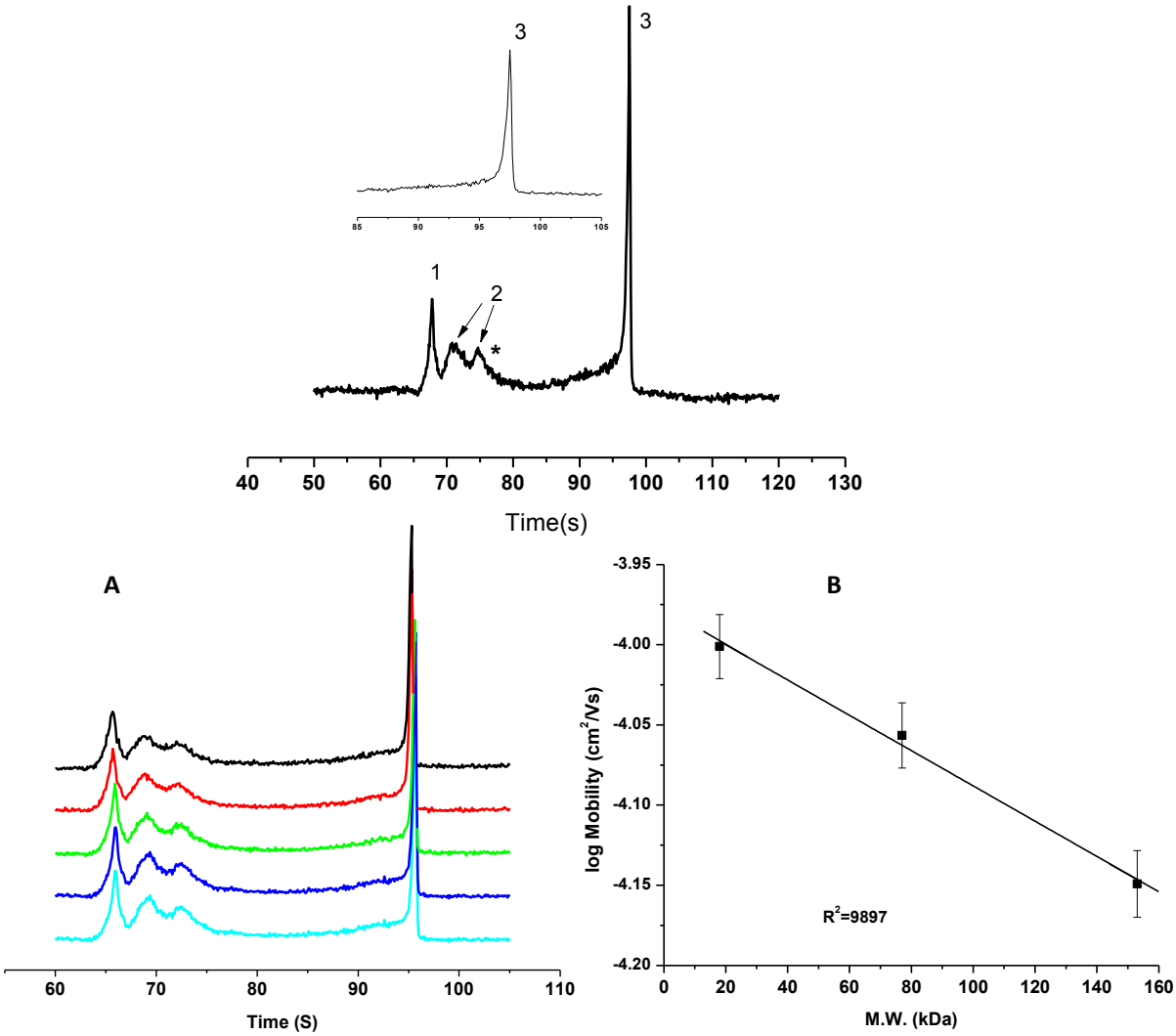

Figure 5.10. Separation of CaM-CN and CaM-eNOS photoproducts using conditions that suppress the EOF. A PDMS/PMMA simple "T" chip with 3.5 cm separation channel was used and the separation conditions were as follow: 4X TBE, pH 8.3, 0.05% (w/v) HPMC, 10 mM SDS, separation potential 800 V and the detection length was ~1.5 cm. Peak 1 is CaM and peak(s) 2 represent CaM-CN photoproducts. Peak 3 represents CaM-eNOS photoproducts. Insert in the top panel shows the shape of peak 3 (A) Consecutive multiple runs (n=5) show consistent migration times (B) Apparent mobility vs. molecular weight and least square linear fit of the two parameters, R^2= 0.9897 and $\log \mu = -0.001MW - 3.977$. The Peak (CaM-CN) labeled with * used for mobility calculation (top panel).

However, it was not possible to suppress EOF without HPMC. The buildup caused band broadening and clogging of channels. Further, it was very difficult to operate for long period of times with multiple runs due to Joule heating. The maximum usage time of a microchip with those separation conditions was approximately half an hour. Due to operational problems and deformed peaks, it was difficult to use run buffers with HPMC in the separation of a mixture with multiple analytes.

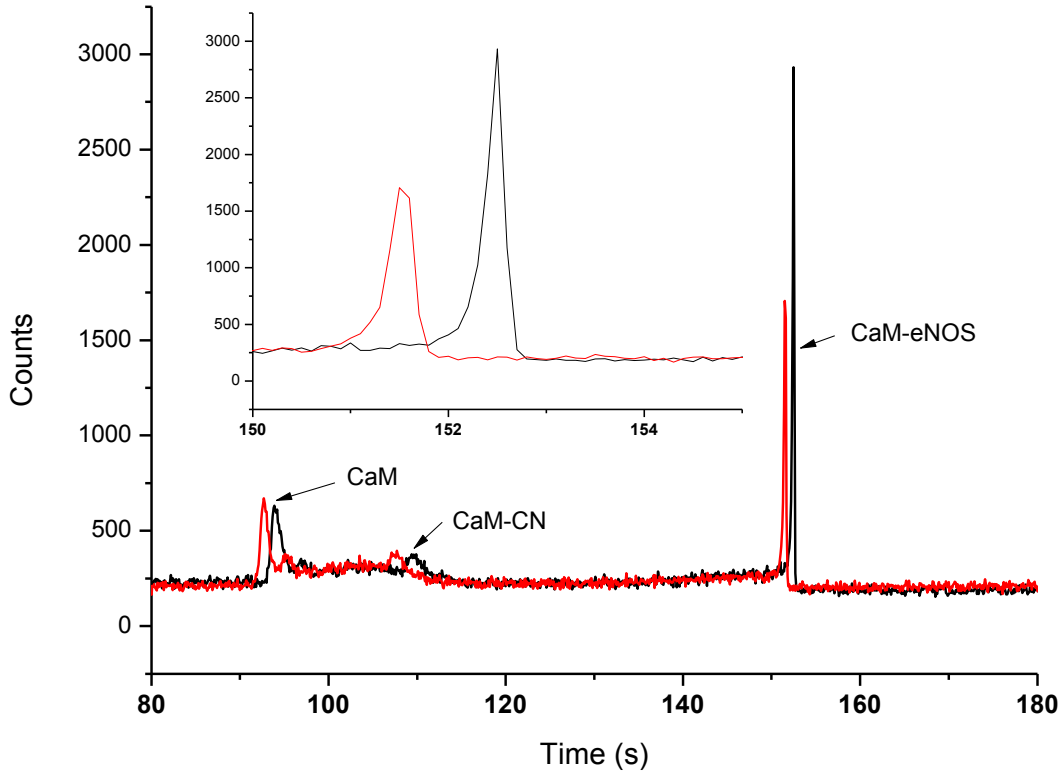

Figure 5.11. Verification of CaM-CN and CaM-eNOS photoproducts using conditions that suppress the EOF. The same chip and separation conditions used in Figure 5.9 were used other than the detection length, which was ~2 cm. Red and black electropherograms shows before and after of spiking with CaM-eNOS. Insert is an enlarged section of the electropherograms to show the effect of spiking of CaM-eNOS.

5.3.3.3. Separation of CaM-CBP photoproducts by Si-nanoparticle chips

A Si-nanoparticle colloidal array in a microchip was next introduced to separate CaM-CBPs. A self-assembled colloidal array with 170 nm Si-nanoparticles in a 1 cm PDMS/glass microchip was used for the analysis. TBE 4X, pH 8.3 with 3.5 mM SDS was used to reduce the conductivity and to get conditions that reduce EOF. The detection length was ~5 mm and the laser beam was focused onto the Si-particle array. Figure 5.12.A, B, and C show the separation of CaM-CN, CaM-eNOS and CaMAF647, respectively.

The separation field strength was 57.85 V/cm. A mixture of CaM-CN and CaM-eNOS photoproducts was separated. The obtained electropherogram is depicted in Figure 5.10D, and the separation filed strength was 42.86 V/cm. The first peak in this electropherogram was CaMAF647, and the broad peak with the highest migration time was assigned as a CaM-eNOS photoproduct. Peak 2 was common to both CaM-CN and CaM-eNOS photoproducts. Peak 3 corresponds to a low abundance photoproduct of CaM-eNOS, which only appears in concentrated samples under relatively low field strengths. Individual peaks were identified by their migration times. As an example, the migration time of CaMAF647 was ~200 s (Figure 5.12A, B, and C). CaM-CN was eluted after the CaMAF647 (Figure 5.12B), followed by CaM-eNOS (Figure 5.12C). This elution order was compatible with the Si-nanoparticle array-based-sieving where smaller analyte elutes first followed by the large analyte (*5*).

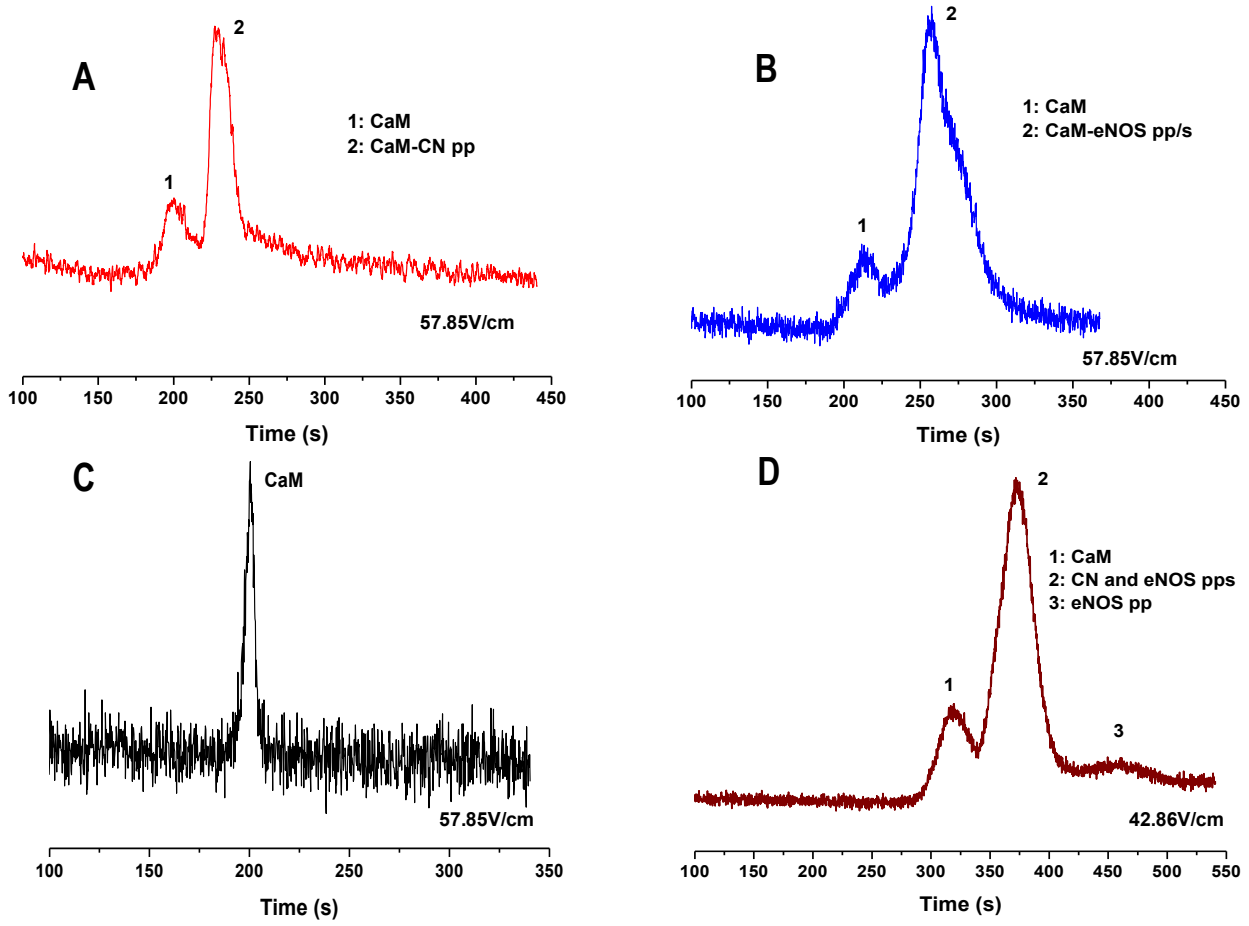

Figure 5.12. Separation of CaM-CBP photoproducts using Si-nanoparticle colloidal array fixed into a PDMS/glass microfluidic device. Separation conditions as follows: 4X TBE, pH 8.5 with 3.5mM SDS, detection length; ~5mm, separation field strength 57.85V/cm (in A, B and C) and in D the field strength was 42.86 V/cm. (A) Separation of CaM-CN photoproducts, total concentration of the mixture ~40 nM. (B) Separation of eNOS photoproducts. Total concentration of the mixture was ~60 nM (C) Separation of CaMAF647 and the concentration of the sample ~10 nM (D) Separation of CN and eNOS photoproducts. Total concentration of the mixture was ~60 nM.

The only difference between Figure 5.12 separation conditions and Figure 5.13 was the concentration of BGE. In Figure 5.12, 4X TBE was used while 3X TBE was used in Figure 5.13. 5X TBE was used to obtain the insert (electropherogram) depicted in Figure 5.13. Peaks 1, 2 and 3 in Figure 5.13 were assigned CaM, CaM-CN and CaM-eNOS, respectively using migration

times. Change of ionic strength of BGE did not alter the elution order and it was as same as in 4X TBE. The insert in Figure 5.13 shows the separation of CaM-CBP complexes in 5X TBE, pH 8.3 buffer. The effective pore size of the colloidal array in 5X TBE was larger than that in 3X TBE, and consequently, the resolution of three peaks was low. The effective pore size of the colloidal array plays a major role in sieving-based separations with a short detection length (~5 mm). The thickness of the electrical double-layer around a Si-nanoparticle depends on the ionic strength of the BGE (*19*). A BGE with low ionic strengths creates a relatively wider electrical double layer than a BGE with high ionic strengths. Therefore, 3X TBE creates a lower effective pore size than 5X TBE, and thus proteins move slower in 3X TBE than in 5X TBE. For the same detection distance, 3X TBE offers slower moving of proteins and thus enhances the band separation while 5X TBE facilitates faster moving of proteins and thus low resolution.

The elution order of separation of CBPs is; peaks 1, 2, and 3 are CaM, CaM-CN and CaM-eNOS, respectively (Figure 5.13 A). The relationship between log μ and MW (M) was derived by the Ogston sieving model (Chapter three, Equation 10). Further, the analyte mobilities are consistent with the theoretical elution order of Si-nanoparticle colloidal array-based separation which can be explained by the Ogston sieving model (*16*). However, the linear least-squares fit between the molecular weight and log of apparent mobility shown in Figure 5.13B gives low R^2 values (R^2=0.6899). This may be a result of uncertainties in the molecular weight of the CaM-CBP photoproducts. Mainly for CaM-eNOS the actual MW could not be verified due to unavailability of mass spectrometry data. Also with low resolution (of peaks) the apparent mobilities of the proteins could not be determined accurately.

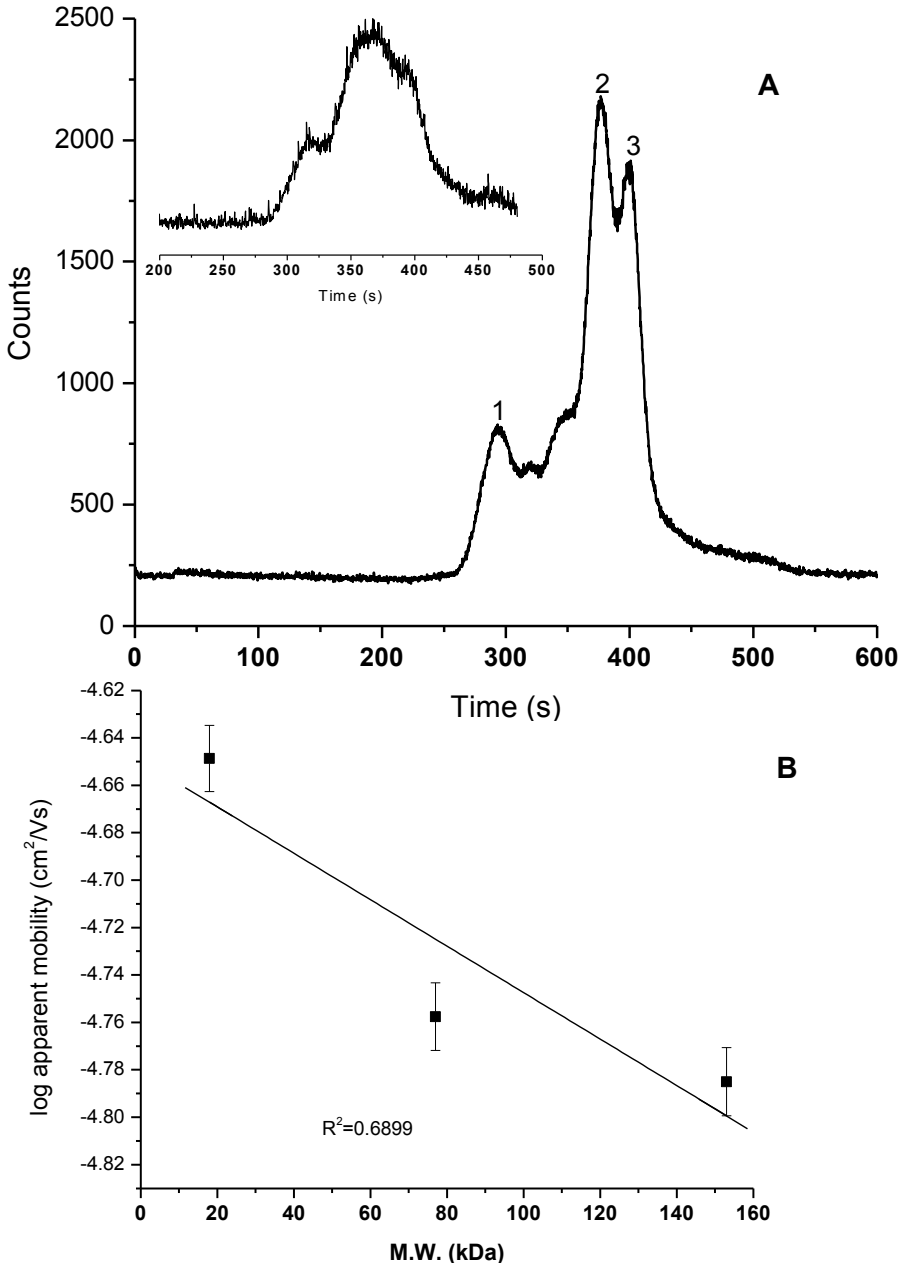

Figure 5.13. Separation of CaM-CBPs photoproducts using Si-nanoparticle self-assembled colloidal array fixed in PDMS/glass microfluidic device. (A) Separation conditions as follows: 3X TBE, pH 8.5 with 3.5mM SDS run buffer, detection length; ~5 mm, separation field strength was 57.85 V/cm. Insert shows the separation of the photoproducts with 5X TBE, pH 8.3 and the same type of Si-nanoparticle chip was also used in this analysis under the same conditions. Peak 1, 2 and 3 are CaM, CaM-CN and CaM-eNOS, respectively. (B) Apparent mobility vs. molecular weight of analytes and the linear least squares fit of the two parameters, R^2=0.6899 and log μ = - 0.001MW - 4.649. The number of separations (using 3X TBE) used for the calculation was, n=3.

Conversely, the reduction of ionic strength of BGE was not successful. Low ionic strength buffers created a relatively large EOF, and it was against the direction of the sample flow. Therefore, it was difficult to get reproducible injections with low ionic strength buffers. Also, to obtain the cross-injection and sieving-based separation mechanism, it was necessary to have conditions that suppress EOF.

Si-nanoparticle-based separation and any sieving based separations utilize porous beds with very small pour sizes (*20*). Zeng and Harrison characterized the effect of pore size on protein and DNA separations (*5*). The size of the silica spheres was selected based on the pore size of colloidal array. In this analysis, the separation mechanism is consistent with the Ogston theory; the fractional volume available in a sieving media is proportional to the mobility of an analyte (*20-22*). Hence, when the pore size of the media accommodates the analyte, separation will be based on the size of the analytes. Small analytes elute first followed by the large analytes. The theory explains the separation of globular analytes that have close relationship with the size of the analytes and the pore size in the sieving matrix (*5, 20, 23*).

This three dimensional porous medium and the high ionic strength buffer effectively created conditions that suppress EOF, and the analyte movement was based on the electrophoretic migration. Also, this well-defined sieving structure is ideal to separate large protein molecules, such as cross-linked CaM-CBP complexes. Deviations of migration times of proteins were observed in consecutive runs, likely due to the adsorption of the proteins onto the Si-array. The adsorption was unfavorable to the resolution and to gain consistent injections. Further, surface adsorption increased background, which might result in low sensitivity to species with low abundance. It was observed in the experiments that the peak shape, intensity, and migration time changed over the time.

Even though we assume one photoproduct (CaM-eNOS) there may more than one photo product that can be formed by the photo cross-linking reaction. Multiple labeling of CaM with the cross-linker which generated many different photo-reactive species, and non-specific reaction of diazirine, which reacts with any C-H bond, are responsible for the formation of multiple photoproducts. Further, the other photoproduct concentrations could be relatively low. The MCE-based method was successfully applied for the standard protein separation (Chapter three). Conversely, I came across many challenges during CBP photoproduct separation as discussed throughout this chapter. The main problem encountered during these separations was the low peak capacity, and it may be related to many photoproducts formed during the photo cross-linking reaction. Additionally, the low abundance of target photoproducts was adversely affected the separation.

5.4. Conclusion

I demonstrated detection of CaM binding model proteins using different microfluidic devices and separation modes. In this analysis, I used microfluidic devices with dynamically modified channel surfaces. Dynamic coating with additives such as SDS, DDM, and HPMC were used to control the surface adsorption of proteins. Further photoproducts with low abundance could not be separated as a result not only of co-migration but also due to band broadening. The best separations were obtained under conditions that suppress EOF and using sieving. Further, the separation of photoproducts was also challenged by the multiple cross-linked products which were formed as a result of chemical cross-linking. A mixture of CaM-CN and CaM-eNOS photoproducts could not be resolved completely by Si-nanoparticle chips.

However, individual photoproducts of CaM-CN and CaM-eNOS were identified by Si-nanoparticle separations.

5.5. References

1. Chin, D., and Means, A. R. (2000) Calmodulin: a prototypical calcium sensor, *Trends Cell Biol 10*, 322-328.
2. O'Neil, K. T., and DeGrado, W. F. (1990) How calmodulin binds its targets: sequence independent recognition of amphiphilic alpha-helices, *Trends Biochem Sci 15*, 59-64.
3. Devore, M. S., Gull, S. F., and Johnson, C. K. (2013) Reconstruction of calmodulin single-molecule FRET states, dye-interactions, and CaMKII peptide binding by MultiNest and classic caximum entropy, *Chem Phys 422*.
4. Hulvey, M. K., Frankenfeld, C. N., and Lunte, S. M. (2010) Separation and detection of peroxynitrite using microchip electrophoresis with amperometric detection, *Anal Chem 82*, 1608-1611.
5. Zeng, Y., and Harrison, D. J. (2007) Self-assembled colloidal arrays as three-dimensional nanofluidic sieves for separation of biomolecules on microchips, *Anal Chem 79*, 2289-2295.
6. Erickson, D., Sinton, D., and Li, D. (2003) Joule heating and heat transfer in poly (dimethylsiloxane) microfluidic systems, *Lab on a Chip 3*, 141-149.
7. Lion, N., Rohner, T. C., Dayon, L., Arnaud, I. L., Damoc, E., Youhnovski, N., Wu, Z. Y., Roussel, C., Josserand, J., Jensen, H., Rossier, J. S., Przybylski, M., and Girault, H. H. (2003) Microfluidic systems in proteomics, *Electrophoresis 24*, 3533-3562.
8. Tran, N. T., Ayed, I., Pallandre, A., and Taverna, M. (2010) Recent innovations in protein separation on microchips by electrophoretic methods: an update, *Electrophoresis 31*, 147-173.
9. Henry, C. S. (2006) Microchip capillary electrophoresis: an introduction, *Methods Mol Biol 339*, 1-10.

10. Kovarik, M. L., Lai, H.-H., Xiong, J. C., and Allbritton, N. L. (2011) Sample transport and electrokinetic injection in a microchip device for chemical cytometry, *Electrophoresis 32*, 3180-3187.
11. Slentz, B. E., Penner, N. A., and Regnier, F. (2002) Sampling BIAS at channel junctions in gated flow injection on chips, *Anal Chem 74*, 4835-4840.
12. Blas, M., Delaunay, N., Ferrigno, R., and Rocca, J. L. (2007) Numerical simulations of the second-order electrokinetic bias observed with the gated injection mode in chips, *Electrophoresis 28*, 2961-2970.
13. Alarie, J. P., Jacobson, S. C., and Ramsey, J. M. (2001) Electrophoretic injection bias in a microchip valving scheme, *Electrophoresis 22*, 312-317.
14. Weingerber, R. (1993) Practical capillary eletrophoresis, *2nd edition*.
15. Doherty, E. A., Meagher, R. J., Albarghouthi, M. N., and Barron, A. E. (2003) Microchannel wall coatings for protein separations by capillary and chip electrophoresis, *Electrophoresis 24*, 34-54.
16. Fruetel, J. A., Renzi, R. F., Vandernoot, V. A., Stamps, J., Horn, B. A., West, J. A., Ferko, S., Crocker, R., Bailey, C. G., Arnold, D., Wiedenman, B., Choi, W. Y., Yee, D., Shokair, I., Hasselbrink, E., Paul, P., Rakestraw, D., and Padgen, D. (2005) Microchip separations of protein biotoxins using an integrated hand-held device, *Electrophoresis 26*, 1144-1154.
17. Strege, M. A., and Lagu, A. L. (1993) Capillary electrophoretic protein separations in polyacrylamide-coated silica capillaries and buffers containing ionic surfactants, *Journal of Chromatography A 630*, 337-344.
18. Shadpour, H., and Soper, S. A. (2006) Two-dimensional electrophoretic separation of proteins using poly(methyl methacrylate) microchips, *Anal Chem 78*, 3519-3527.
19. Zhou, M. X., and Foley, J. P. (2006) Quantitative theory of electroosmotic flow in fused-silica capillaries using an extended site-dissociation--site-binding model, *Anal Chem 78*, 1849-1858.
20. Han, J., Fu, J., and Schoch, R. B. (2008) Molecular sieving using nanofilters: past, present and future, *Lab Chip 8*, 23-33.
21. Ogston, A. G. (1958) The spaces in a uniform random suspension of fibres, *Trans Faraday Soc 54*, 1754-1757.

22. Rodbard, D., and Chrambach, A. (1970) Unified theory for gel electrophoresis and gel filtration, *Proc Natl Acad Sci U S A 65*, 970-977.

23. Birdsall, R. E., Koshel, B. M., Hua, Y., Ratnayaka, S. N., and Wirth, M. J. (2013) Modeling of protein electrophoresis in silica colloidal crystals having brush layers of polyacrylamide, *Electrophoresis 34*, 753-760.

Chapter Six

Conclusions and Future Directions

6.1. Summary and conclusions

The objective of this dissertation work was to develop a microchip electrophoresis separation method for detecting CBPs. In Chapter two, I described the development of an MCE-based platform to separate proteins using LIF detection. The semi-automated platform contains four basic modules: a separation module, an optical module, a detection module and a control module. The detection module, which contains an APD, was utilized to detect CaMAF647 concentrations as low as 5 nM with high signal-to-noise ratio (S/N=6). The developed platform was capable of implementing two different injection mechanisms (gated and cross injection), and different separation modes, such as MCZE, MEKC, MCGE and sieving based methods (Si-nanoparticle colloidal array). This system can be easily converted to detect different analytes by selecting a compatible fluorophore, and changing the laser and dichroic mirror.

In Chapter three, I demonstrated a baseline separation of standard proteins (CaM, BSA and ConA) by CE with good peak capacity. The standard proteins were also separated using different microfluidic devices and separation modes by MCE. I separated the three standards in 100 s by MCZE with 10 cm and 5 cm glass chips. The standards were baseline-separated and a LOD of <5 nM was obtained for CaMAF647 with Si-nanoparticle devices. Collectively, I demonstrated the capabilities of the developed MCE platform for fast and sensitive separation of the standard proteins.

In Chapter four, I demonstrated photochemical cross-linking of CaM and CBPs. MCE separation conditions such as SDS denaturation disrupt CaM-CBP complexes. Therefore,

photochemical cross-linking was used to maintain CaM-CBP complexes during electrophoresis. CaMAF647 was covalently linked with model CBPs, CN and eNOS. Two different photo-affinity labeling methods and cross-linkers (BPM and NHS-diazirine) were tested. An amine reactive NHS-LC-SDA offered successful crosslinking with CaM and the model CPBs. Photoproducts were analyzed by different methods such as SDS-PAGE, WB, and in-gel digression with trypsin, followed by mass spectrometry.

In Chapter five, I showed the separation of photo cross-linked CaM-CBP complexes by the developed MCE platform. I also discussed the separation of CaM-CBP complexes by CE under conditions that reduced EOF. Different microfluidic devices such as glass, PDMS/glass, and Si-nanoparticle array chips were used to separate the CaM-CBP complexes. Individual photoproducts (CaM and CaM-CN, and CaM and CaM-eNOS separately) were separated under different conditions. But, it was difficult to fully resolve a mixture of photoproducts (CaM-CN and CaM-eNOS). The developed MCE method combined with cross-linking does not have the potential to separate a complex mixture of proteins. Mainly, the low abundance of target photoproducts and the presence of multiple species formed by photo cross-linking might adversely affect the separation.

Cumulatively, microchip electrophoresis can be successfully implemented to separate a simple protein mixture. The task of translating a method that was developed using relatively pure and simple proteins to a more complex protein mixture such as photo cross-linked proteins, presents many challenges including the low-abundance of the analyte of interest and the presence of unknown species. Photochemical cross-linking changed the physical and chemical properties of the protein. Following a photochemical reaction, new chemical species were formed and they can undergo many reaction pathways. As an example, a protein can form high MW structures

(dimers, trimers, and oligomers) by combining with each other or other species in the mixture. Additionally, proteins can convert to new structures. Therefore, the actual outcome of a photochemical reaction might be different from the expected outcome. Hence the implementation of a photo cross-linking procedure to a complex protein mixture should be thoroughly evaluated. Detection of CBPs by MCE may be successful as evident by the standard protein separation; however, a new methodology to capture CaM-CBP complexes is essential.

6.2. Future Directions

The separation of a mixture of CaM-CBP complexes needs to be further optimized. I suggest using a combination of two or more separation modes in a single device. The separation module of the developed platform can be converted in to a 2-D separation method and it would enhance the separation efficiency and peak capacity. A Si-nanoparticle colloidal array can be coupled with MCZE under conditions that reduce EOF, and it would enable us to separate multiple analytes in comparison to a single separation mode. The peak capacity of a 2-D separation method is larger than that of a 1-D separation method. Also, Si-nanoparticle chips can be easily operated using simple buffers, and thus combined with MCZE. In addition to that, the peak capacity and separation efficiency in this two dimensional separation method would be increased. Furthermore, it would be possible to analyze multiple samples with high throughput in a single microfluidic device by integrating the 2-D separation mechanism with a parallel multiple array of separation channels.

As a long-term objective, this method could detect selected CBPs in a single cell. As an example, a sub-set of cancer related CBPs and their expression levels could be detected in a

single cell. Such information would enable this method to be used as a diagnostic tool for early detection of cancer cells. Photochemical cross-linking can be easily adopted to investigate other protein-protein interactions. Especially, this separation platform would be further enhanced to detect protein biomarkers in a single cell.

In conclusion, the work reported in this dissertation demonstrates the development of a rapid and sensitive method for detecting CBPs. Additionally, this method could assist in identifying new pathways of CaM interactions in the cellular environment.